Impact Response and Failure of a Textile Composite Fuselage Frame

Lawrence O. Pilkington

Thesis submitted to the faculty of the Virginia Polytechnic Institute and State University
in partial fulfillment of the requirements for the degree of

Masters of Sciences
In
Aerospace Engineering

E. R. Johnson
S. W. Case
R. L. Boitnott

July, 2004
Blacksburg, Virginia

Keywords: textile composite, impact response, dynamic response, fuselage

Impact Response and Failure of a Textile Composite Fuselage Frame

Lawrence O. Pilkington

(ABSTRACT)

Impact tests are performed on two circular circumferential frame segments using a drop tower apparatus. These frames have a nominal radius of 120 inches, a forty-eight - degree included angle, a thin-walled cross section in the shape of the letter J, and are typical of the transverse fuselage frames found in a large transport aircraft. The material is a 2D triaxial braided composite of carbon fiber yarns. Impact speeds of the 91.6 lb drop mass are 23.7 ft/s or less. This speed range is the order of the vertical speed considered in a survivable crash on a runway. Transient response characteristics and failure sequence are compared to nominally identical frames tested quasi-statically in a previous study. The peak load at the first major failure event and the corresponding displacement are larger in impact tests than in the quasi-static tests. However, the fracture sequence in the vicinity of the impact location is similar to what was observed in the static tests. Preliminary transient simulations of the frame impact tests using the LSDyna software were also performed. Using the available composite material failure criteria in the software, reasonable correlation was achieved between the simulation and the tests on the load-displacement plot. The computed strains distributions did not compare as well to the measured strains at the first major failure event.

Acknowledgements

The work discussed herein was sponsored by NASA grant NGT1-03024 through the NASA Graduate Student Researchers Program, and was administered by the NASA/Langley Office of Education.

All experimental work was conducted at the NASA/Langley Impact Dynamics Research Facility under the direction of Dr. Richard Boitnott and with the help of Nelson Seabolt, Victor Jenkins, and George Palko.

I would like to thank my advisor, Dr. Eric Johnson, and my committee members, Dr. Richard Boitnott and Dr. Scott Case, for their support and guidance. I would also like to extend my gratitude to Ms. Betty Williams, Ms. Gail Coe, and Ms. Wanda Foushee of the AOE Department of Virginia Tech.

Without the support of my parents, Jim and Vivian Pilkington and Ron and Sue Kelton, this work would not have been possible. And I most certainly must thank Mr. Kenneth Pettigrew for the sanity check- may it never bounce.

Table of Contents

List of Figures

List of Tables

Chapter 1 Crash-type loading of circumferential fuselage frames

1.1 Role of fuselage frames in crash survivability

The motivation for this project is the crashworthiness of composite aircraft structures, particularly the survivability of occupants in crashes involving large transport aircraft. As noted by Woodson, the typical survivable crash occurs near the airport at a flight velocity of 150 knots, and a vertical speed below 21 feet per second.[1] Assuming that the plane does not hit an obstruction during the crash, the horizontal speed is reduced slowly as the plane slides along the ground, whereas the vertical speed decreases quickly upon impact with the ground. This rapid reduction of vertical speed leads to high acceleration loads on passengers and cargo. A crashworthy design attempts to mitigate this acceleration through the stroking of the landing gear, the crushing of the lower fuselage, and the stroking of the seat or cargo supports. This project is concerned with the energy absorbed during the crushing of the lower fuselage.

1.1.1 Fuselage testing

A series of drop tests performed on increasingly complex composite fuselage sections was conducted by Carden.[2] The sections tested started as just the circumferential fuselage frame, then increased to a skeletal sub-floor section including the frames and stringers, and finally a full sub-floor section with frames, stringers, and the outer skin. In all these of the substructure tests, the circumferential frames dominated the fundamental response and failure of the sections.

It was also noted by Carden that the composite frames fail by a brittle fracture mode. Cracks developed across the entire frame cross section, first at the point of load

application, then at 45-50 degrees on either side of the application point. The sections of the frame between these cracks essentially separate from the rest of the frame. This failure mode lowers the energy absorbed by the fuselage frame because very little of the material participates in the crush. In contrast, an aluminum fuselage frame tends to maintain integrity through yielding and folding. Matching or exceeding the energy absorbed by aluminum frames is an important goal if composite frames are to achieve wide-spread acceptance.

Following the fuselage subsection tests performed by Carden, a series of tests of on several frames made of unidirectional carbon fiber tape layup were performed by Moas and Perez.[3,4] Delamination and cracking dominated the failure modes of these frames.

1.2 Textile composite frames

The two textile composite frames utilized in this study were part of five frames originally supplied to NASA Langley Research Center under NASA contract NAS1-19348 (Structures and Material Technologies for Aircraft Composite Primary Structures) by Lockheed Aeronautical Systems Company. A $[0^{\circ}_{18k}/\pm 64^{\circ}_{6k}]$ 39.7% axial 2D triaxial braided preform of AS-4 carbon fiber was injected with 3M PR500 epoxy using resin transfer molding (RTM).[5,6] The notation is explained in detail in Section 1.2.1. The frame dimensions were specified as a 118-inch inner mold line radius, a length of 102 inches, and a depth of 4.8 inches. A J-shaped cross section was specified. The thickness of each section of the frame was specified to carry a 55,000 lb-in load (skin in compression) with 2463 lb axial tension, and -38,887 lb-in with 4470 lb axial tension. Nominal dimensions for the frames are show in Figure 1.1. Detailed measurements of each frame are provided in Chapter 2.

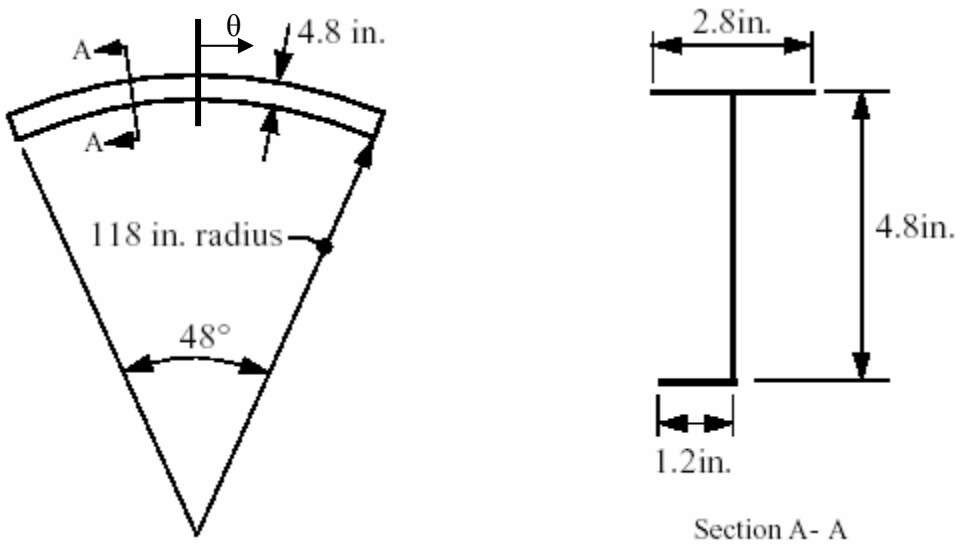

Fig. 1.1: Nominal dimensions of the textile composite frames.[4]

1.2.1 Triaxial braided textile composites

Textile composites are fabricated from dry preforms made by weaving, braiding, or knitting fiber yarns. This undulation of the fibers in textile composites leads to higher through-thickness strength and resistance to damage when compared to tape laminates. Additionally, fibers in adjacent layers nest together during the RTM process, forming a mechanical bond through the matrix that is not present in a tape layup. The bond between layers offers improved resistance to delamination, increasing the ability to carry load after initial failure and thus increasing the amount of energy absorbed during impact. This fabrication process also allows the textile preform to be made in the final shape of the part, offering increased savings in automated manufacturing.[7]

Individual yarns are composed of fibers formed into continuous linear strands that are both strong and flexible. Fibers may be formed from graphite, glass, aramids, steel, even ceramics. Because of its high strength-to-weight and stiffness-to-weight ratios, graphite has become the choice of fiber for composites where high stiffness and strength are needed and minimal weight is a necessity.[7]

Braiding is a textile process in which two or more systems of yarns are intertwined in a diagonal pattern. The preforms are fabricated over a cylindrical mandrel, one layer braided on top of the last, until the desired thickness is reached. A single layer of a 2D

braid consists of either two or three intertwined yarns. The braider yarns follow the $+\theta_b^\circ$ and $-\theta_b^\circ$ directions and usually interlace in either a 1x1 or a 2x2 pattern. A 1x1 pattern (Fig. 1.2) is similar to the interlacing in a plain weave fabric (Fig. 1.3), while in a 2x2 pattern a $+\theta_b^\circ$ braider yarn continuously passes over two $-\theta_b^\circ$ braider yarns and then under two $-\theta_b^\circ$ braider yarns and vice versa. A triaxial braid adds yarns that run parallel to the braiding axis and are inserted between the braider yarns (Fig. 1.4). These axial yarns are ideally not crimped.

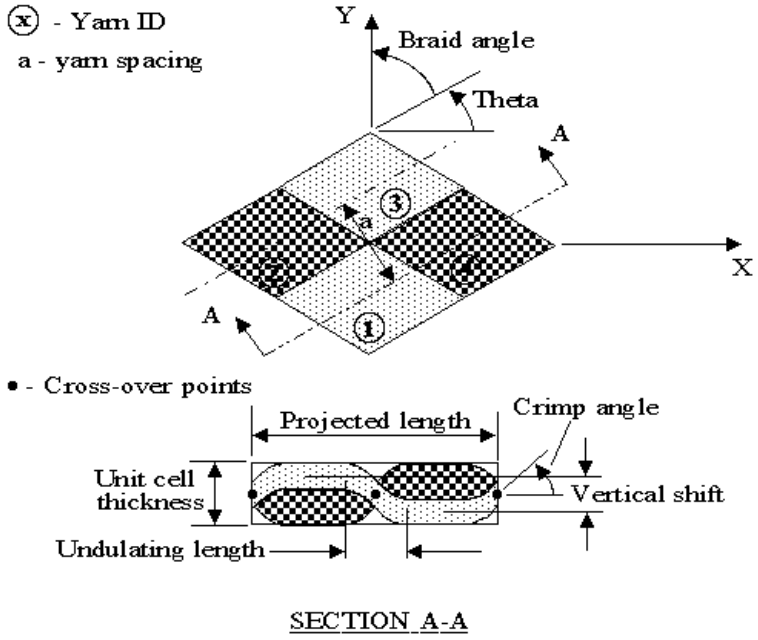

Fig. 1.2: 2D braid unit cell.[8]

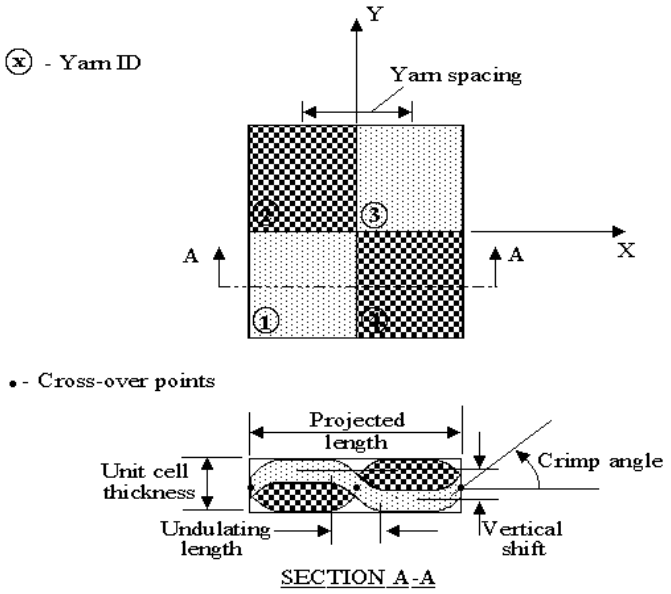

Fig. 1.3: Plain weave unit cell.[8]

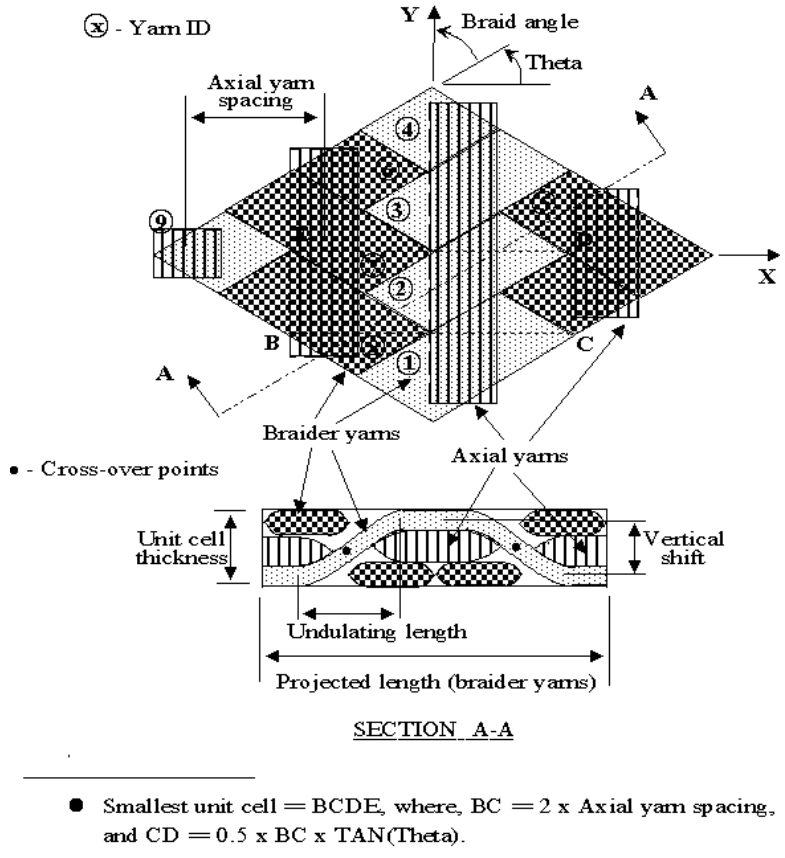

● Smallest unit cell = BCDE, where, BC = 2 x Axial yarn spacing, and CD = 0.5 x BC x TAN(Theta).

Fig. 1.4: 2D triaxial braid unit cell.[8]

After braiding, the preform is removed form the mandrel, cut along the axis, flattened, and border stitched. It is then ready for manufacturing of the final part. In general, the preform is placed in a mold and resin is introduced by RTM. As with all composite materials, it is important to minimize the occurrence of trapped air, so usually this process is done at elevated temperatures and high pressures. The final part is still a 2D composite because there are no yarns that actually go through the thickness of the material.

Standard nomenclature for textile composites defines the bias angle, tow size, and the percentage of material that is aligned with the braiding axis. In the case of the frames used in this research, the material is a $[0^{\circ}_{18k}/\pm 64^{\circ}_{6k}]$ 39.7% axial 2D triaxial weave meaning the bias yarns are placed at $\pm 64^{\circ}$ to the braiding axis, the axial yarns have 18,000 fibers per yarn, the bias yarns have 6,000 fibers per yarn, and the axial yarns account for 39.7% of the unit cell volume.

1.3 Quasi-static frame tests and finite element analysis

Drop tests of fuselage sections show that the failure sequence of static tests and dynamic tests are nearly the same, especially in the range of survivable impact velocities.[2] Quasi-static, radially-inward tests were performed on two of the available textile frames, denoted as Frames B and C, by Perez.[4] A sketch of the test apparatus can be seen in Figure 1.5; a similar fixture utilizing the same I-beam and end blocks, and a similar loading platen, is used for the current dynamic research as explained in detail in Chapter 2.

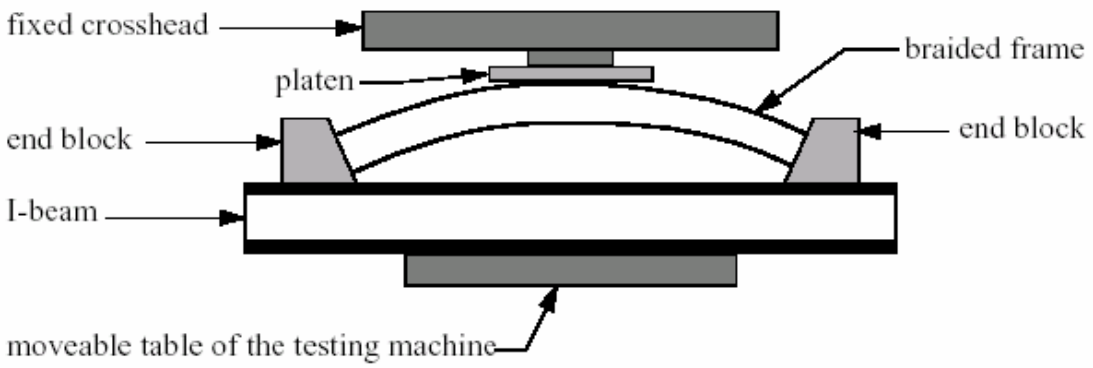

Fig. 1.5: Static test apparatus.[4]

Both Frames B and C failed near the point of load application. The outer flange buckled, then developed a crack, and eventually fractured; followed by cracking and fracture of the web; and finally cracking and fracture of the inner flange. On both frames, the noodle, a filler strip of braided carbon fiber that is placed on the outer flange at the junction of the flange and the web, also delaminated. Frame B experienced the first failure event at 5791.6 lbs and a radial deflection of 0.4782 in, corresponding to crack initiation in the outer flange. Let θ denote the polar angle as shown in Fig. 1.1, and $\theta=0^\circ$ be the apex of the frame. Cracks developed in Frame B at $\theta=0^\circ$ in the outer flange and web, and at the end supports ($\theta=\pm 21.4^\circ$) in the inner flange. Frame C experienced first failure at 6331.9 lb and 0.5187 in. Several failure events followed the first, but the load did not surpass this first peak. Cracks were observed at $\theta = 0^\circ$, $\pm 5^\circ$, and -7° in the outer flange and at $\theta=-5^\circ$ in the web; there were no cracks at the ends of Frame C.

A branched shell finite element analysis of the frames tested in Ref. 4 was conducted by Hart.[9] The branched shell finite element model of the frame included geometric nonlinearity and contact of the load platen of the testing machine with the frame. Intralaminar progressive failure was based on a maximum in-plane stress failure criterion followed by a moduli degradation scheme. Interlaminar progressive failure was implemented using an interface finite element to model delamination initiation and the progression of delamination cracks. Inclusion of both the inter- and intra- laminar progressive failure models in the FEA of the frame correlated very well with the load-displacement response from the test through several major failure events.

1.4 Objectives and outline

The objective of the current research is to perform dynamic drop tests on the remaining two textile frames, denoted as Frames CF6F and D. Results are compared to the static tests conducted by Perez,[4] with particular interest in the peak load, the deflection at this load, and the area under the load-defection plot.

The test apparatus and procedures are discussed in Chapter 2, with test results presented in Chapter 3. Chapter 4 outlines preliminary dynamic FEA utilizing the commercial code LSDyna, developed and marketed by Livermore Software Technology Corp. The dynamic FEA results are compared to the experimental data from the dynamic drop tests. Concluding remarks are presented in Chapter 5.

Chapter 2 Composite Frame Dynamic Drop Tests

Dynamic drop tests were performed on two textile composite, circumferential fuselage frame segments. Each frame was mounted convex side up in a fixture that essentially imposed clamped boundary conditions at each end of the frame. A load-induction fixture was placed on top of the frame at its center, which is the apex of the circular frame segment. This assembly was placed in a drop tower and impacted by a mass released from a variable height. The following sections discuss the frames, test apparatus, instrumentation, and the test procedure.

2.1 Textile Composite Fuselage Frames

Five textile composite frames, labeled A, B, C, D, and CF6F, were produced under NASA contract NAS1-19348 by Lockheed Aeronautical Systems Company in Marietta, Georgia[5]. All five frames were made from AS-4 carbon fiber braided textile preforms with a $[0_{18K}/\pm 60_{6K}]$ 39.7% axial architecture. The preforms were placed in a mold and infiltrated with 3M PR500 epoxy resin through Resin Transfer Molding.

Frame A was found to have many voids and other defects; it was cut into smaller sections for coupon tests and short-column compression tests.[4,9] Frames B and C were subjected to a quasi-static radially-inward load until failure.[4] Frames D and CF6F are the subject of the current research, and are subjected to a dynamic radially-inward load until failure.

All frames have a J-shaped cross section, as shown in Fig. 2.1; detailed measurements of each frame are provided listed in Table 2.1. The discrepancies in the thicknesses of the outer flange, web, and inner flange arose from the manufacturing process. The number of braided textile layers in the web and inner flange is the same, but the inner

flanges are from 15% to 28% thicker than the webs. Hence, the inner flanges have a decreased fiber volume fraction with respect to the webs, which results in a reduced stiffness and strength of the inner flange with respect to the web. The outer flange is formed by separating the layers in the web, and folding each half at a right angle to the web.

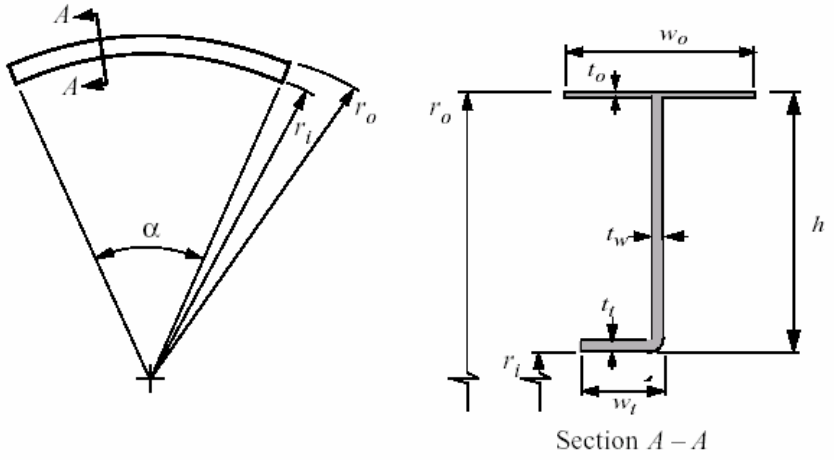

Fig. 2.1: J-section Fuselage Frame.[4]

Table 2.1: Braided composite frame measurements.[4]

Dimension as shown in Fig.2.1	Frame				
	A	*B*	*C*	*D*	*CF6F*
weight, lb	n/a	6.74	6.99	6.88	6.80
w_i, in	1.24	1.25	1.27	1.26	1.27
w_o, in	2.78	2.77	2.80	2.79	2.80
t_i, in	0.198	0.204	0.202	0.203	0.200
t_o, in	0.0892	0.0885	0.0920	0.0892	0.0823
t_w, in	0.162	0.159	0.172	0.177	0.162
h, in	4.78	4.80	4.81	4.81	4.79
r_i, in	117.25	117.85	118.92	116.23	116.59
r_o, in	122.03	122.65	123.73	121.04	121.38
α, degrees	48.18	47.21	47.46	47.56	47.09

A V-shaped void is left in the outer flange at this junction, which is filled with a braided strand of axial fibers that runs circumferentially around the frame, referred to as the 'noodle'. An illustration of this discontinuity is shown in Fig. 2.2.

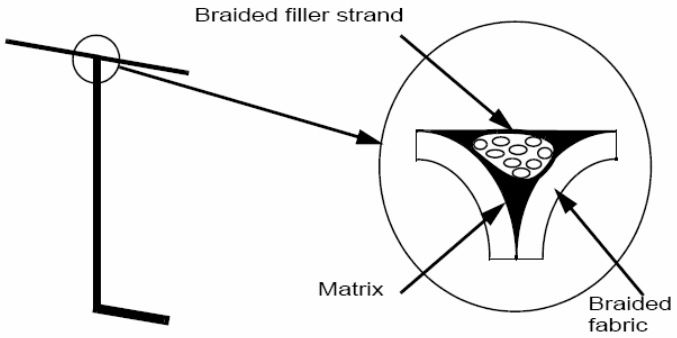

Fig. 2.2: V-shape void and braided filler strand.[9]

The computer program Textile Composite Analysis for Design, or TEXCAD, was used to estimate the stiffness and strength of the textile material.[8] TEXCAD implements a micro-mechanical constitutive analysis using data of the architecture and constituent material properties to estimate unit cell properties. The output from TEXCAD and the results of the coupon tests are presented in Table 2.2.[9] The TEXCAD values are used in a material model for the finite element analysis presented in Chapter 4.

Table 2.2: Tri-Axial braid properties for V_f = 55.26%.[9]

Properties	TEXCAD[8]	Tension Tests[4]
Axial Modulus (E_{11}, psi)	7.06×10^6	7.09×10^6
Transverse Modulus (E_{22}, psi)	6.59×10^6	n/a
Through thickness Modulus (E_{33}, psi)	1.53×10^6	n/a
Poisson's Ratio (υ_{12})	0.231	0.26
Poisson's Ratio (υ_{13})	0.216	n/a
Poisson's Ratio (υ_{23})	0.298	n/a
In Plane Shear Modulus (G_{12}, psi)	1.91×10^6	n/a
Transverse Shear Modulus (G_{13}, psi)	0.601×10^6	n/a
Transverse Shear Modulus (G_{23}, psi)	0.645×10^6	n/a
Maximum Compressive Axial Stress (X^C, psi)	71,000	n/a
Maximum Tensile Axial Stress (X^T, psi)	91,370	76,880
Maximum Compressive Transverse Stress (Y^C, psi)	56,890	n/a
Maximum Tensile Transverse Stress (Y^T, psi)	73,140	n/a
Maximum In-Plane Shear Stress (S^C, psi)	30,460	n/a
Tensile Failure Strain (ε_1^T, $\mu\varepsilon$)	14,071	10,588
Compressive Failure Strain (ε_1^C, $\mu\varepsilon$)	10,108	n/a

2.2 Test Apparatus

A photograph of Frame D ready for testing is shown in Fig. 2.3. The large block connected to the hook via an eye bolt in the photograph is the aluminum drop mass. Below this drop mass is an aluminum honeycomb wedge whose function is to shape the pulse, or time history, of the impact force, as will be explained in Section 2.2.4. The wedge is placed on top of the load induction fixture, which is centered on the frame at its apex. The frame itself is secured by a steel I-beam and end blocks.

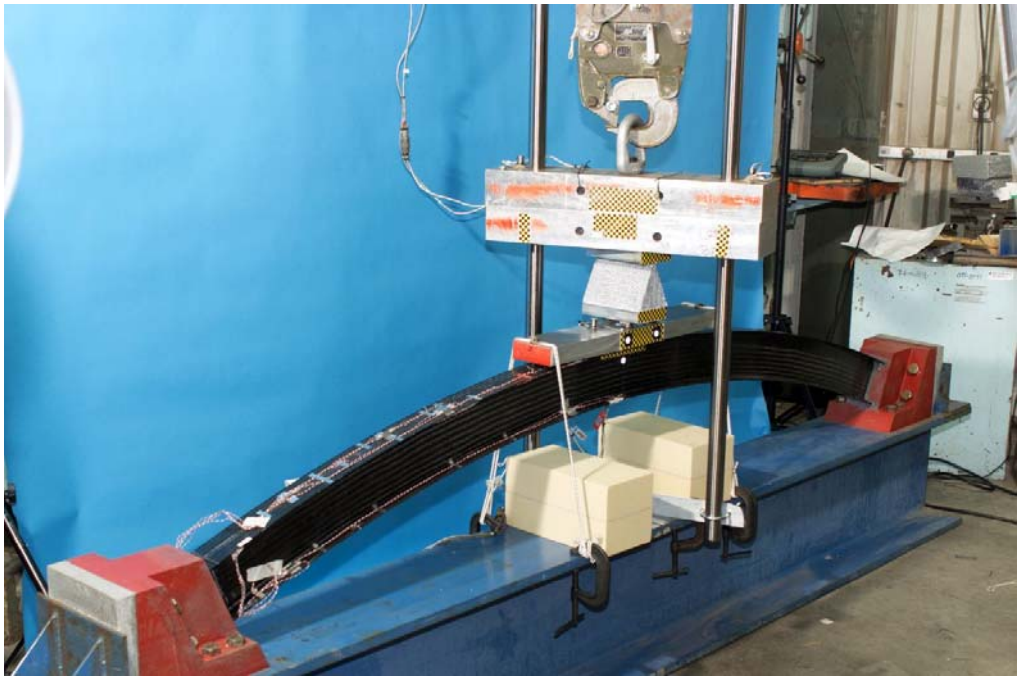

Fig. 2.3: Frame D prior to test.

2.2.1 Frame Fixture

The fixture in which the frame is mounted is the same fixture that was used for the static frame tests.[4] This fixture is composed of a 10 ft long steel I-beam and two steel end blocks. Each end block had an over-sized, J-shaped slot milled into it to allow the end of the frame to be inserted and then potted into the block. The end blocks were bolted to the I-beam; slots drilled in the I-beam allowed for horizontal adjustment of the spacing of the end blocks. A back plate was welded to the I-beam behind each end block and spacers and shims were placed between the end block and the back plate to ensure that the end block did not slide under load. A photograph of one end of the frame secured in the end block is shown in Figure 2.4.

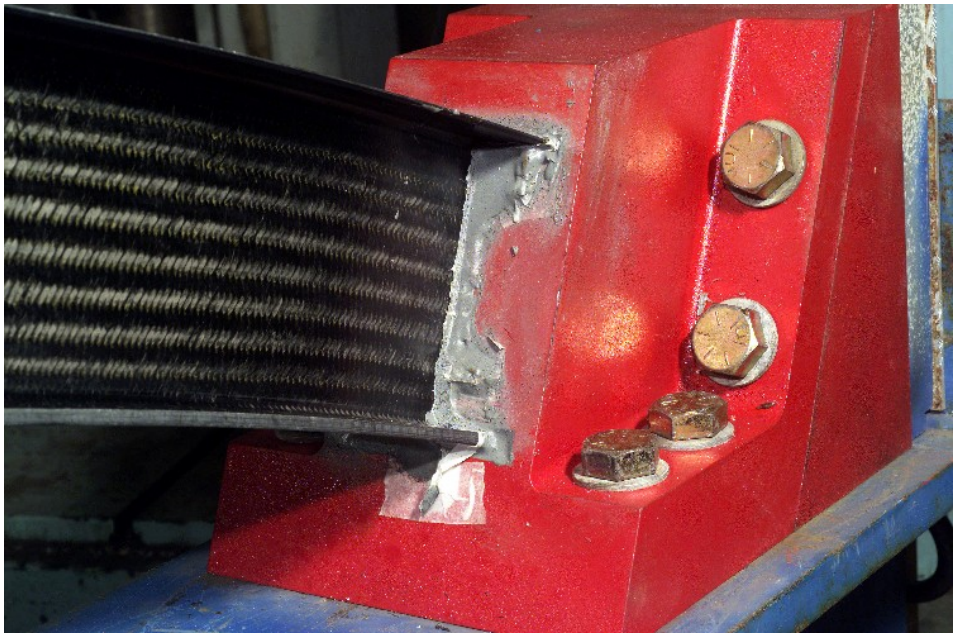

Fig. 2.4: End block with frame potted in place.

To position the frame in the support fixture, the end blocks were slipped over the ends of the frame; the frame was centered, leveled, and clamped into place; and the end blocks were bolted in place. Spacers were placed around the frame ends to keep the ends centered in the slots in the end blocks. One end of the I-beam was raised until the end block face was level, then the frame was potted in place using an epoxy filled with 25% glass beads by weight. This mixture was injected into the space around the frame with an air-powered syringe. Care was taken to ensure that the epoxy flowed into the slot in a manner that minimized trapped air pockets, a problem that was encountered during the static tests. Removal of the end blocks after testing showed that this technique filled the slots in the end blocks almost entirely.

2.2.2 Drop Tower

The small drop tower at the NASA/Langley Impact Dynamics Research Facility (IDRF) was utilized for these tests. This drop tower consisted of two guide rods that were held vertically in an A-frame structure and a drop head that slid on the guide rods. The A-frame was secured to a balcony in one of the hangers at the IDRF. An electric winch that was bolted to the top of the A-frame raised the drop head, and an electrically-

actuated release hook allowed for remote release of the drop head. A photograph of the drop tower, with the composite frame in place, is shown in Fig. 2.5.

Fig. 2.5: Drop tower with frame in place for testing.

The I-beam was placed between the guide rods at an angle to allow high-speed video coverage perpendicular to the plane of the frame. The camera can be seen on the far right of Fig. 2.5, on the black tripod.

The guide rods were two 14 ft long, 1.5 in. diameter, polished steel rods. One end of each rod was tapped for a bolt that secured the rod to the A-frame. The bottom of each

rod was restrained by U-bolts and a piece of angle-aluminum that was clamped to the I-beam, as seen in the photograph in Fig. 2.6.

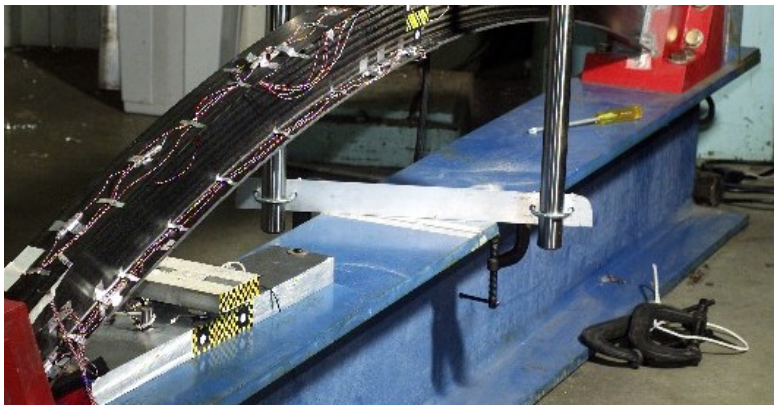

Fig. 2.6: Guide rod clamp.

The drop head was composed of aluminum blocks that could be used separately for a mass of 48 lb, or combined for a mass of 96.1 lb; when combined, the blocks were bolted together. Each block had two holes with a brass bushing for the guide rods to pass through, and a hole in its center to receive the eye-bolt. The release hook of the drop tower was inserted through the eye-bolt. For the composite frame tests, the eye-bolt was secured by a section of threaded rod that passed through the drop head and was threaded into a 1 in. thick aluminum plate that was sized to match the base of the honeycomb wedge.

The height above the frame from which the head was released determined the impact velocity of the mass. As discussed in the first chapter, a survivable impact occurs at vertical velocities of less than 21 ft/s. Available drop heights with the frame and fixture in place ranged up to 104.5 in., which correspond to impact velocities up to 23.7 ft/s.

2.2.3 Load Induction Fixture

A load induction fixture was designed to 1) spread the load evenly across the apex of the frame to simulate an impact with the ground, and 2) provide a mounting fixture for the load cells to measure the load. The fixture was composed of a lower platen and an upper platen that were bolted together with the load cells between the two platens. An effort was made to keep the load fixture as light as possible so that its inertia would have minimal influence on the load imposed on the frame.

2.2.3.1 Lower Platen

The lower platen was in direct contact with the frame. It was made sufficiently long to load the frame with a flat contact up to the first failure event and to ensure that the ends of the platen did not cut into the frame during the test. Holes for the head of the bolts that tie the upper and lower platen together were spaced in the lower platen so that they cleared the width of the radially outboard flange of the frame, requiring the lower platen to be 4 in. wide. To ensure that the ends of the platen did not contact the frame, the platen length was set to 24 in.; this number was calculated assuming that the frame would deflect 0.5 in. at failure as in the static test, then placing a chord line across the 123 in. outer arc of the frame. The platen used for the static tests was 34 in. long, but was sized to a larger expected displacement at failure.

The thickness of the platen was designed to allow less than 1%, or 0.024 in., deflection of its ends at maximum load. Assuming a line load across the middle of the platen, the deflection was found using

$$\delta = \frac{FL^3}{48EI} \qquad (2.1)$$

where F is the expected load, 7000 lbs; L is half the length of the platen, 12 in.; E is Young's Modulus of aluminum, 10.5×10^6 psi; and I is the second area moment of the rectangular cross section of the platen. The final thickness of the platen was determined to be 2 in. The final weight of the lower platen was 15.0 lbs.

2.2.3.2 Upper Platen

The upper platen was sized to the same maximum deflection as the lower platen. Additional requirements included requiring the upper platen to be at least as large as the base of the honeycomb wedge and thick enough to be tapped to accept the bolts that hold the fixture together. This last constraint was the driving variable as it was found that the deflection of the upper platen with a 1 in. thickness was negligible in the range of sizes needed for the wedge. The final size of the upper platen was 4 in. long, 6 in. wide, and 1 in. thick, arrived at after the wedge was sized. The final weight of the upper platen was 1.875 lbs.

2.2.3.3 Assembly

The upper and lower load platens were bolted together with 3, 0.25 in. bolts placed in a triangular pattern. Clearance holes were drilled in the lower platen, and the upper platen was tapped to accept the threads of the bolts. Each bolt was passed through the lower platen, then a steel washer, a ring-shaped load cell, and a second steel washer was placed over the bolt, then the bolts were threaded into the upper platen. A diagram of the assembly can be seen in Fig. 2.7.

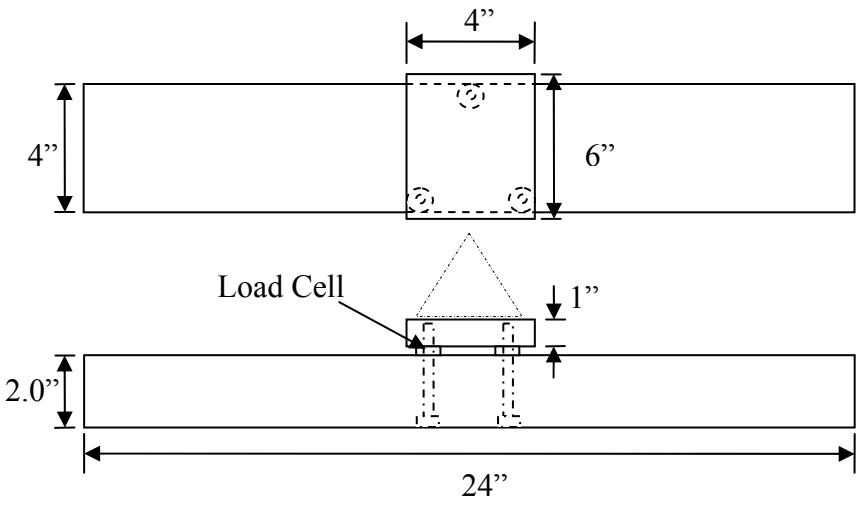

Fig. 2.7: Diagram of load introduction fixture.

2.2.4 Honeycomb Wedge

The aluminum honeycomb wedge was used to tailor the pulse shape, or time history of the force applied to the frame. This technique has been used at the IDRF in previous dynamic tests to simulate the stroking of the undercarriage of an aircraft; the result is that the load pulse resembles a sine wave more than a step load, which is more realistic in an actual crash senario.[10]

To size the honeycomb wedge, a two-spring, two-mass model of the test was developed and programmed in Matlab to perform a modal analysis of the system. See Fig. 2.8 for a sketch of the model. The Matlab program is listed in Appendix 1. The program predicted the displacement history and peak load acting on the frame given the

input parameters. The drop mass had two possible values, as discussed above, but since it was difficult to change the mass between tests, only the heavy mass of 91.6 lbs was used. The mass of the platen was assumed, then iterated as the base size of the wedge changed the size of the upper platen. The spring-stiffness assumed for the frame was taken from the initial load-deflection response of the frame under static loading. These input selections left a value for the effective stiffness of the honeycomb wedge and the initial velocity of the drop mass as the only design parameters.

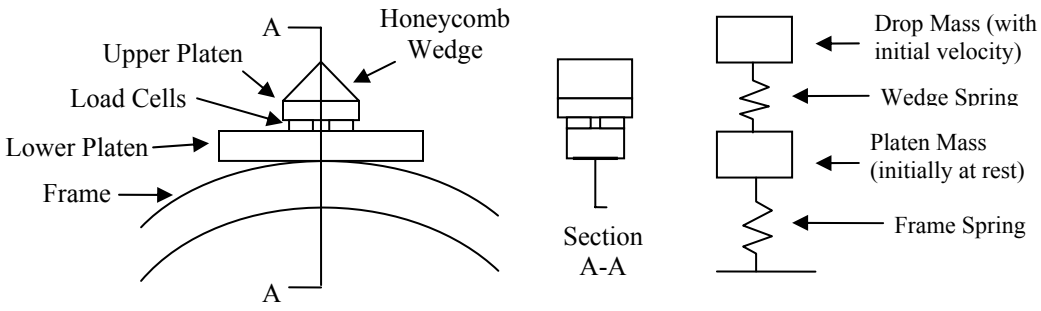

Fig. 2.8: Spring-mass system model.

Since the honeycomb was cut as a uniform triangular cross section along the width of the flange, or the y-axis, the area over which the applied force acts increases linearly with the depth of the crushed pyramid section. This linearly increasing force with crush depth leads to behavior analogous to a simple, linear spring. However, the linear relation between the force and depth of the crush is irreversible, since the honeycomb wedge material behaves as an ideally rigid-plastic material. A sketch of the honeycomb wedge is shown in Fig. 2.9.

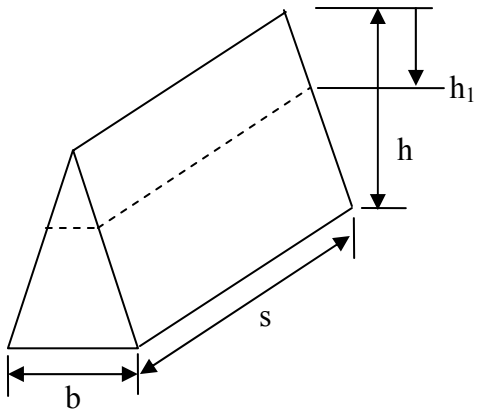

$b_1 = h_1\, b/h$

$F_1 = X^C\,(s\, b_1) = (X^C\, s\, b)\, h_1/h$

$F_1 = K_W\, h_1$

$K_W = X^C\, s\, b/h$

Fig. 2.9: Linear spring behavior of honeycomb wedge.

Let h_1 denote the crush depth of the wedge, b_1 the length of the base of the crushed portion of the wedge at this crush depth, F_1 the force corresponding to this crush depth, s the width of the base of the wedge, and X^C the compression strength of the honeycomb material. Then, $F_1 = X^C\,(s\, b_1)$. But $b_1 = h_1\, b/h$, where b is the length of the base of the wedge. Eliminating b_1 we find $F_1 = (X^C\, s\, b)\, h_1/h$. Therefore, the constant of proportionality, or "spring stiffness" of the wedge, is:

$$K_W = X^C \frac{sb}{h} \qquad (2.2)$$

The design parameters for the wedge were the width s, the length b of the base, the height h of the wedge, and the crush strength X^C of the honeycomb material. At the IDRF, there was honeycomb available with compression strengths of 90, 200, 400, 640, and 900 psi. A sample wedge of 4x4x4 in. with 400 psi strength was used as the starting point for the parametric design of the final wedge shapes, whose dimensions will be given in Section 2.4. As seen in Fig. 2.11, the predicted displacement history of the frame matches the actual displacement until the nonlinear material and geometric properties of the frame begin to dominate the response.

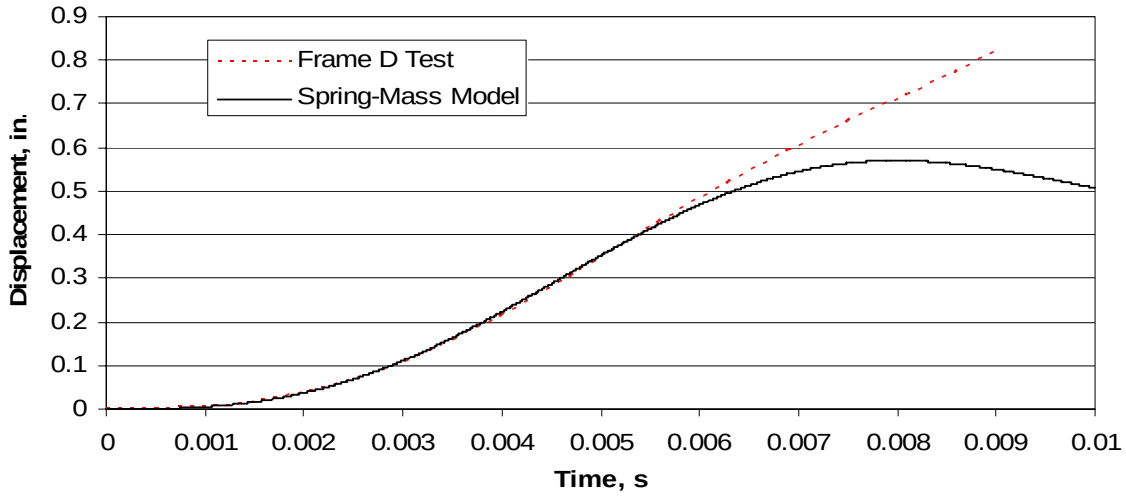

Fig. 2.10: Matlab prediction compared to actual displacement data.

2.3 Instrumentation

The drop head was instrumented with two accelerometers, ENDEVCO of San Juan Capistrano, CA, model 2262-200, one near each guide rod. Two more accelerometers were placed on the lower load platen, adjacent to the upper platen. Three load cells, Transducer Techniques of Temecula, CA, model LW0-10K, were placed between the upper and lower platen, as described above. Three load cells were used instead of one because a single load cell may provide erroneous data if placed in bending as was experienced in the tests. Each bolt was torqued to 20 ft-lbs to provide a preload on the load cell; these load cells only read compressive loads unless a preload is applied and the effective zero load is shifted. These instruments are identified in Fig. 2.11; note that one of the load cells is on the back side of the picture and is not visible.

Fifteen electrical-resistance stain gages, model CEA-06-500UW-350, were placed on each frame to match the placement of the strain gages in the static tests. Due to budget limitations of the dynamic tests, only gages that yielded interesting information in the static tests were matched. Figures 2.12 and 2.13, and Tables 2.3 and 2.4, describe the location of the gages from the dynamic tests, and which gages they match from the static tests. As noted in Fig. 2.12, the positive-y direction is the direction in which the inner flange projects from the web. This side is referred to as the front of the frame, and the

negative-y side as the back, because of the orientation to of the frame to the camera during the dynamic tests.

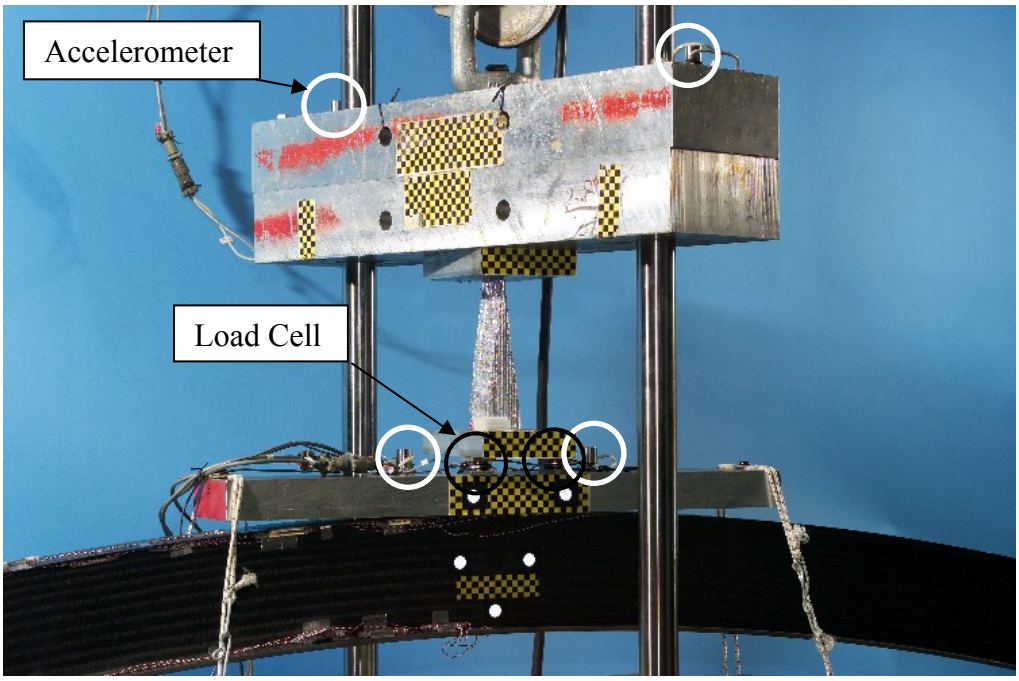

Fig. 2.11: Instrumentation detail.

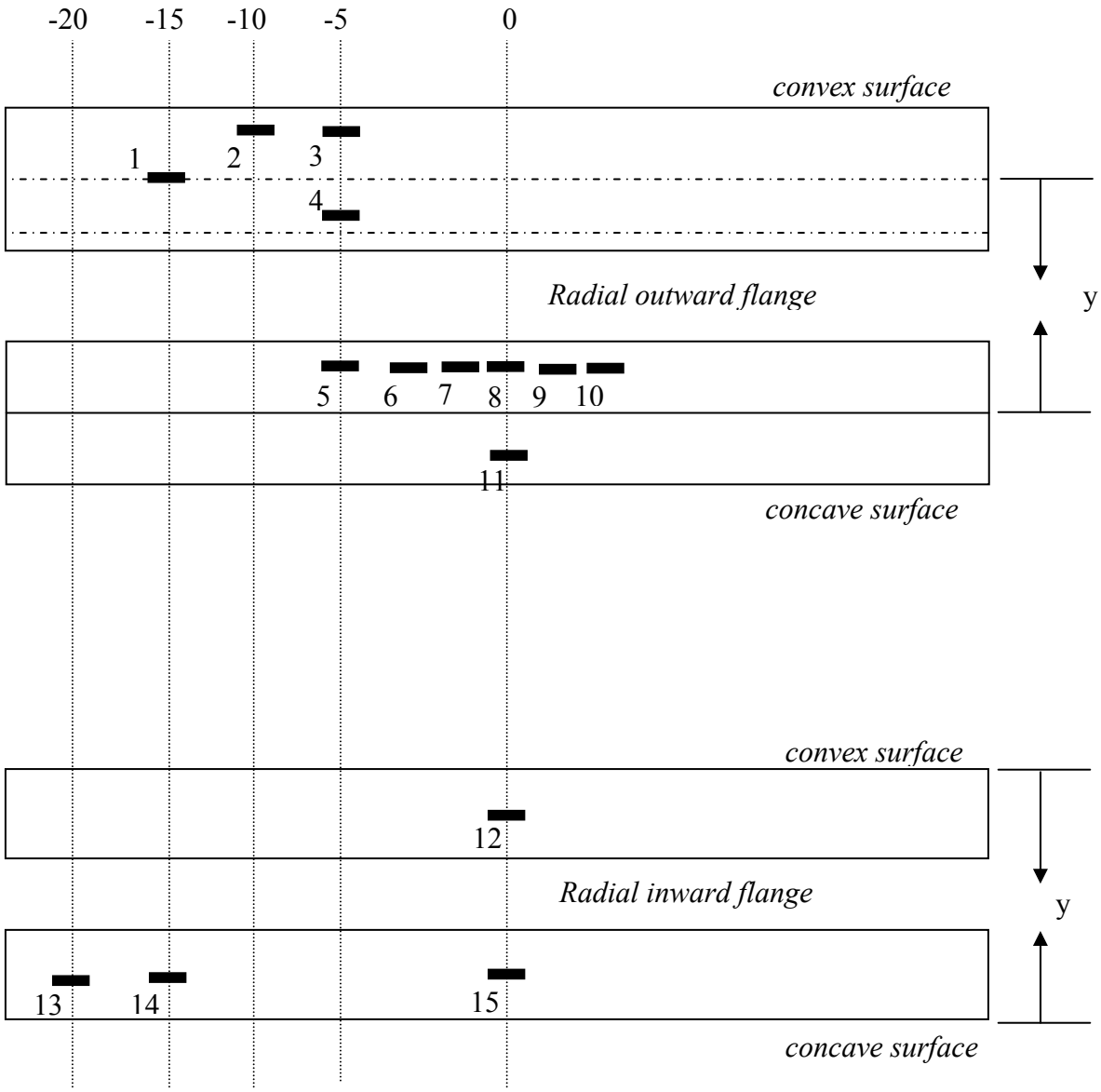

Fig. 2.12: Strain gage layout on composite frames.

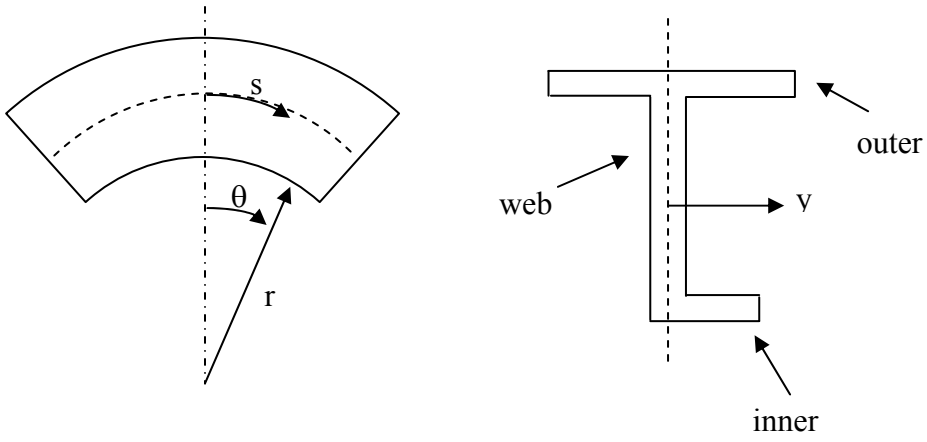

Fig. 2.13: Coordinate definition for Tables 2.3 and 2.4.

Table 2.3: Circumferential, out-of-plane, and radial locations of the strain gages on the braided composite Frame D.

Strain Gage Number	Angle θ, degrees	s, inches	y, inches	Radius r, inches
1	-15	-31.69	0	121.04
2	-10	-21.13	-0.693	121.04
3	-5	-10.56	-0.693	121.04
4	-5	-10.56	0.693	121.04
5	-5	-10.55	0.693	120.95
6	-2.5	-5.28	0.693	120.95
7	-1	-2.11	0.693	120.95
8	0	0	0.693	120.95
9	1	2.11	0.693	120.95
10	2.5	5.28	0.693	120.95
11	0	0	-0.693	120.95
12	0	0	0.625	116.43
13	-20	-40.57	0.625	116.23
14	-15	-30.43	0.625	116.23
15	0	0	0.625	116.23

Table 2.4: Circumferential, out-of-plane, and radial locations of the strain gages on the braided composite Frame CF6F.

Strain Gage Number	Angle θ, degrees	s, inches	y, inches	Radius r, inches
1	-15	-31.48	0	120.23
2	-10	-20.98	-0.693	120.23
3	-5	-10.49	-0.693	120.23
4	-5	-10.49	0.693	120.23
5	-5	-10.49	0.693	120.15
6	-2.5	-5.25	0.693	120.15
7	-1	-2.10	0.693	120.15
8	0	0	0.693	120.15
9	1	2.10	0.693	120.15
10	2.5	5.24	0.693	120.15
11	0	0	-0.693	120.15
12	0	0	0.625	116.67
13	-20	-40.73	0.625	116.59
14	-15	-30.455	0.625	116.59
15	0	0	0.625	116.59

2.3.1 Calibration

Calibration tests were run by placing known loads on the load introduction fixture to verify that the sum of the load cell readings was the true applied load. The fixture was placed in universal test machine with a calibrated load cell stacked on top of the upper platen. The press was run in displacement control mode, applying a quasi-static load to the fixture and calibrated load cell. The loads registered by the calibrated load cell and the load cells in the fixture were recorded by the same data acquisition system used during the dynamic tests. The loads measured by the load cells in the fixture were summed and compared to the load measure by the calibrated load cell.

It was found that the load cells only read 72.5% of the applied load; part of the load was shunted through the bolts that held the fixture together. As seen in Fig. 2.14, when the correction faction was applied to the raw fixture data as $F_{Corr} = F_{Raw}$ /0.725, the

corrected curve matches the calibrated data exactly, with $R^2 = 1$ in the regression analysis. This correction factor was used during the data analysis discussed in Chapter 3.

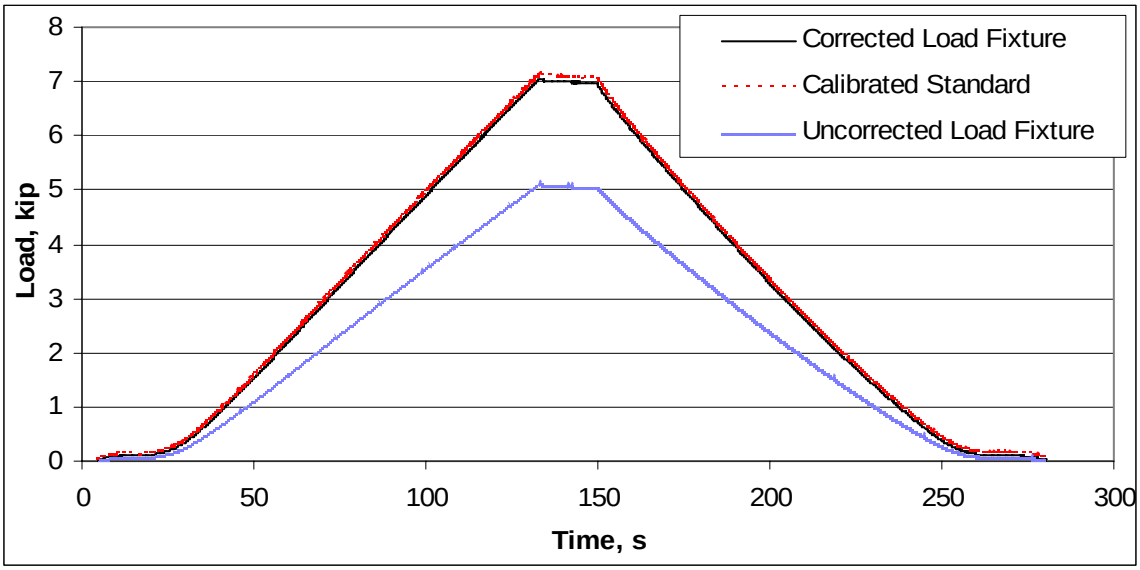

Fig. 2.14: Comparison of corrected fixture data and calibrated standard data.

2.4 Test Procedure

Several tests were designed with increasing peak loads. It was expected that the frames would fail under dynamic loading at 115% of the static load, or about 6900 lbs.[10] The initial failure test was thus designed for 7000 lbs. Tests were designed with peak loads of 1000, 2000 and 7000 lbs by varying the geometry and strength of the honeycomb wedge. Frame CF6F was tested with these load conditions. When the frame did not fail at 7000 lbs, a 10,000 lb peak load test was designed; Frame CF6F failed during this test. Frame D was tested at 1000 and 10,000 lb peak loads. Table 2.5 lists parameters for each test. The lower-load tests have low velocities because of the use of a constant drop mass.

Table 2.5: Dynamic test parameters.

Test Type	Designed Peak Load, lb	Frame(s) Tested	Aluminum Honeycomb Wedge Parameters				Drop Mass Parameters		Notes
			s, in.	b, in.	h, in.	X^c, psi	Height, in.	Velocity, ft/s	
Static[4]	To Failure	B, C	n/a	n/a	n/a	n/a	n/a	n/a	
Dynamic	1000	CF6F, D	2	1.5	3.125	400	18.534	10	
Dyn.	2000	CF6F	4	1.5	3.125	400	41.925	15	
Dyn.	7000	CF6F	6	4	4	400	90.182	22	
Dyn.	10,000	CF6F, D	6	4	3.25	640	98.571	23	failure

Before each test was run, the frame position within the drop tower was verified and the wedge for the given test was placed on top of the load introduction fixture and secured with double-sided tape. Several cameras, including two high-speed film cameras, two standard video cameras, and one digital high-speed camera, were placed around the test frame. The digital high-speed video camera was placed perpendicular to the plane of the frame and was focused on the apex of the frame. The other cameras were places are various locations for more wide-angled views of the test. A 3200L Digital Acquisition System by EME Corp., of Arnold, MD, with up to 31 channels, each with a built in A/D converter, was used to convert the analog data signals and interface with a laptop computer. Software provided by EME Corp. sampled the data at 10,000 Hz and wrote a text file for each channel that was later imported to Microsoft Excel and Matlab.

Care was taken during the test to ensure the safety for the staff involved. Lexan shields were placed several feet away from the drop tower, and all personnel were required to stand behind the shields during the test. Any equipment, such as the cameras and release hook, that had to be triggered during the test were wired so that they could be actuated remotely.

The results from the dynamic tests are compared to the static test results in Chapter 3.

Chapter 3 Analysis of the Dynamic Test Data

The response data from the dynamic tests of Frames CF6F and D are compared to the corresponding data from the quasi-static tests of Frames B and C. The first section of this chapter discusses the analysis of the raw data that led to the load and displacement at failure. Next, the loads and displacements at the first major failure events, defined as a drop in the load, of Frames CF6F and D are compared to Frames B and C. Additionally, load-displacement response curves from the lower peak-load dynamic tests are compared to corresponding response curves from the static tests. High-speed video clips and post-test photos are examined to compare the failure sequence of the dynamic tests to the static failure sequence. Lastly, strain gage data are compared between the tests.

3.1 Load and displacement analysis

The load imparted to the frame was found using the following equation:

$$F_{frame}(t) = CF \cdot \left[\sum_{i=1}^{3} F_i(t) - F_i(0) \right] + A_{platen}(t) \cdot m_{platen} \quad (3.1)$$

where CF (0.725) is the load calibration factor for the load fixture, F_i is the load measure by load cell i, $F_i(0)$ is the initial offset of load cell i, m_{platen} (17.867 lbs) is the mass of the load introduction fixture, and the acceleration of the lower platen, denoted by A_{platen}, is found by:

$$A_{platen} = \frac{filter(A_{rear}) - avg(A_{rear}^{freefall}) + filter(A_{front}) - avg(A_{front}^{freefell})}{2} \quad (3.2)$$

where *filter(A)* is the data from the accelerometer after it has been filtered by the process described below, and $avg(A^{freefall})$ is the average of the accelerometer data from the start of the test to the impact event; this zeros the accelerometer data.

During analysis, it was found that the accelerometers on the lower platen recorded an erroneous harmonic during the failure sequence, oscillating between the extreme values that the accelerometers could register (± 200 g). Examination of the high-speed video did not show any large, sudden displacements that would correspond to such high accelerations, and these oscillations caused spikes in the load data that did not correspond to physical events. Consequently, the data from each accelerometer on the platen was filtered using a 4-point, moving average filter implemented in Matlab using the *filtfilt* command, as can be seen in Appendix B.[11] A comparison of the filtered and unfiltered accelerometer and load data from the failure test of Frame CF6F is shown in Figs. 3.1 and 3.2.

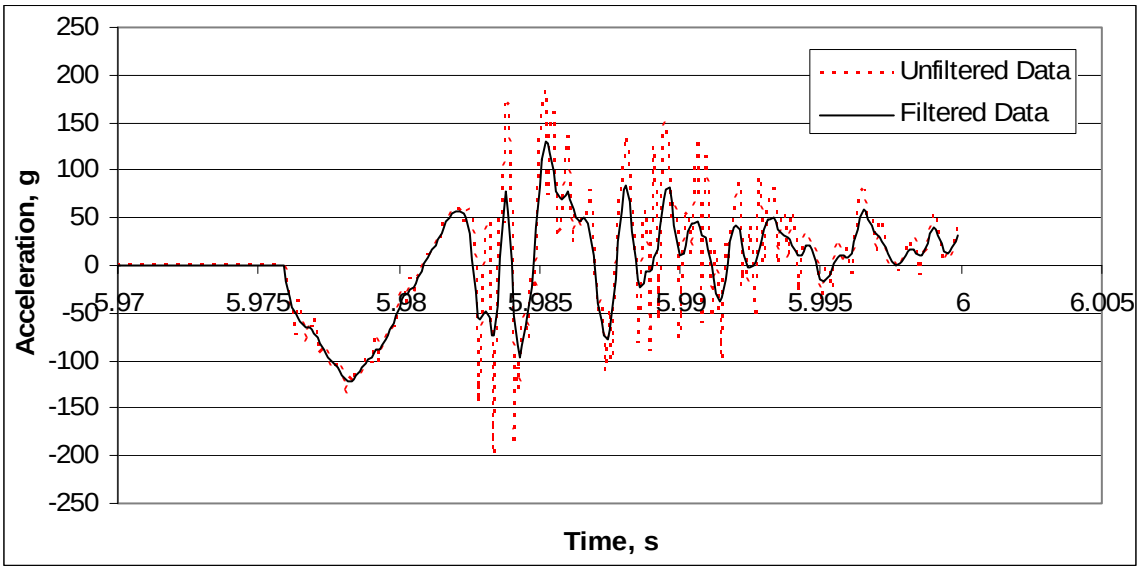

Fig. 3.1: Comparison of unfiltered and filtered accelerometer data from Frame CF6F failure test.

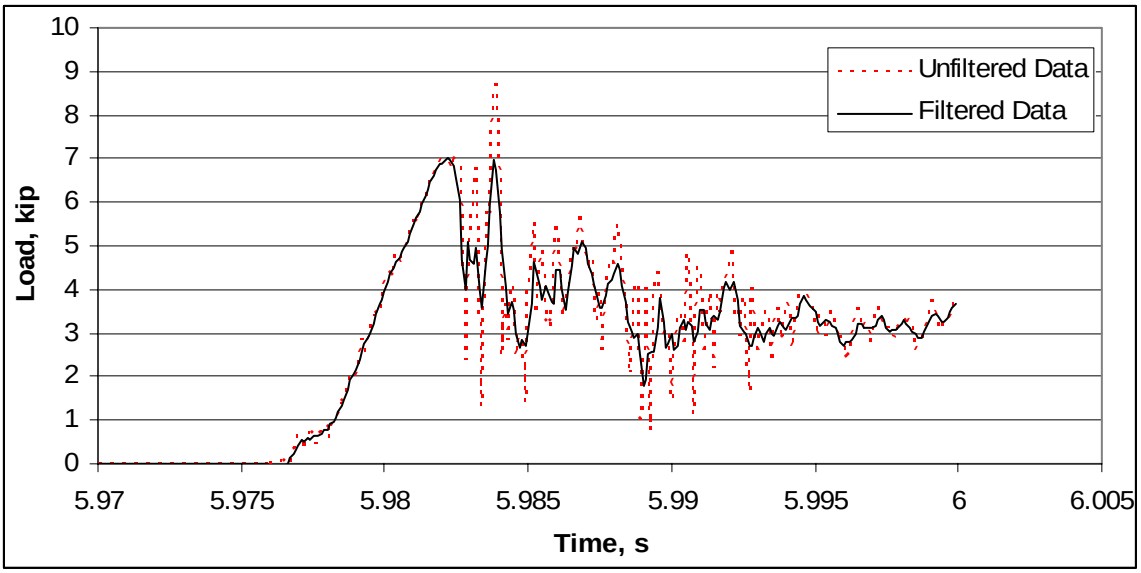

Fig. 3.2: Comparison of unfiltered and filtered load data from Frame CF6F failure test.

The displacement of the apex of the frame was assumed to be equal to the displacement of the lower platen. This displacement was found by twice integrating A_{platen} using the trapezoidal rule:

$$Vel^{n}_{platen} = \sum_{i=1}^{n-1} \frac{1}{2}(A^{i}_{platen} + A^{i+1}_{platne})\Delta t^{i}$$
$$X^{m}_{platen} = \sum_{i=1}^{m-1} \frac{1}{2}(Vel^{i}_{platen} + Vel^{i+1}_{platen})\Delta t^{i} \qquad (3.3)$$

where Vel^{n}_{platen} is the velocity of the platen at time step n, X^{m}_{platen} is the displacement of the platen at time step m, and Δt is the time step, or 0.0001 sec for a 10,000 Hz sampling frequency. The displacement was saved at each time step, and then plotted against the load.

3.2 Loads and displacements at failure

The load and displacement data of each frame at the first major failure event are listed in Table 3.1, where the load and displacement are measured in the radial inward direction at the apex of the frame.

Table 3.1: Loads and displacements of frames at failure.

Frame	Load at failure (lb)	Displacement of apex at failure (in.)
B (static)	5791	0.4782
C (static)	6331	0.5187
CF6F (dyn.)	7014	0.5651
D (dyn.)	7495	0.7143

Both frames in the dynamic tests failed at a greater load and displacement than the load and displacement at failure of the two frames in the quasi-static tests. On average, the dynamic tests yielded an increased load of 1193 pounds, an increase of 20%, which is slightly greater than the expected 115% static load. The average displacement at failure in the dynamic tests increased 0.1413 in., or 28%, with respect to the quasi-static tests.

As seen in Figures 3.3 and 3.4, the load-displacement response in the dynamic tests had a similar stiffness to the static test response. The dynamic tests also exhibit softening of the response at a lower load than occurs during the static tests. Subsequent failure events in the dynamic tests continue this trend, exhibiting a similar pattern of failure events but at larger loads and displacements than in the static tests, though the load drop following each failure event is higher in magnitude during the dynamic tests.

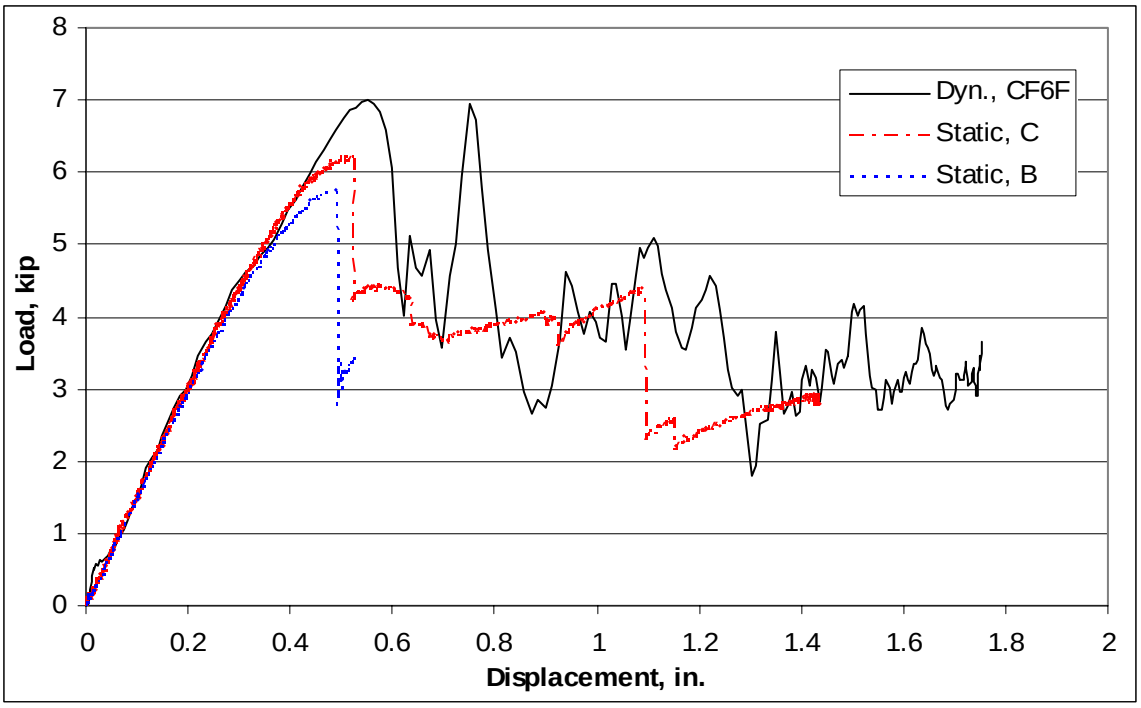

Fig. 3.3: Load-Displacement curve of failure tests, comparing Frame CF6F to static tests

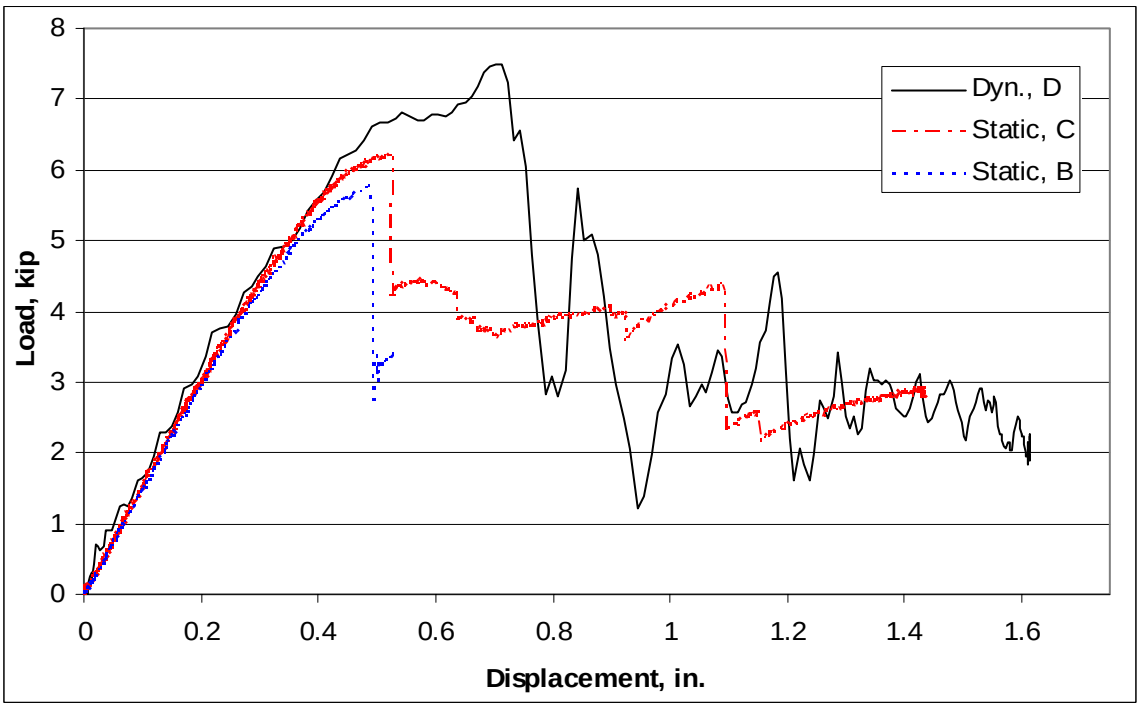

Fig. 3.4: Load-Displacement curve of failure tests, comparing Frame D to static tests.

The energy absorbed by the frames during the failure tests was calculated by integrating the load-displacement curve from 0 in. to the maximum displacement. The trapezoidal rule was again used for this integration. The initial kinetic energy imparted to the system by the impact of the drop mass was 9.47 kip-in. Frame CF6F absorbed 6.84 kip-in., and the wedge used in the test absorbed 2.35 kip-in., for a total of 9.17 kip-in. Frame D absorbed 6.15 kip-in., and the wedge 2.51 kip-in., for a total of 8.66 kip-in. The discrepancy between the initial energy and the total absorbed energy can be accounted for by the fact that the load and displacement was only measured in the vertical direction and the frame displaced and twisted out-of-plane. Table 3.2 lists the energy absorbed by each frame and wedge during the failure events, as well as the pertinent wedge parameters including the angle of the crushed portion which can be used to estimate the angle of twist of the frame at the first failure event.

Table 3.2: Energy absorbed during dynamic failure tests.

Frame	Initial Energy, kip-in	Frame Energy		Wedge Crush, in.	Wedge Angle, deg.	Wedge Energy, kip-in	Total Energy Absorbed
		kip-in	% of total				
CF6F	9.47	6.84	75.5	2.284	1.50	2.35	9.17
D	9.47	6.15	71.0	2.250	2.38	2.51	8.66

3.3 Failure sequence

As noted by Perez, in the quasi-static test of Frame B, cracks developed in the outer flange and progressed radially inward in the web at the apex of the frame (θ=0˚), and in the inner flange at $\theta = \pm 21.4$˚.[4] The origin of the polar angle θ is at the apex, or center, of the frame segment. Frame C developed crack in the outer flange at θ = 0˚, ±5˚, and -7˚, and in the web and inner flange at θ = -5˚. Also, the circumferential filler material, or the so-called the noodle, in the outer flange, separated from the outer flange from -9˚ to +9˚. In both static tests, the first major failure event, corresponding to the first drop in load, is the initiation of a crack in the outer flange, followed by a second drop in load when the outer flange cracks through. A third drop in load corresponds to the cracking of the web.

In Frame C, the crack in the web then propagates into the inner flange at complete failure, while in Frame B the inner flange cracks through far from the web crack.

The dynamic failure of Frames CF6F and D followed a sequence similar to that observed in the quasi-static tests: the outer flange cracked near the apex, then this crack propagated into the web at the junction of the outer flange and web, then propagated radially inward in the web to the junction of the web and the inner flange. The inner flange of Frame CF6F did not completely fracture, leaving the frame intact, while the crack in the web of Frame D propagated into the inner flange and the frame fractured into two pieces. During the static tests, the platen was attached to the loading head and thus partially restrained the twisting and out-of-plane bending of the frames along the platen contact under the radially inward load, similar to the stringers and skin of a full fuselage section. In the dynamic tests the platen did not restrict this out-of-plane motion as much, and the inner flange and web of both Frame CF6F and D rotated significantly about the circumferential reference axis; the dynamic tests are less like a real crash impact than the static tests in this respect. However, the platen remained almost level, so the rotation of the frame led to half of the outer flange folding towards the web. Cracks also developed along the noodle from the apex to ±10˚. Figures 3.5 through 3.8 show this sequence from frames taken from the high-speed video and the post-test photos.

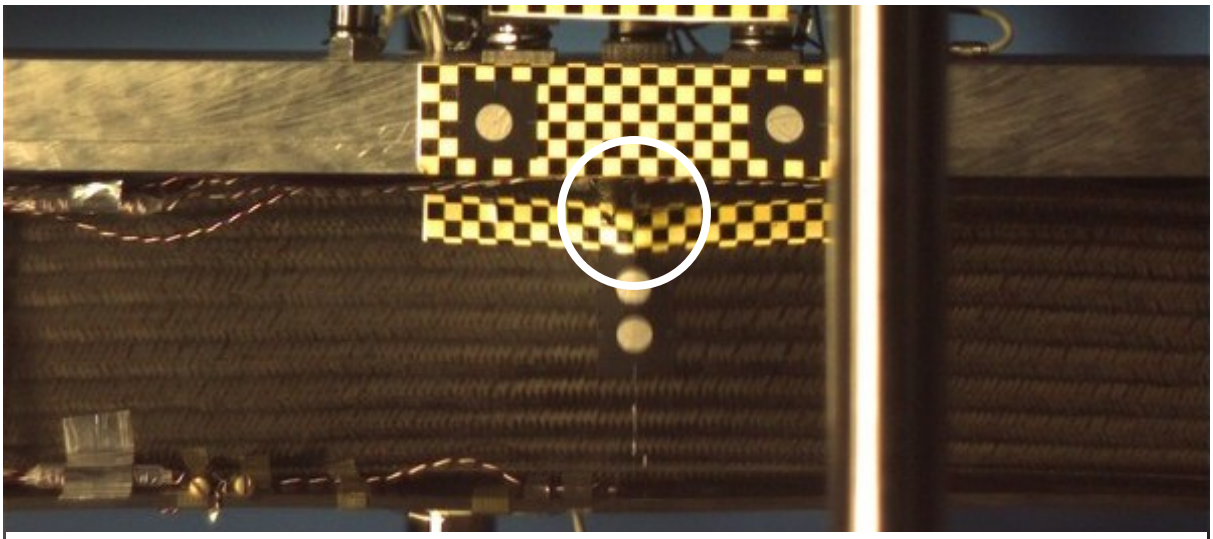

A: Note crack has propagated to junction of web and outer flange. This is the first failure event at 6854 lb load, 0.56 in. displacement, and 0.0063 s after impact.

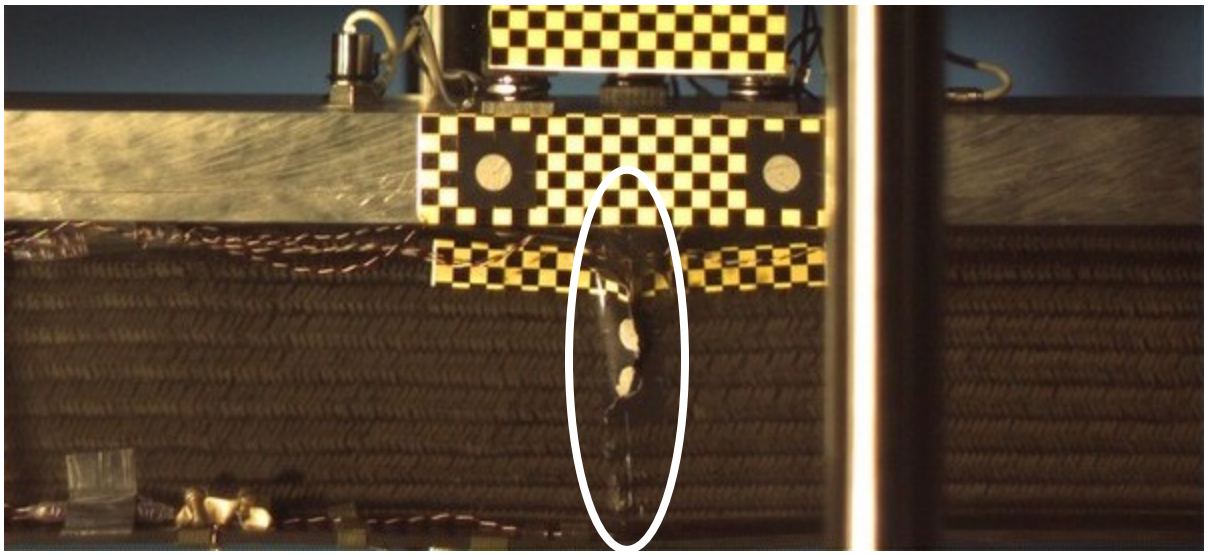

B: Note crack has propagated down web to junction of web and inner flange. This is just prior to maximum deflection of 1.75 in., 0.0240 s after impact

Fig. 3.5 A and B: Frame CF6F crack propagation.

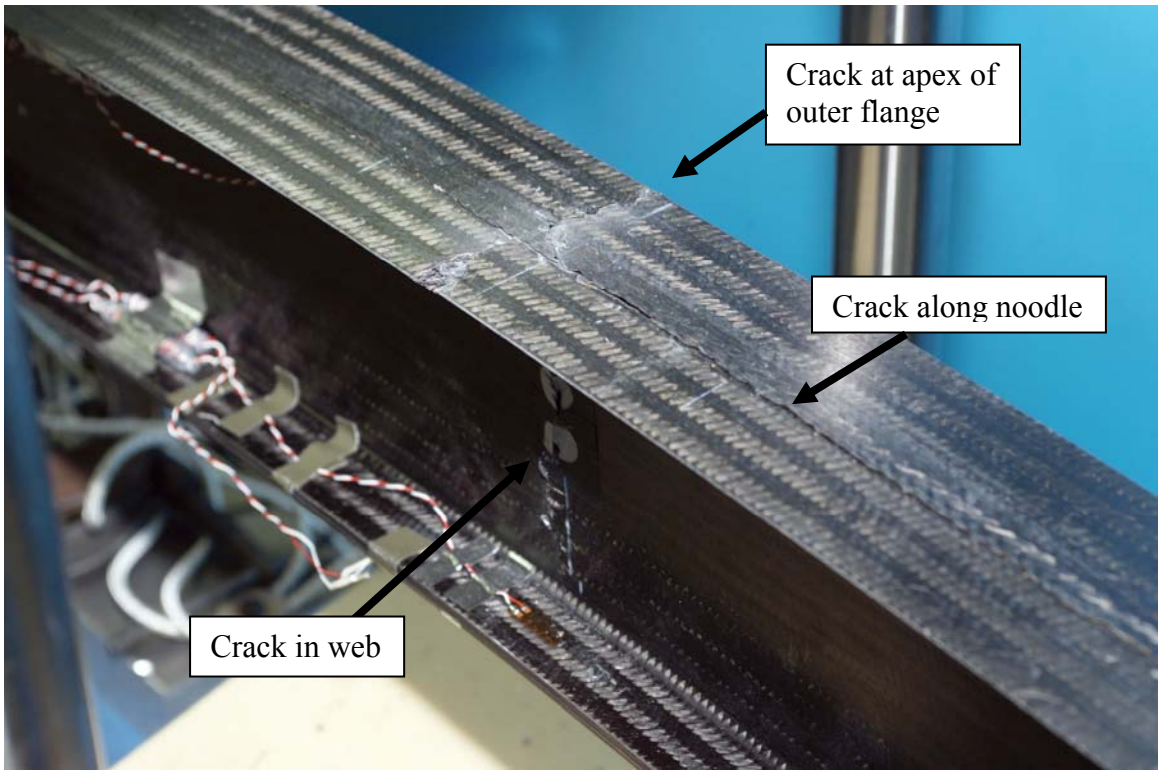

Fig. 3.6: Failed Frame CF6F.

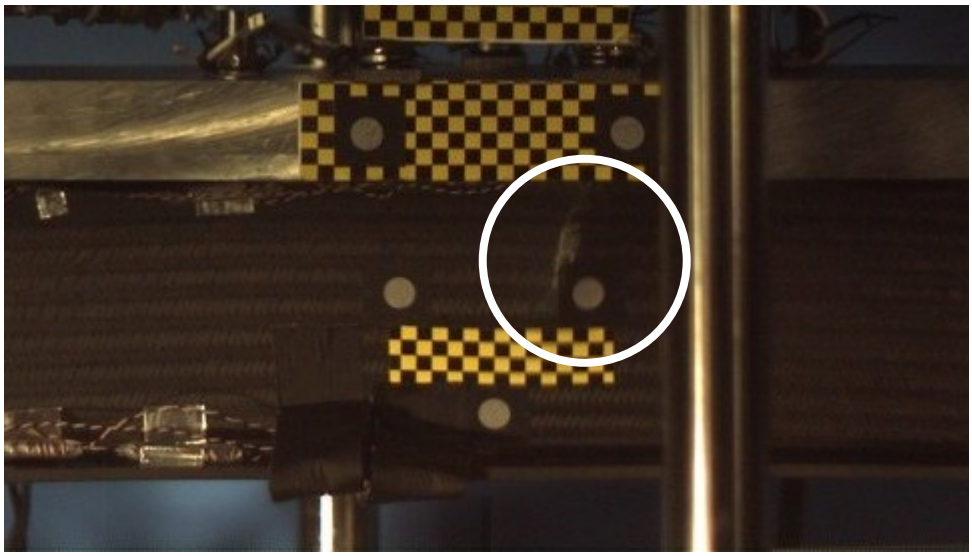

A: Note crack starting to propagate into web from outer flange at ~+1˚. This is the first failure event at 7344 lb load, 0.71 in. displacement, and 0.0077 s after impact.

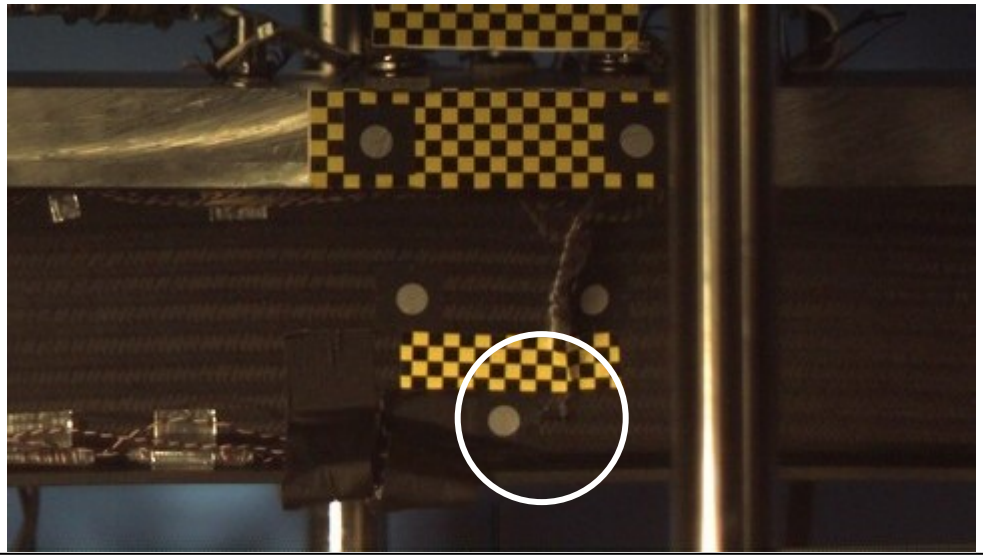

B: Note crack has propagated to junction of web and inner flange. This is the second failure event at 4410 lb., 0.0092 s after impact.

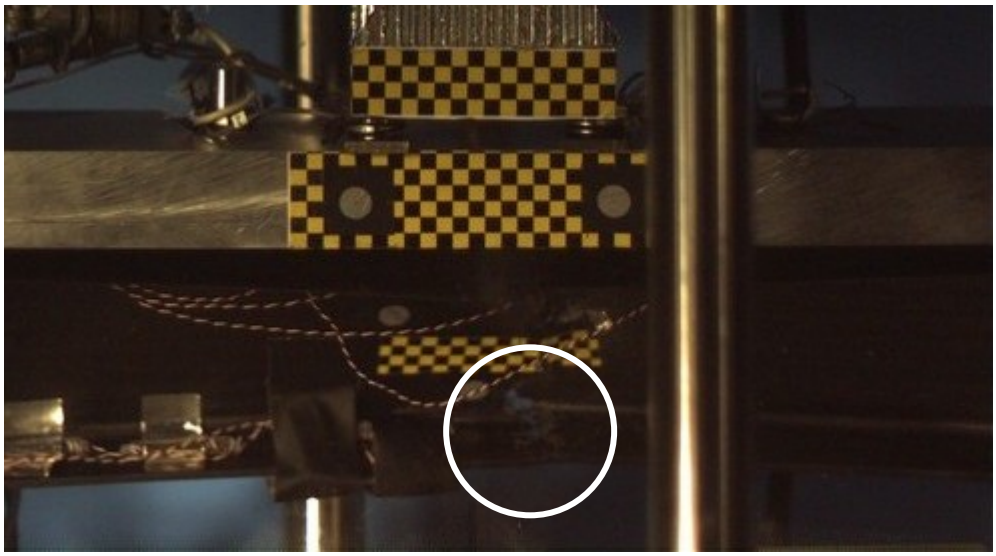

C: Note inner flange has fractured, and the frame has twisted out-of-plane. This is at maximum deflection of 1.61 in., 0.0240 s after impact.

Fig. 3.7 A, B, and C: Frame D crack propagation.

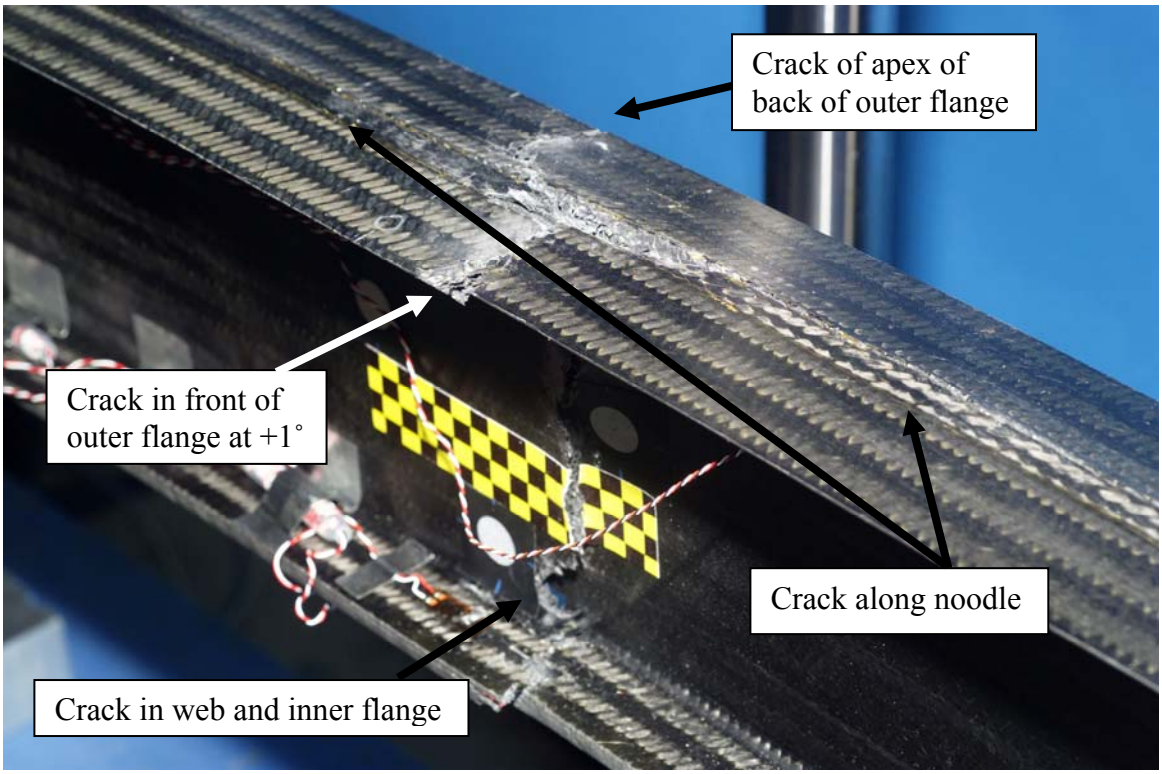

Fig. 3.8: Failed Frame D.

3.4 Lower peak-load tests

In addition to the dynamic tests to complete failure, several tests with lower peak loads were conducted. Frame CF6F was subjected to 1000, 2000, and 7000 lb peak-loads. As mentioned in Section 2.3, the 7000 lb test was expected to fail the frame, but did not cause any apparent damage. Frame D was subjected to a 1000 lb test. The data from these tests were compared to the portion of the static test that corresponds to a similar load, as shown in Figures 3.9 through 3.12.

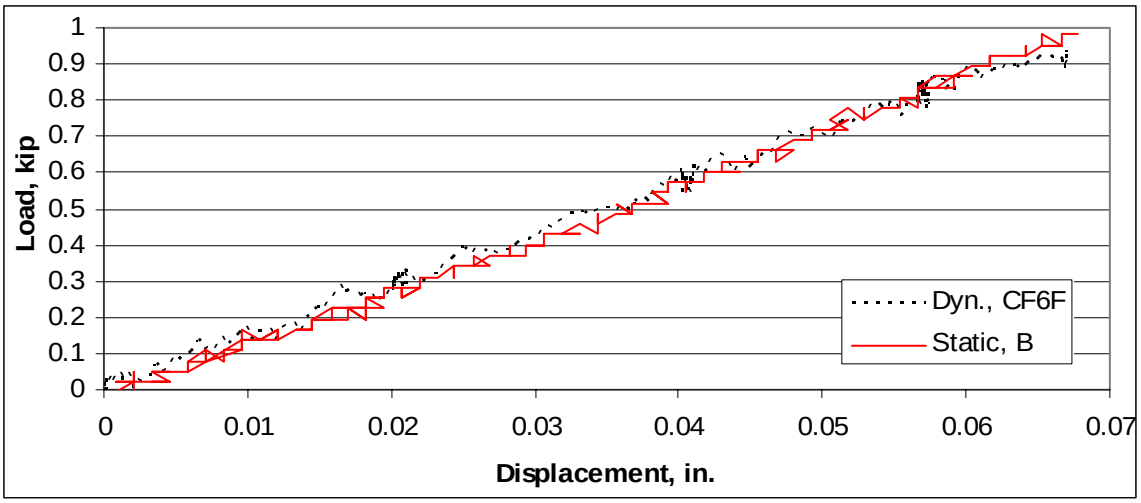

Fig. 3.9: 1000 lb test, comparison of Frames CF6F and B.

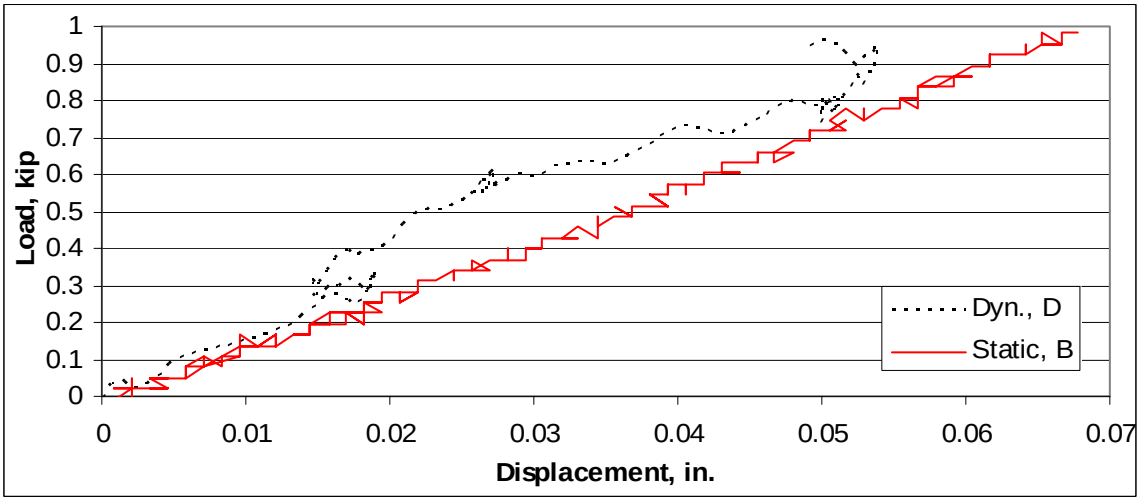

Fig. 3.10: 1000 lb test, comparison of Frames D and B.

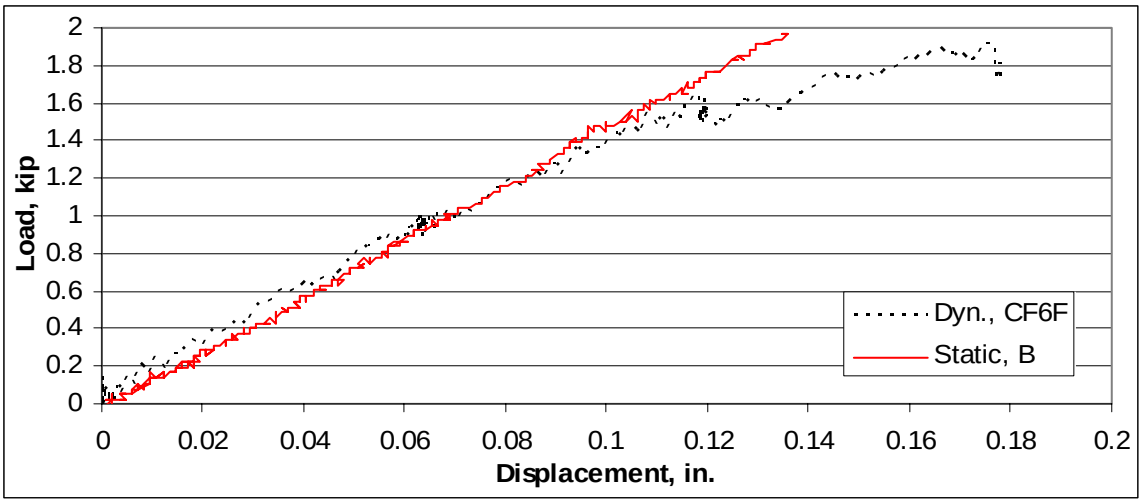

Fig. 3.11: 2000 lb test, comparison of Frames CF6F and B.

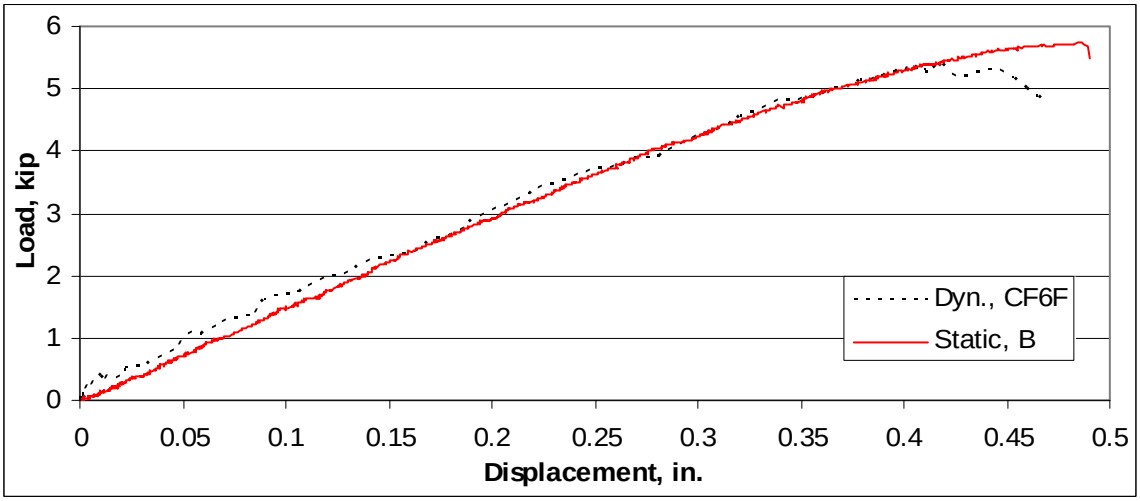

Fig. 3.12: 7000 lb test, comparison of Frames CF6F and B.

Frame CF6F is linear in its response to 1000 lb, mirroring the static tests. The response of Frame D is also linear to 1000 lb, though there is a step-decrease in displacement at a load of 300 lb. Under the 2000 lb test, the response of CF6F is linear until about 1600 lb, then the slope begins to decrease as the displacement increases. For the 7000 lb test, CF6F again exhibits a linear response that mirrors the static test until about 5300 lb load, and again the slope decreases. This decrease in slope is due to the dynamics of the system, not damage to the frame. The decrease in structural stiffness during the static tests was attributed to a softening of the frame material just before failure; note that the failure of Frame B at 5791 lbs is apparent in Fig. 3.12. This

apparent loss of stiffness is also seen the in the 2000 and 7000 peak load dynamic tests, but there was no discernable damage to the frame and the initial response of the frame during the next load test matches the response from the previous tests.

3.5 Strain gage data

As noted in Section 2.2.5, 15 strain gages were placed on Frames CF6F and D in a pattern similar to Frames B and C. The following sections discuss (1) the strain distributions in the outer and inner flanges from all dynamic tests in comparison to the static tests, and (2) the bending of the inner and outer flanges by looking at data from back-to back gages placed on opposite sides of the flanges.

3.5.1 Strain distributions in outer flange

Figures 3.13 through 3.18 show the outer flange strain gage readings along the circumference at various load magnitudes. These uni-directional gages are oriented circumferentially on the flanges, and positive values correspond to tensile strains and negative values correspond to compressive strains. Again, the polar angle θ denotes the circumferential position of the strain gages with the apex of the frame at $\theta = 0^{\circ}$. Larger magnitudes of the circumferential strains occur in the dynamic tests with respect to the static tests, but with the same circumferential distribution as measured in the static tests. The largest tensile strains are near the fixed ends of the frame and the largest compressive strains are near the apex, with the change from tensile to compressive strain near $\theta = -12^{\circ}$ Again, this is similar to the static tests with tension near the frame ends and compression at the apex, and the inflection point from the static tests was at $\theta = -9^{\circ}$.[4] One difference in the dynamic strain distributions with respect to the static strain distributions is a larger circumferential gradient, accompanied by increased magnitudes, in the compressive strain in the vicinity of the apex at the larger load magnitudes.

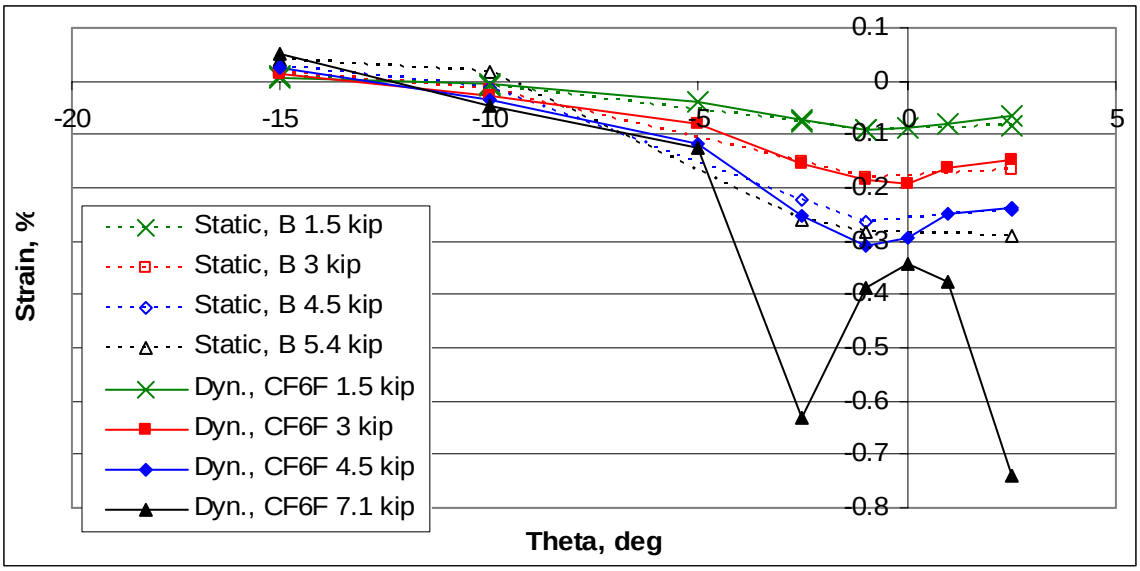

Fig. 3.13: Frame CF6F strain distributions in outer flange during failure test, compared to Frame B.

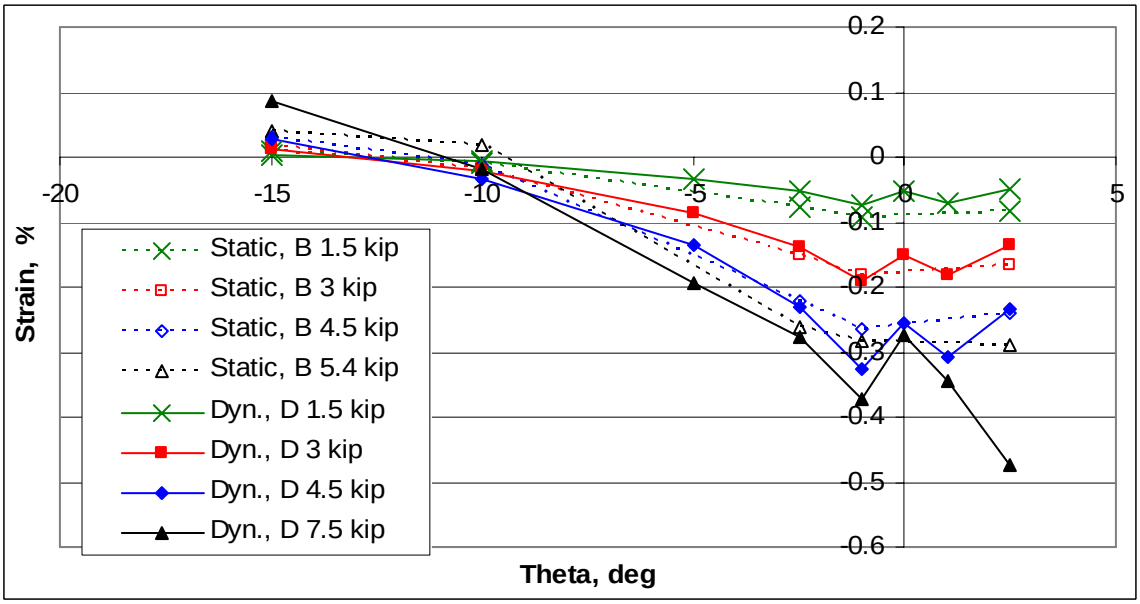

Fig. 3.14: Frame D strain distributions in outer flange during failure test, compared to Frame B.

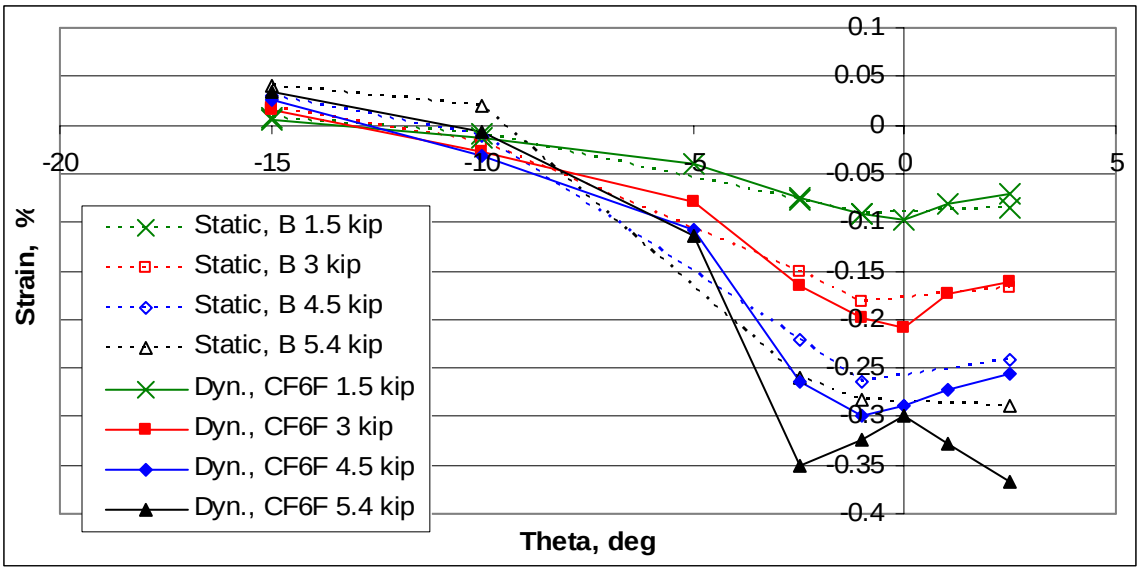

Fig. 3.15: Frame CF6F strain distributions in outer flange during 7000 lb test, compared to Frame B.

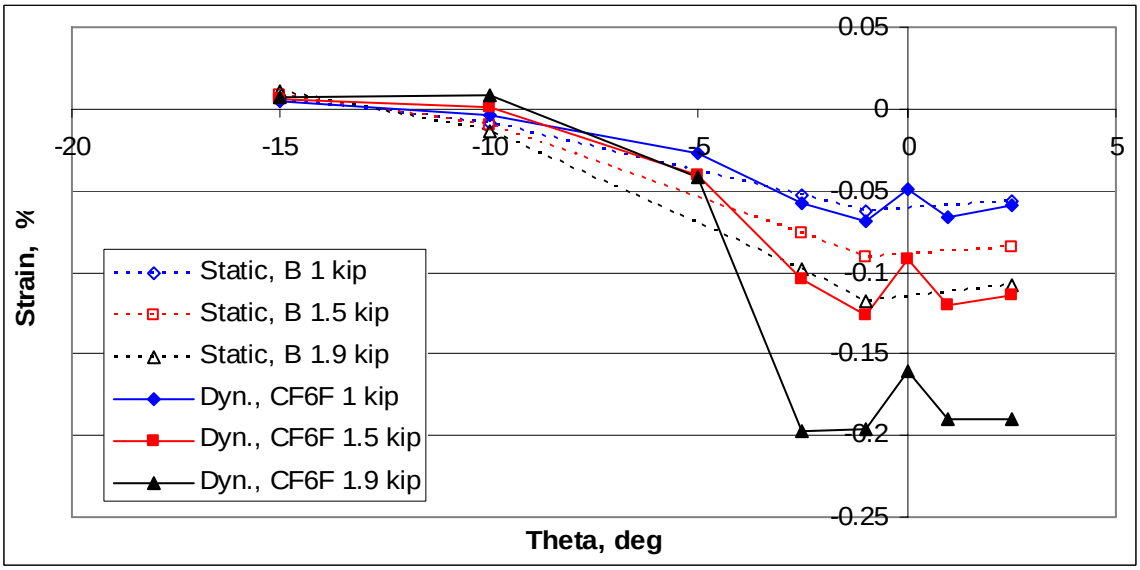

Fig. 3.16: Frame CF6F strain distributions in outer flange during 2000 lb test, compared to Frame B.

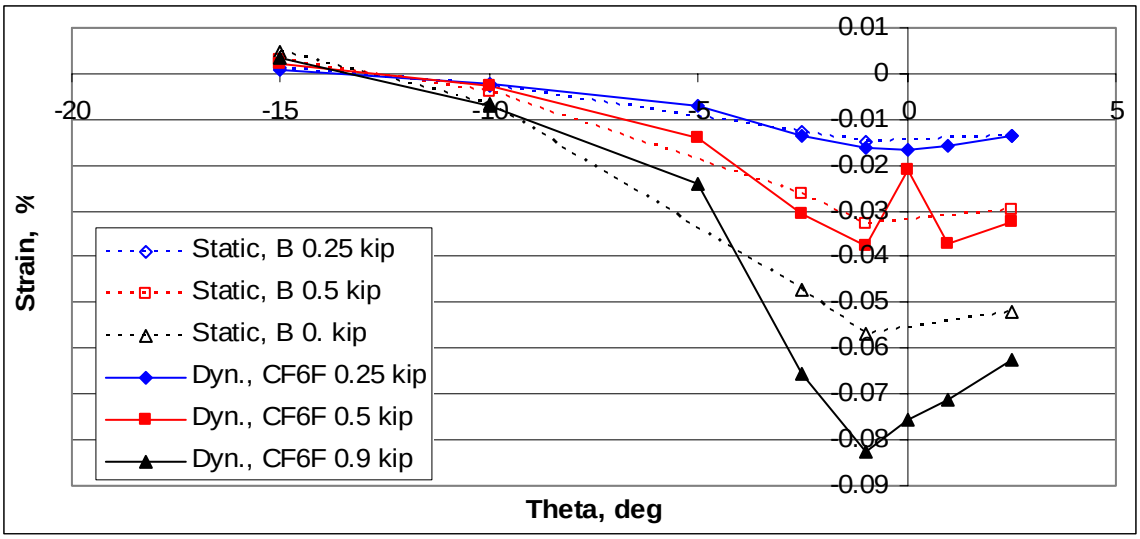

Fig. 3.17: Frame CF6F strain distributions in outer flange during 1000 lb test, compared to Frame B.

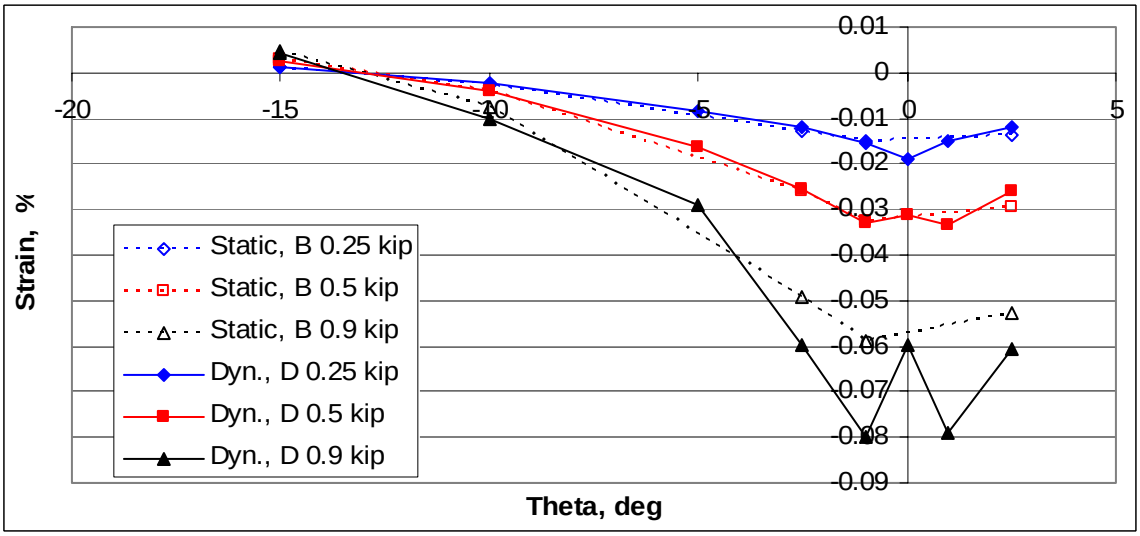

Fig. 3.18: Frame D strain distributions in outer flange during 1000 lb test, compared to Frame B.

3.5.2 Strain distributions in inner flange

Figures 3.19 through 3.24 show the strain levels of the inner flange at various load levels. The strain magnitudes are generally higher for a given load level in the dynamic tests while exhibiting a similar pattern of tensile and compressive strains over the arc of the frame.

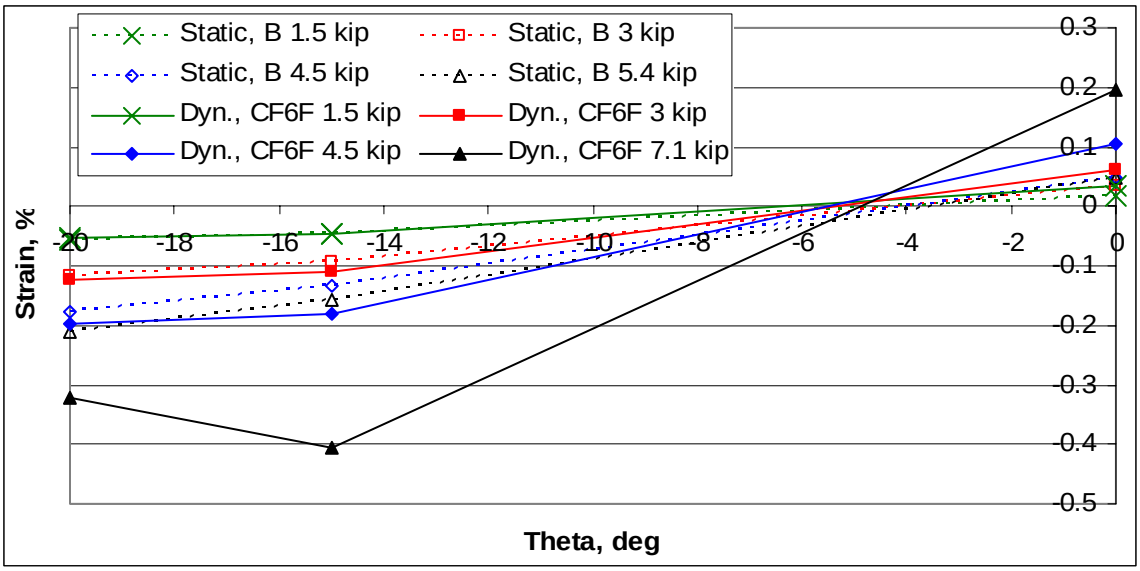

Fig. 3.19: Frame CF6F strain distributions in inner flange during failure test, compared to Frame B.

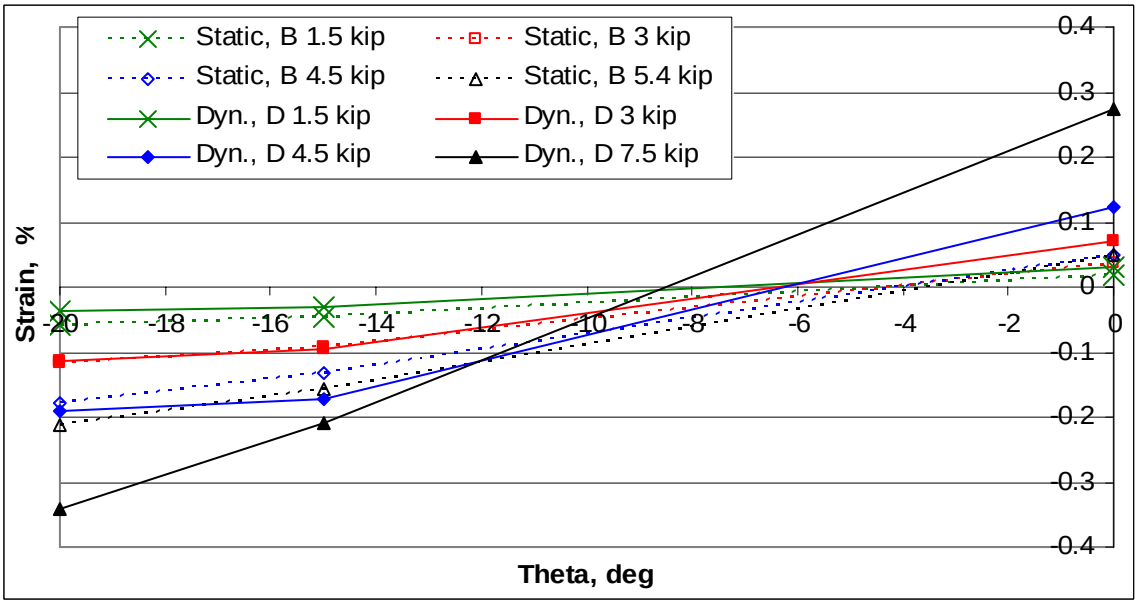

Fig. 3.20: Frame D strain distributions in inner flange during failure test, compared to Frame B.

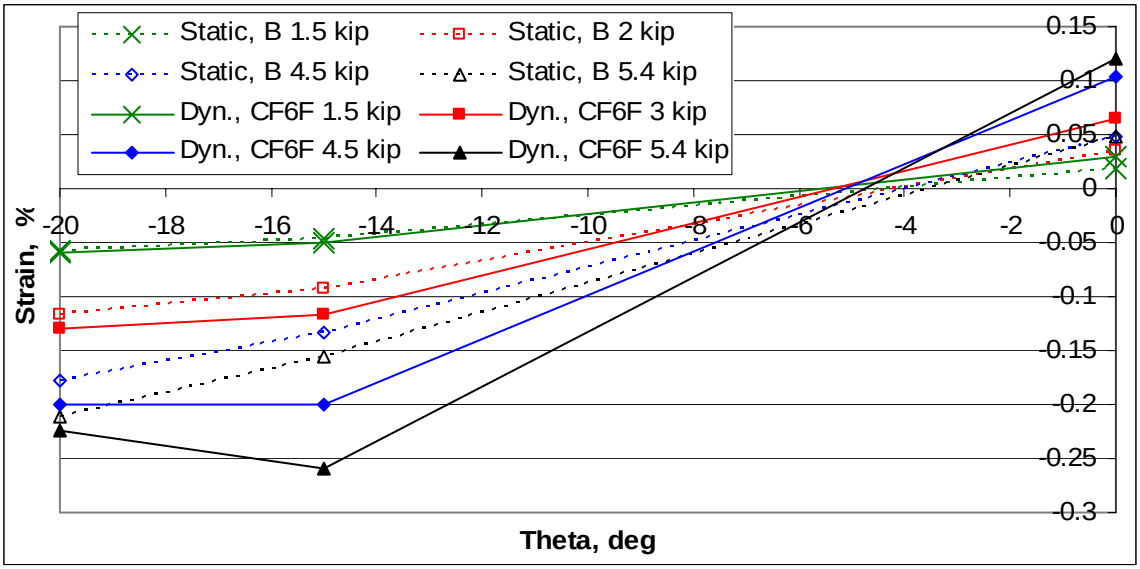

Fig. 3.21: Frame CF6F strain distributions in inner flange during 7000 lb test, compared to Frame B.

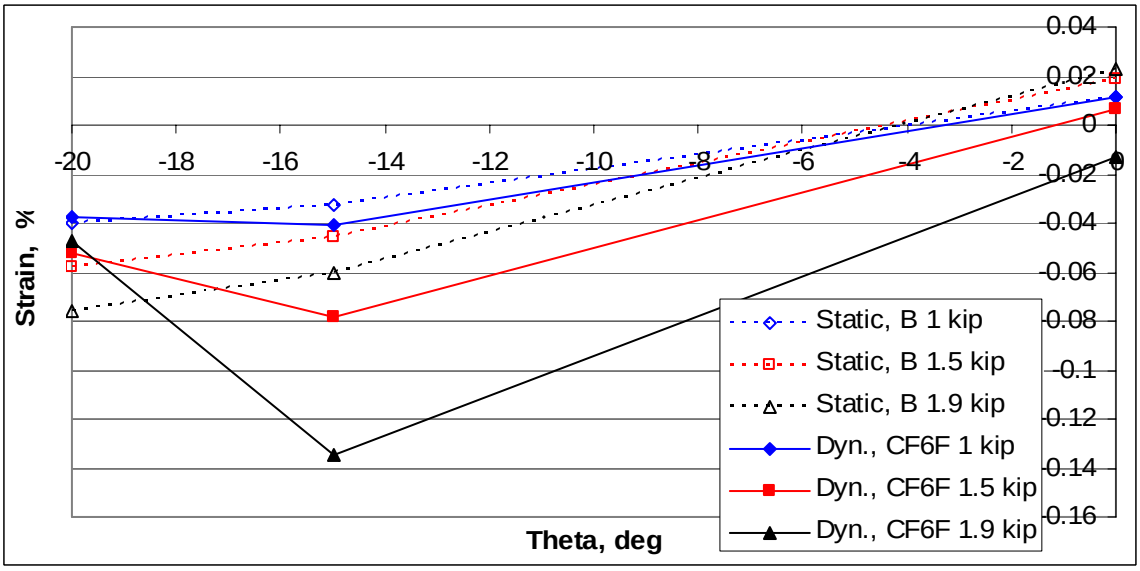

Fig. 3.22: Frame CF6F strain distributions in inner flange during 2000 lb test, compared to Frame B.

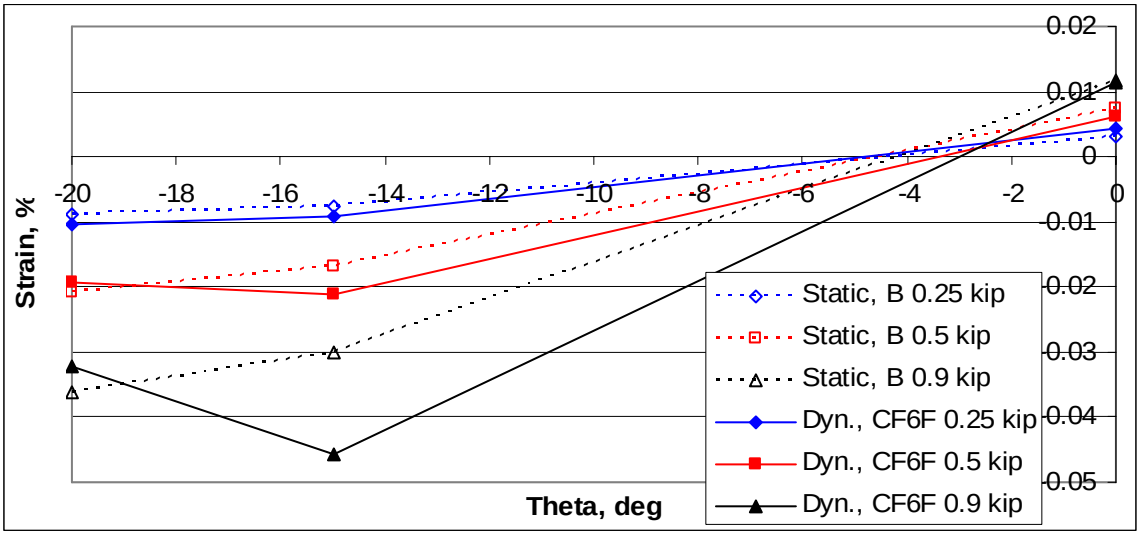

Fig. 3.23: Frame CF6F strain distributions in inner flange during 1000 lb test, compared to Frame B.

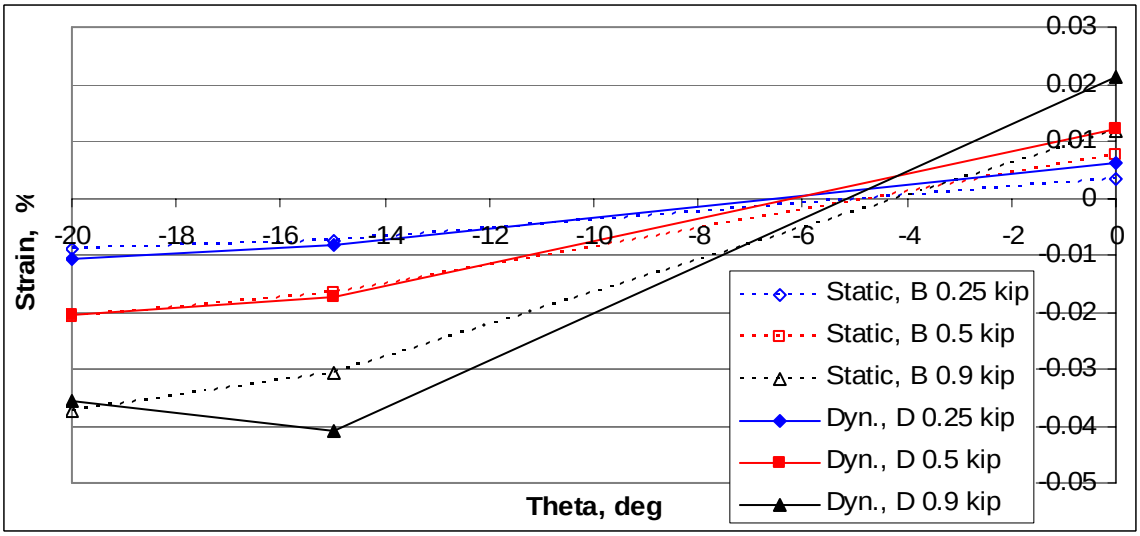

Fig. 3.24: Frame D strain distributions in inner flange during 1000 lb test, compared to Frame B.

3.5.3 Back-to-back strain gage data

There were three pairs of back-to-back circumferential strain gages located on opposite surfaces at the same circumferential location on the frame. Gages 4 and 5 are bonded on the top and bottom surface of the outer flange in the positive-y direction (front

side) at -5˚ on the top and bottom surface, respectively (see Fig, 2.12). Gages 8 and 11 are placed on the bottom surface of the outer flange at 0˚ on either side of the web. Gages 12 and 15 are placed on the inner flange at 0˚, front side, on the top and bottom surface, respectively. Bending and/or extension of the flanges can be inferred by looking at the difference and average, respectively, in the strains measures by these back-to-back pairs of gages.

During both dynamic failure tests, gages 4 and 5 both record compressive strain but gage 5 records a lower magnitude of strain, as seen in Figures 3.25 and 3.26. This suggests that the frame was in compression overall, but there was also a localized circumferential bending of the flanges. Both Frame CF6F and Frame D exhibit the same response with increasing load, but Frame D experiences much larger compressive strain on the upper surface as shown in Fig. 3.26, roughly double that of Frame CF6F.

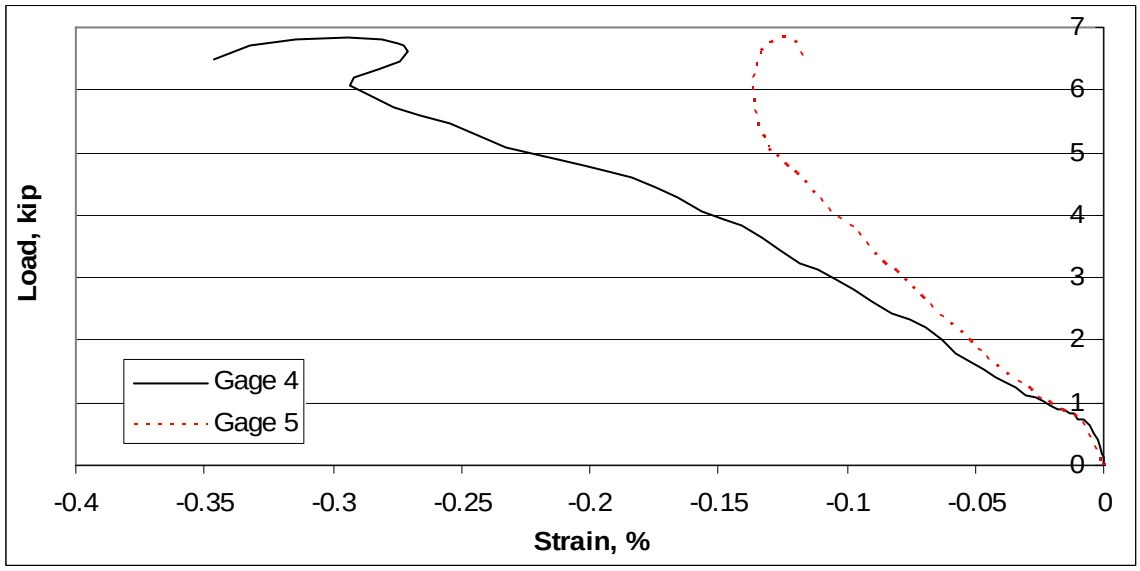

Fig. 3.25: Strains from back to back gages at -5˚ on Frame CF6F, failure test.

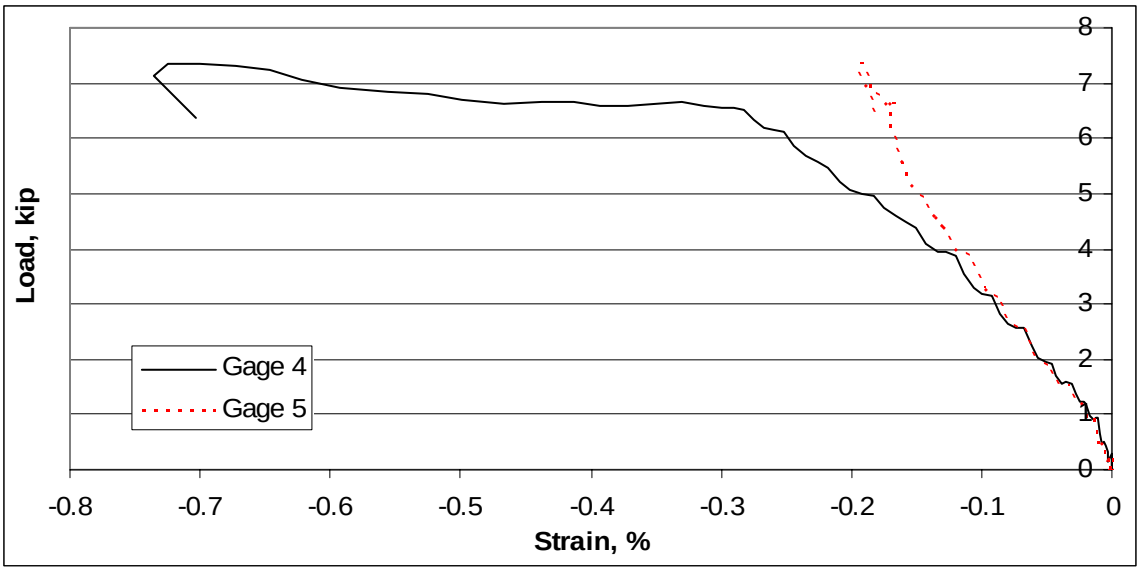

Fig. 3.26: Strains from back to back gages at -5˚, outer flange, Frame D failure test.

Gages 8 and 11, at the apex of the outer flange, register almost the same compressive strain up to 5000 lb load in the failure test of Frame CF6F (Fig. 3.27), then gage 11 returns almost to 0 strain, suggesting that the outer flange was nearly in pure circumferential compression for most of the test, then at about 4900 lbs a significant amount of out-of-plane bending occurs for increased loads. Frame D exhibits a similar pattern, but the bending does not dominate until right at the failure load (Fig. 3.28). This bending becomes more apparent immediately after failure as gage 11 goes into tension of the same magnitude as gage 8. This out-of-plane bending is observed in the video footage of the tests.

Overall, this pattern of a nearly a pure compressive strain response followed by bending of the outer flange as the load increases is similar to the strain patterns observed in the static tests, though the back to back gages were at -2.5˚ and -1˚ in the latter tests. Also, the magnitude of the circumferential strains in the dynamic tests at failure initiation, roughly -0.3% strain, are on a par with the strain levels in the static tests. In both test cases, the failure strains are well below the predicted failure strain of -1%, suggesting that the TEXCAD model did not account for all failure modes within the material.

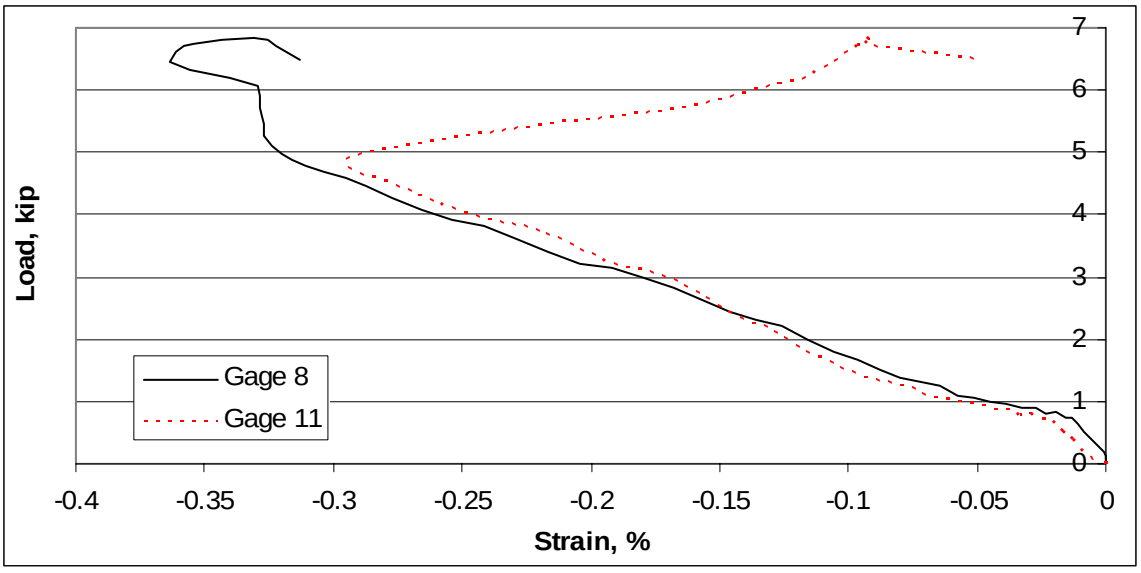

Fig. 3.27: Strains from back to back gages at 0˚, outer flange, Frame CF6F failure test.

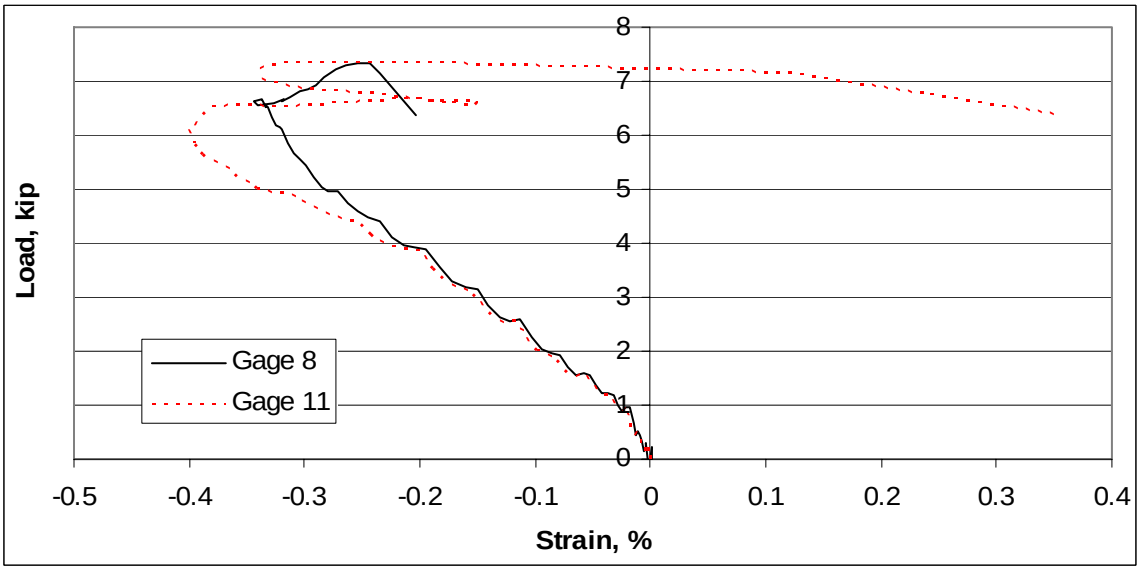

Fig. 3.28: Strains from back to back gages at 0˚, outer flange, Frame D failure test.

The back-to-back gages at the apex of the frame on the inner flange, gages 12 and 15, shown in Figs 3.29 and 3.30, record tensile circumferential strains to the failure load, though the difference in the magnitude of these back-to-back gages again suggests that the inner flange is also in localized bending. The strain magnitudes, about 0.2% strain, are roughly 0.05% strain larger than the magnitudes seen in the static tests.

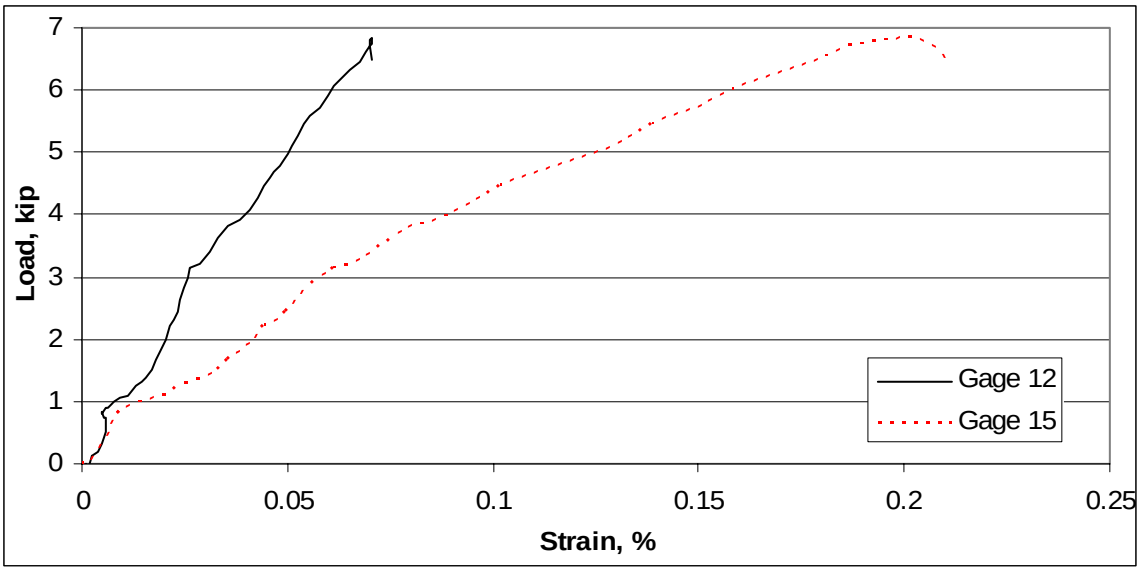

Fig. 3.29: Strains from back to back gages at 0˚, inner flange, Frame CF6F failure test.

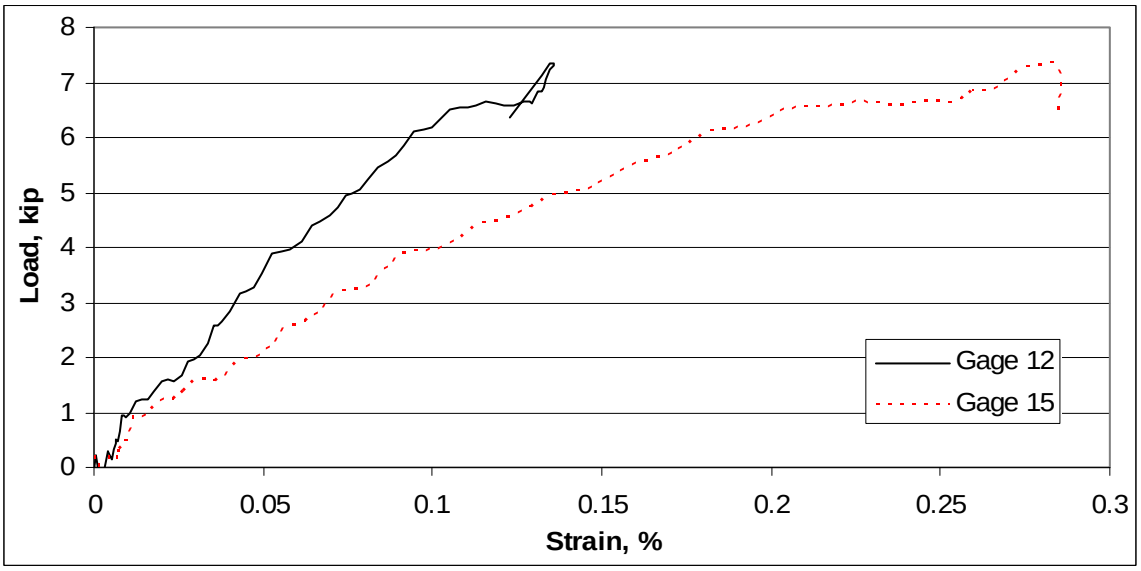

Fig. 3.30: Strains from back to back gages at 0˚, inner flange, Frame D failure test.

The examination of the strain gage data suggests that the frames behave in a very similar fashion under both static and dynamic failure. The overall magnitude of the strains are larger in the dynamic tests, but the pattern of strain distribution and the flange bending suggested by the back-to-back gages is similar to the static strain patterns. This conclusion parallels the load and displacement discussion earlier in this chapter.

Chapter 4 Finite Element Analysis of Dynamic Frame Tests

A finite element analysis (FEA) of the dynamic frame tests was conducted utilizing LSDyna, a commercially available dynamic FEA code from Livermore Software Technology Corp. in Livermore, CA. LSDyna is an explicit FEA that uses a modified central difference scheme to solve the nonlinear ordinary differential equations of motion.[12] Input files are simple text files; an example input file is presented in Appendix C. This chapter discusses two preliminary LSDyna analyses: one analysis compares the a discrete element representation of the frame to the modal analysis conducted in Section 2.2.4, and the second analysis compares one of the composite material models available in LSDyna to a previous composite-coupon study. The last section describes the LSDyna simulation of the transient response of the textile composite frame tests.

4.1 Preliminary analyses

Two simple problems were used to gain confidence in the use of LSDyna. The first problem was a lumped-mass-spring model of the frame tests, and the results were compared to the model that was used for the modal analysis in Section 2.2.4. To verify the material models, the second problem was a model of composite coupon tests conducted by van Wamelen.[13]

4.1.1 Two-mass, two-spring model

The two-spring, two-mass model as described in Section 2.2.4 and the FEA model are shown in Fig. 4.1. The spring stiffness of the frame, K_f, was taken from the initial stiffness of the static tests. The effective spring stiffness of the honeycomb wedge, K_W,

was found using equation 2.2, $K_W = X_C\ s\ b\ /h$. The drop mass used in the tests and the mass of the load induction fixture platens were both measured quantities. Table 4.1 lists the values for each parameter of the model.

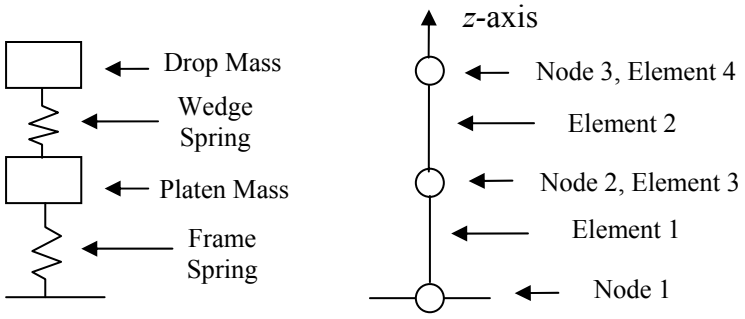

Fig. 4.1: Two-spring, two-mass modal analysis and FEA models.

Table 4.1: Parameters used in the two-spring, two-mass FEA model.

Parameter	English units	SI units
Drop mass	91.600 lbs	41.550 kg
Platen mass	17.867 lb	8.105 kg
Frame stiffness, K_F	15 kip/in.	2.6267 MN/m
Wedge stiffness, K_W	5.0215 kip/in	879.4 KN/m

The FEA model of this system consisted of three nodes, Node 1 at the ground station, Node 2 at the platen station, and Node 3 at the drop mass station, or $z = 0$ m, $z = 2$ m, and $z = 3$ m, respectively. Two discrete-beam elements modeled the springs. Element 1, with $K = K_F$, was placed between Nodes 1 and 2, and Element 2, with $K = K_W$, between Nodes 2 and 3. Two lumped-mass elements modeled the platen mass and the drop mass, Element 3 at Node 2 and Element 4 at Node 3, respectively. Node 1 was restricted to no translation and no rotation, while Nodes 2 and 3 were only allowed to translate in the *z*-direction. Node 3 was given an initial velocity of -23 ft/s, or -7.0104 m/s, in the z-direction. The displacement of Node 2, compared to the motion of the platen during the modal analysis, is shown in Fig. 4.2. There are no discernable differences between the two curves.

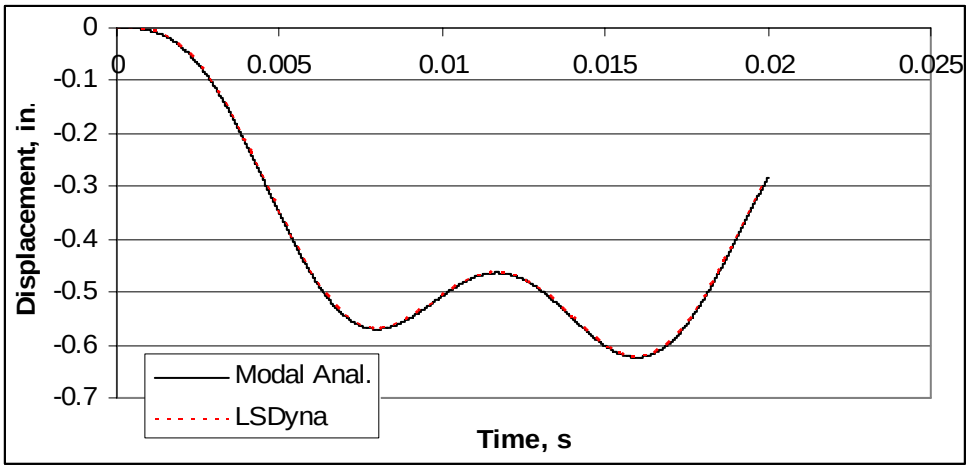

Fig. 4.2: Comparison of modal analysis and FEA two-spring, two-mass model.

4.1.2 Composite coupon model

Van Wamelen conducted coupon tests of a $[0/90/45/0/90/-45/90/0]_s$ carbon fiber laminate. Two test cases were run, a tensile load to failure in the 0˚ direction, and a tensile load to failure 10˚ off-axis.[13] Figures 4.3 and 4.4 show typical results from these coupon tests, including the original failure predictions from van Wamelen.

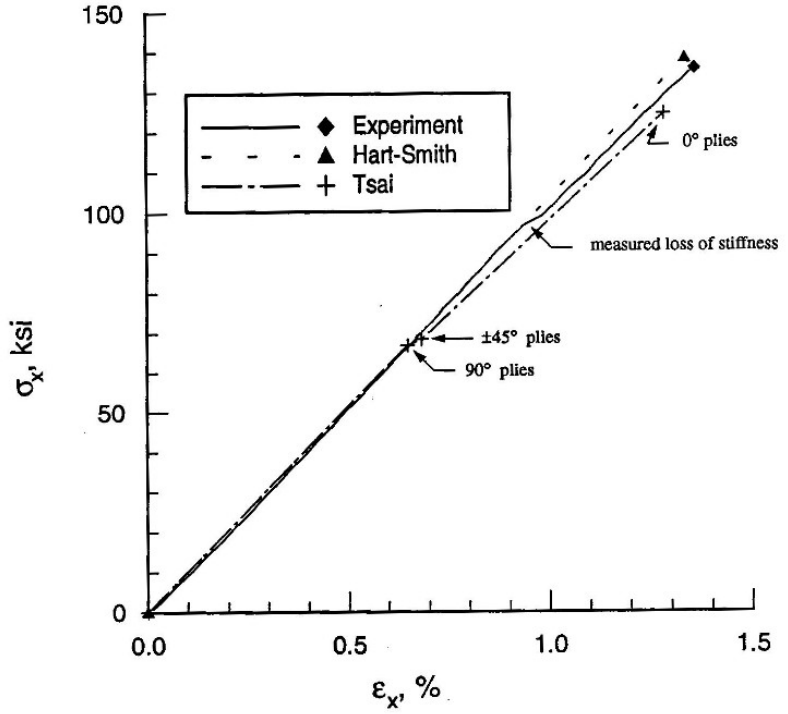

Fig. 4.3: Typical results from 0˚ on-axis coupon tests.[13]

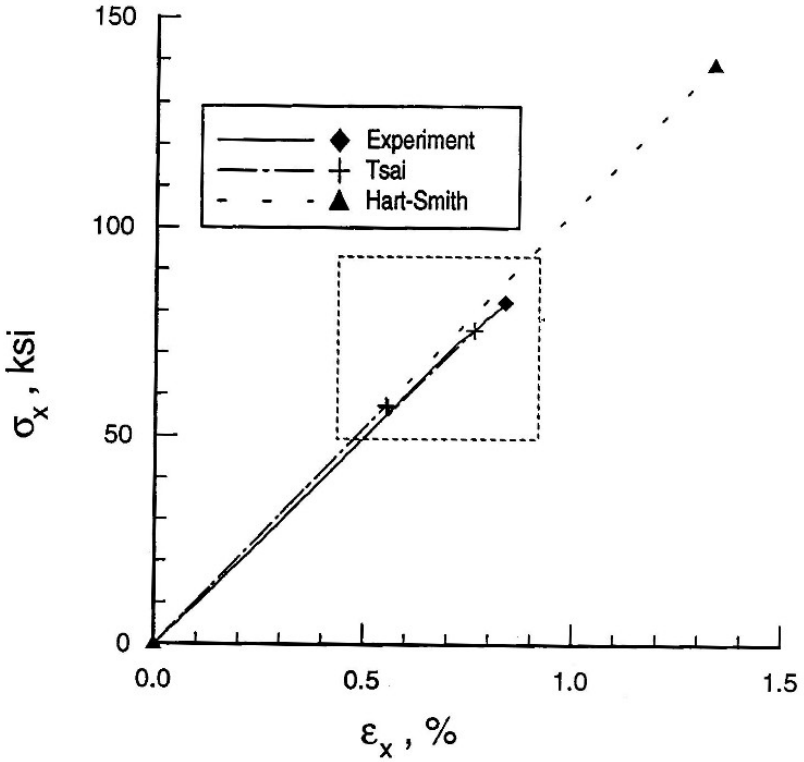

Fig. 4.4: Typical results from 10˚ off-axis coupon tests.[13]

For the FEA, a coupon size of 0.1 m wide and 0.3 m tall was used, and each layer was assumed to have a 0.15 mm thickness for a total coupon thickness of 0.0024 m. The lower edge of the coupon was clamped, while the top edge was given a prescribed displacement that resulted in a steady rate of 1.5% strain in 1 second. Four-node, shell elements were used for the FEA model. The element formulation was the default LSDyna option, based on the Hughs/Lin four-node shell with uniformly reduced integration.[14] Initially, each shell was set with 16 integration points through the thickness so that each layer of the laminate was included in the model; each integration point had an angle associated with it that set the fiber angle of the material at the point.[15] The LSDyna material model was MAT_022, an orthotropic, elastic, composite-damage model with failure criteria based on suggestions from Chang/Chang:[16]

fiber breakage:

$$F_{fiber} = \left(\frac{\sigma_1}{X^T}\right)^2 + \bar{\tau} > 1 \qquad (4.1)$$

compressive failure:

$$F_{comp} = \left(\frac{\sigma_2}{2S^C}\right)^2 + \left[\left(\frac{Y^C}{2S^C}\right)^2 - 1\right]\frac{\sigma_2}{Y^C} + \bar{\tau} > 1 \qquad (4.2)$$

matrix cracking:

$$F_{matrix} = \left(\frac{\sigma_2}{Y^T}\right)^2 + \bar{\tau} > 1 \qquad (4.3)$$

where σ_1 is the stress in the fiber direction, σ_2 is the transverse stress, τ_{12} is the shear stress in the 1-2 plane, X^T is tensile strength of the material in the fiber direction, Y^T is the transverse tensile strength, Y^C is the transverse compressive strength, G_{12} is the shear modulus in the 1-2 plane, and:

$$\bar{\tau} = \frac{\frac{\tau_{12}^2}{2G_{12}} + \frac{3}{4}\alpha\tau_{12}^4}{\frac{S^{C^2}}{2G_{12}} + \frac{3}{4}\alpha S^{C^4}} \qquad (4.4)$$

where α is the nonlinear shear stress term.

If the failure criteria for an integration point in an element was satisfied, then the model set $E_1 = E_2 = G_{12} = 0$.[16] This reduction in stiffness resulted in a drop in the load

carried by the coupon. The material constants used in the model were the same as those used by van Wamelen and are listed in Table 4.2.[13]

Table 4.2: Material constants for coupon FEA model.[13]

Constant	English Units	SI Units
E_{11}	22.04 msi	151.8 GPa
E_{22}	1.322 msi	9.115 GPa
E_{33}	1.322 msi	9.115 GPa
υ_{12}	0.286	0.286
$\upsilon_{13} = \upsilon_{12}$	0.286	0.286
υ_{23}, *typical*[17]	0.458	0.458
G_{12}	1.04 msi	7.17 GPa
$G_{13} = G_{12}$	1.04 msi	7.17 GPa
G_{23}, *typical*[17]	0.693 msi	3.20 GPa
X^C $(=X^T)$	295.01 ksi	2.034 GPa
X^T	295.01 ksi	2.034 GPa
Y^C	35.67 ksi	245.9 MPa
Y^T	7.5 ksi	51.71 MPa
S^C	11.3 ksi	77.91 MPa
α *(suggested)*[16]	0.25	0.25

The FEA model for the on-axis load case was initially built using one element for the coupon. This single element did exhibit damage just before failure stress, as shown in Fig. 4.5, but the load drop at damage was large when compared to the experimental data in Fig. 4.3. For subsequent on-axis tests, and for the 10˚ off-axis tests, a second model was built with four elements by splitting the coupon into two sections vertically and horizontally; the material was still modeled as one shell, i.e., only one element thick. As shown in Table 4.3, this model exhibited damage at a lower stress than the experiments, but the magnitude of the load drop was in better agreement than the one-element model. Failure of the four-element FEA model occurred at a lower stress than the experimental data for the on-axis test, but was accurate for the off-axis test as shown in Table 4.3.

A third model was built by splitting each of the four elements into 16 layers, each 0.15 mm thick and with a defined angle that set the fiber direction of the layer such as a laminate in the coupon lay-up, i.e. layer one is set at 0˚, layer 2 is set at 90˚, etc. With the layers stacked this way, LSDyna enables the user to define the stack as a laminated composite in an attempt to correct for the effects of a non-constant shear strain through the thickness of the element, where each layer is under a different shear strain, ε_{12}, because each layer is at a different angle to the applied load.[18] In the on-axis tests, as can be seen in Fig. 4.5, the 64-element model without not defined as a laminate was almost as accurate at the 4-element model, while the accuracy of the model defined as a laminate was not close. In the off-axis tests, the 64-element model, with or without lamination, did not match the 4-element model as shown in Fig. 4.6.

Table 4.3 compares the stresses and strains of initial damage and failure across all tests. The results of this problem, while not a perfect match with the experimental data, were encouraging, and the FEA continued to the next step: modeling the full frame.

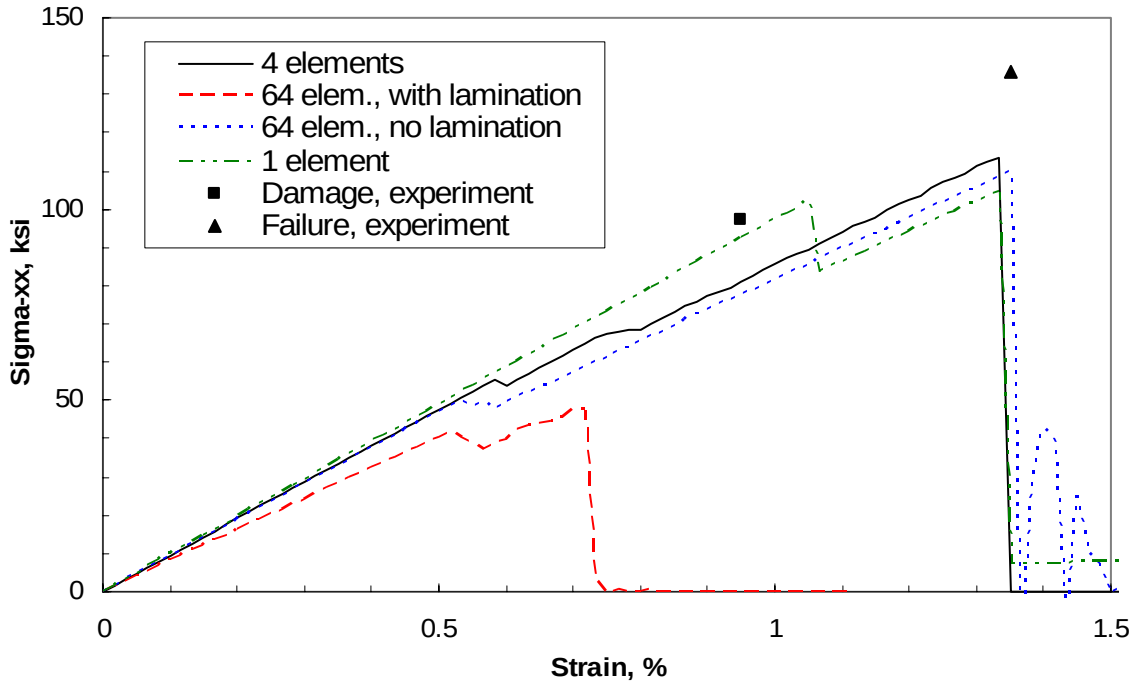

Fig. 4.5: On-axis FEA of coupon tests; comparison of finite element formulations.

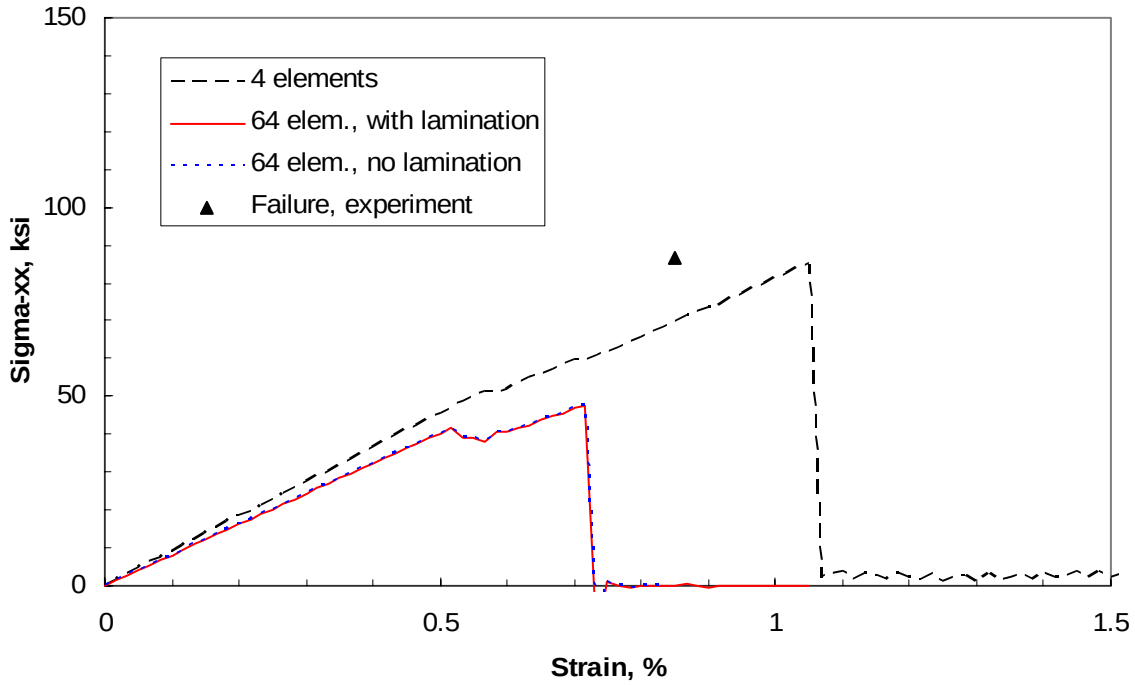

Fig. 4.6: Off-axis FEA of coupon tests; comparison of finite element formulations.

Table 4.3: Comparison of damage and failure stress and strain of coupon tests and FEA.

Test	σ_{damage}, ksi	ε_{damage}, %	$\sigma_{failure}$, ksi	$\varepsilon_{failure}$, %
0˚, experiment	97.0	0.95	135.93	1.35
0˚, FEA, 1-element	102.0	1.05	104.0	1.33
0˚, FEA, 4-element	55.6	0.58	113.0	1.33
0˚, FEA, 64-element	50.2	0.53	110.0	1.35
0˚, FEA, 64-element with lamination	41.6	0.52	47.5	0.72
10˚, experiment	n/a	n/a	86.05	0.85
10˚, FEA, 4-element	51.5	0.57	85.1	1.05
10˚, FEA, 64-element	41.6	0.52	47.5	0.72
10˚, FEA, 64-element with lamination	41.6	0.52	47.5	0.72

4.2 Full textile composite frame FEA

The nodes and elements for the full frame model were defined using a Matlab script, presented in Appendix D. This script outputs the coordinates of the nodes for the complex geometry of the frame, and then defined the elements based on this node list. The two lists were then copied into the input text file for LSDyna. Based on the previous material-model study in Section 4.2.1, the frame was modeled with a single layer of shell elements that varied in thickness as the thickness of the cross section varied (see Table 2.1). The same four-node shell element as the coupon test was employed in the full frame model, and the material model was the same MAT_022. The material constants used in the model were taken from the TEXCAD model as presented by Perez and are listed in Table 4.4.[4]

Table 4.4: Material constants for frame FEA model, taken from TEXCAD.[4]

Constant	English Units	SI Units
E_{11}	7.06 msi	48.6 GPa
E_{22}	6.59 msi	45.4 GPa
E_{33}	1.53 msi	10.5 GPa
υ_{12}	0.231	0.231
υ_{13}	0.216	0.216
υ_{23}	0.298	0.298
G_{12}	1.91 msi	13.1 GPa
G_{13}	0.601 msi	4.14 GPa
G_{23}	0.645 msi	4.44 GPa
X^C *(used in later models)*	71.0 ksi	489 MPa
X^T	91.37 ksi	630.0 MPa
Y^C	56.89 ksi	392.2 MPa
Y^T	73.14 ksi	504.3 MPa
S^C	30.46 ksi	210.0 MPa
α *(suggested)*	0.25	0.25

A rigid-body load platen was placed on top of the frame at the apex, just as in the dynamic tests. The displacement of the platen was found by integration of the accelerometer data, as describe in Section 3.1. This displacement as a function of time was prescribed as the z-direction displacement of the rigid platen in LSDyna; the platen was restricted in all other translations and rotations. In the contact modeling feature of LSDyna, the platen is specified as the 'master', forcing the 'slave' frame nodes to move when the platen came into contact with them. A coefficient of friction between the platen and the frame of $\mu = 0.3$ was set to keep the frame from sliding out of its plane. The reaction load exerted on the platen by the frame was tracked during the FEA run and compared to the experimental load.

The initial model was based on elements roughly 1 in. on each side. As seen in the response curve of Fig. 4.7, this model was not accurate when compared to the experimental data. A second model with elements roughly 0.5 in. on each side more accurately captured the loading of the frame, including a reloading after initial failure, but the load at initial failure was 25% higher than experimental data as shown in Fig. 4.7. A third model with 0.25-in. elements was built in hopes that mesh refinement would lead to a more accurate model, but this model exhibited almost exactly the same loading as the 0.5-in. model, also shown in Fig. 4.7. Since the 0.5-in. element model required far less computer time than the 0.25-in. element model, the simpler model was used for subsequent analyses. The 0.5-in. model had 3441 elements, with 3641 nodes and 21,548 active degrees of freedom. A screen-shot of this model is shown in Fig. 4.8. Further attempts to more accurately model the dynamic frame tests were accomplished by refining the material model.

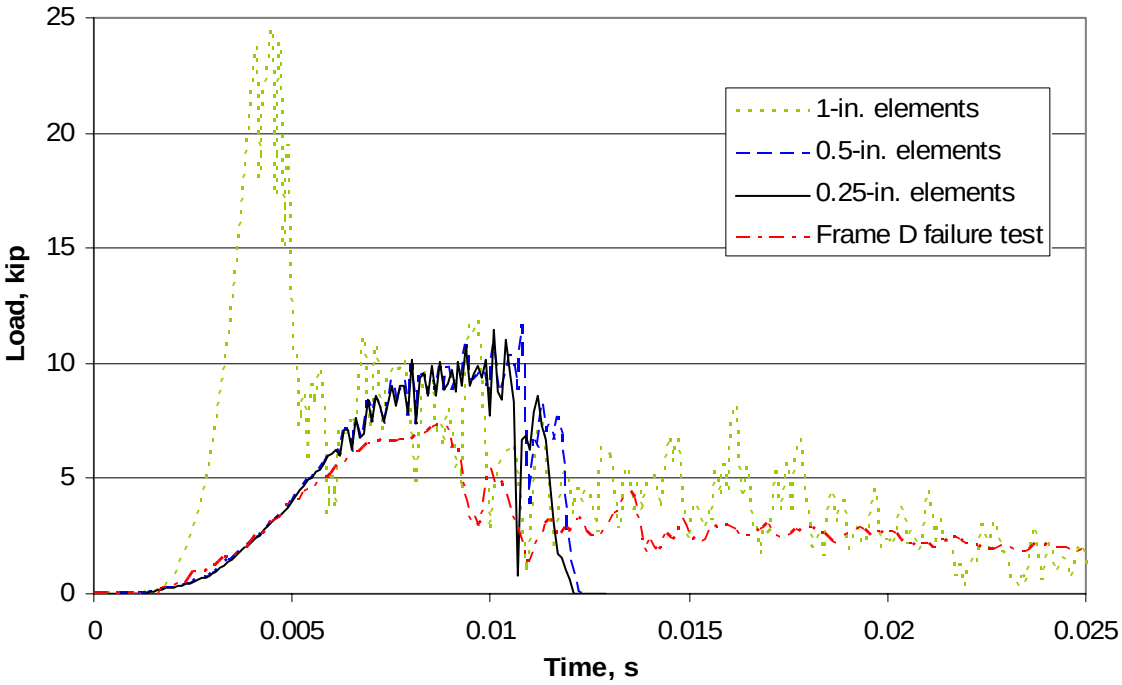

Fig. 4.7: Comparison of element size for the full frame FEA.

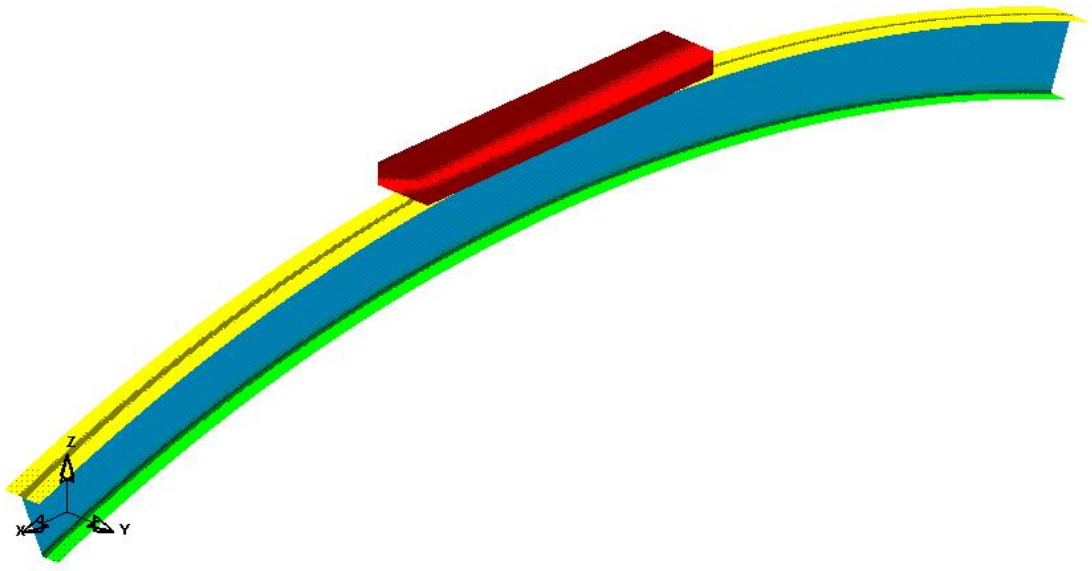

Fig. 4.8: Screen shot of 0.5-in. element FEA model.

4.2.1 Material model refinement for full frame FEA

4.2.1.1 Reduced strength models

The previous material model, MAT_022, does not distinguish between compressive and tensile failure strength in the fiber direction. This assumption is valid for some composites, such as the coupon material tested in the Section 4.1, but the textile composite material has $X^T \neq X^C$, as seen in Table 4.4. Since the failure mode of the experimental tests was dominated by fractures occurring in the circumferential compression region at the apex of the frame, one attempt to increase the accuracy of the model was to decrease X^T in the MAT_022 input data. Figure 4.9 shows the results of several of these reduced-strength runs, and Table 4.5 lists initial failure loads and displacements for each run.

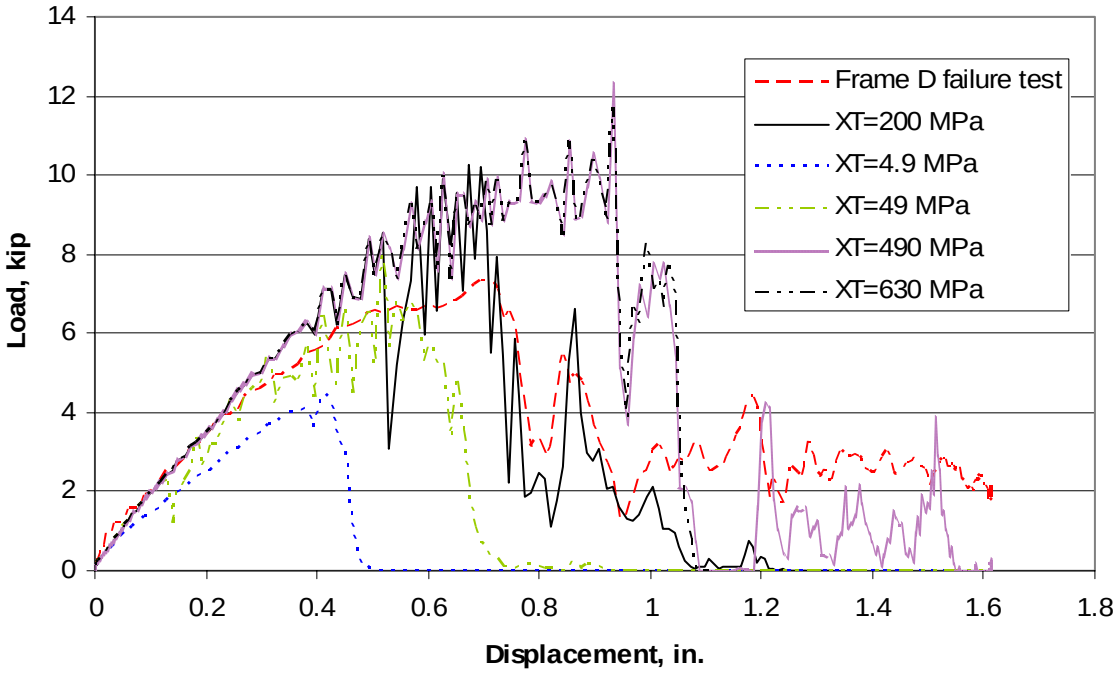

Fig. 4.9: Comparison of Load-Displacement curves for the reduced-strength MAT_022 models and experimental data.

Table 4.5: Comparison of load and displacement of at failure, and energy absorbed during run, of the reduce-strength MAT_022 models and experimental data.

Test	$F_{failure}$, kip	Error,%	$D_{failure}$, in.	Error,%	Energy,kip-in	Error,%
Experiment	7.5	0	0.75	0	6.15	0
X^T = 630 MPa	12.3	+64.0	0.93	+24.0	7.33	+19.0
X^T = 490 MPa	12.3	+64.0	0.93	+24.0	7.33	+19.0
X^T = 200 MPa	10.4	+38.7	0.70	-6.7	4.73	-23.2
X^T = 49.0 MPa	8.0	+6.6	0.52	-30.7	2.80	-54.5
X^T = 4.90 MPa	4.5	-40.0	0.42	-44.0	1.19	-80.7

Setting $X^T = X^C$ = 485.89 MPa had the same result as the initial run, predicting a failure load 64% and displacement 24% higher than the experimental data. Reducing X^T further to 200 MPa led to a failure predicted very close to the actual displacement, but with a failure load 38.7% high. Reducing X^T further did not get any closer to the experimental data in displacement.

Instead of comparing loads or displacement at failure, another method of assessing the accuracy of the FEA results is to compare the total energy absorbed during the impact. The integration for all tests was computed from 0.0 to 1.62 in. displacement, the maximum displacement measured in the Frame D failure test tests. Values of the energy absorbed for each case are listed in Table 4.5. If this metric is employed, the best model was either the original model with X^T = 630 MPa, or the second model with $X^T = X^C$ = 490 MPa, both with an error of +19%.

An important feature of the predicted load curves using MAT_022 was the fact that a reloading is seen after the initial failure. In particular, the FEA run with X^T = 200 MPa matched the displacement and load level of the second drop in load well, but only the runs with a high X^T continued to carry load beyond this second drop in load. Another feature was the apparent softening of the material, seen as a decreasing slope of the Load-Displacement curve, as the first failure is approached. Both of these features were also observed in the experimental data.

4.2.1.2 Additional material models

LSDyna has several other material models that could apply to composite failure events. Two of these models are based on MAT_022: MAT_054 and MAT_055. These models use similar failure criteria as MAT_022, but incorporate an X^C that is not assumed to be X^T. For both MAT_054 and MAT_055, the failure criteria are:[19]

fiber tensile failure:

$$e_f^2 = \left(\frac{\sigma_1}{X^T}\right)^2 + \beta\left(\frac{\tau_{12}}{S^C}\right) - 1 \geq 0 \qquad (4.5)$$

where $\beta = 0$ gives the maximum stress criteria, which is assumed to be closer to experimental data; fiber compressive failure:

$$e_c^2 = \left(\frac{\sigma_1}{X^C}\right)^2 - 1 \geq 0 \qquad (4.6)$$

matrix tensile mode:

$$e_m^2 = \left(\frac{\sigma_2}{Y^T}\right)^2 + \left(\frac{\tau_{12}}{S^C}\right)^2 - 1 \geq 0 \qquad (4.7)$$

with the difference being:

matrix compressive failure for MAT_054:

$$e_d^2 = \left(\frac{\sigma_2}{2S^C}\right)^2 + \left[\left(\frac{Y^C}{2S^C}\right)^2 - 1\right]\frac{\sigma_2}{Y^C} + \left(\frac{\tau_{12}}{S^C}\right)^2 - 1 \geq 0 \qquad (4.8)$$

matrix compressive failure for MAT_055, based on Tsai/Wu criterion:

$$e_{ed}^2 = \frac{\sigma_2^2}{Y^C Y^T} + \left(\frac{\tau_{12}}{S^C}\right)^2 + \frac{\left(Y^C - Y^T\right)\sigma_2}{Y^C Y^T} - 1 \geq 0 \qquad (4.9)$$

where σ_1 is the stress in the fiber direction, σ_2 is the transverse stress, τ_{12} is the shear stress in the 1-2 plane, X^T is the tensile strength in the fiber direction, X^C is the compressive strength in the fiber direction, Y^T is the transverse tensile strength, Y^C is the transverse compressive strength, and S^C is the shear strength. Again, if any of the failure criteria are met, the material constants are set to zero.

Another feature of the MAT_054/055 model is that failure can also be controlled by the strain of the elements. If no failure strain is specified, the element fails as in MAT_022. Since the goal of using the MAT_054 material model was to improve the results obtained from MAT_022, the tensile failure strain of $\varepsilon^T = 1.5\%$ and a compressive

failure strain of ε^C = -1.0%, taken from the TEXCAD[4] model, was set in the input data for MAT_054/055. A third strain, called the effective failure strain, or *EFS*, could also be set and is the limiting strain if it is not set to zero in the input data. Several cases were run with different values of *EFS*, as shown in Fig. 4.10 and tabulated in Table 4.6. To change from MAT_054 to MAT_055, one simply changes a flag in the input data. There was no discernable difference in the response of MAT_055 when compared to MAT_054, so only the results from MAT_054 are discussed.

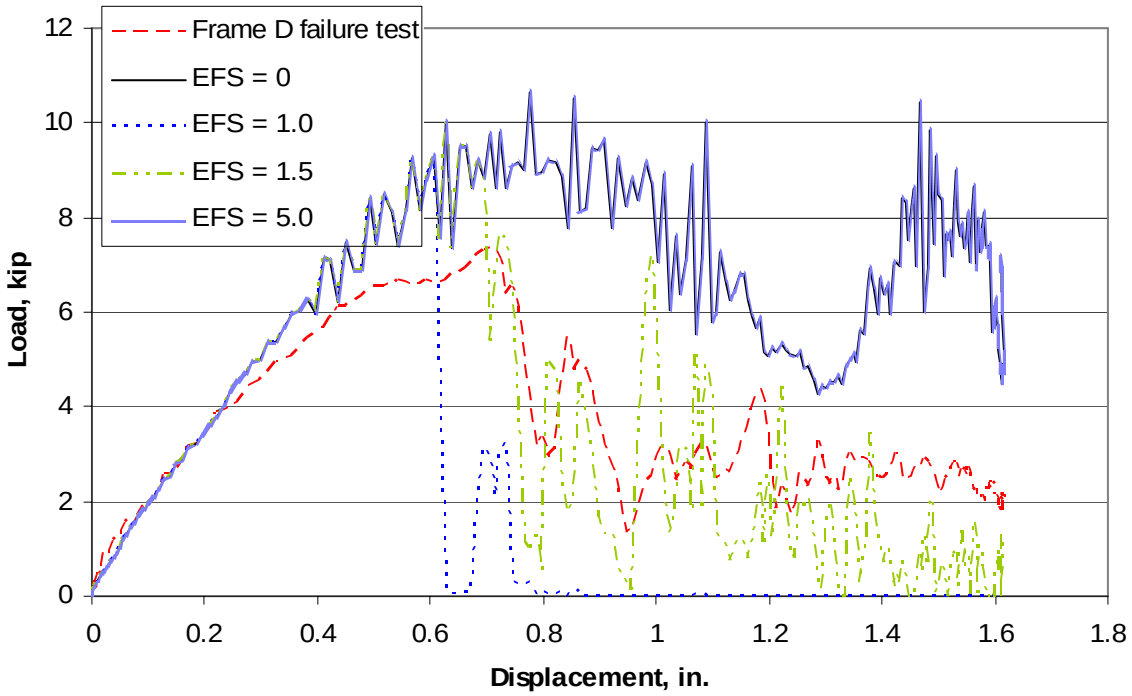

Fig. 4.10: Comparison of Load-Displacement curves MAT_054 models and experimental data.

Table 4.6: Comparison of load and displacement at failure, and energy absorbed during run, of MAT_054 models and experimental data.

Test	$F_{failure}$, kip	Error,%	$D_{failure}$, in.	Error,%	Energy, kip-in	Error,%
Experiment	7.5	0	0.75	0	6.15	0
EFS = 0	10.6*	+41.3	1.09	+45.3	10.5	+70.5
EFS = 1.0%	9.3	+24.0	0.61	-18.7	3.26	-47.1
EFS = 1.5%	9.5	+26.7	0.66	-12.0	5.63	-8.60
EFS = 5.0%	10.6*	+41.3	1.09	+45.3	10.5	+70.5

***This is the highest load, while the displacement is taken at the first large drop in load.**

With only the tensile and compressive failure strains set in the input (*EFS* = 0), MAT_054 predicted a failure load and displacement 41.3% larger than the experimental data. With *EFS* = 1.0%, i.e. the compressive failure strain, the model failed at a 24% higher load, but under-predicted the displacement at failure by 18.7%. With *EFS* = 1.5%, i.e. the tensile failure strain, the failure load prediction increased, but the failure displacement was closer, only -12%. With *EFS* = 5.0%, the results were the same as when there was no effective failure strain specified. One interesting feature of the MAT_054/055 models was that the load curve was the same up to failure. Also, unlike MAT_022, MAT_054 always predicted a load carried beyond the first failure event, and with the effective failure strain set to the tensile failure strain, the load curve closely followed the experimental data in displacement, if not load.

Comparing the energy absorbed by the FEA frame model during the analyses, the best model in this respect was with *EFS* = 1.5%, the tensile failure strain. This model was better than the best model with MAT_022.

A third material model investigated was MAT_059, a composite failure model. There are no notes in the LSDyna manuals on the specific failure criteria used in this material model. The difference in the input data between MAT_059 and MAT_022 is X^C is included in the formulation, and between Mat_059 and MAT_054/055 is there are no provisions for failure strains.[20] The results, shown in Fig. 4.11, were the same as MAT_054 up to failure displacement at 1.09 in. Beyond this displacement, the model did not carry as much load as the MAT_054 model, but did exhibit a reloading and second failure. The energy absorbed by the model with MAT_059 was 8.85 kip-in., an error of +43.7%, which was no better than the best MAT_054 model.

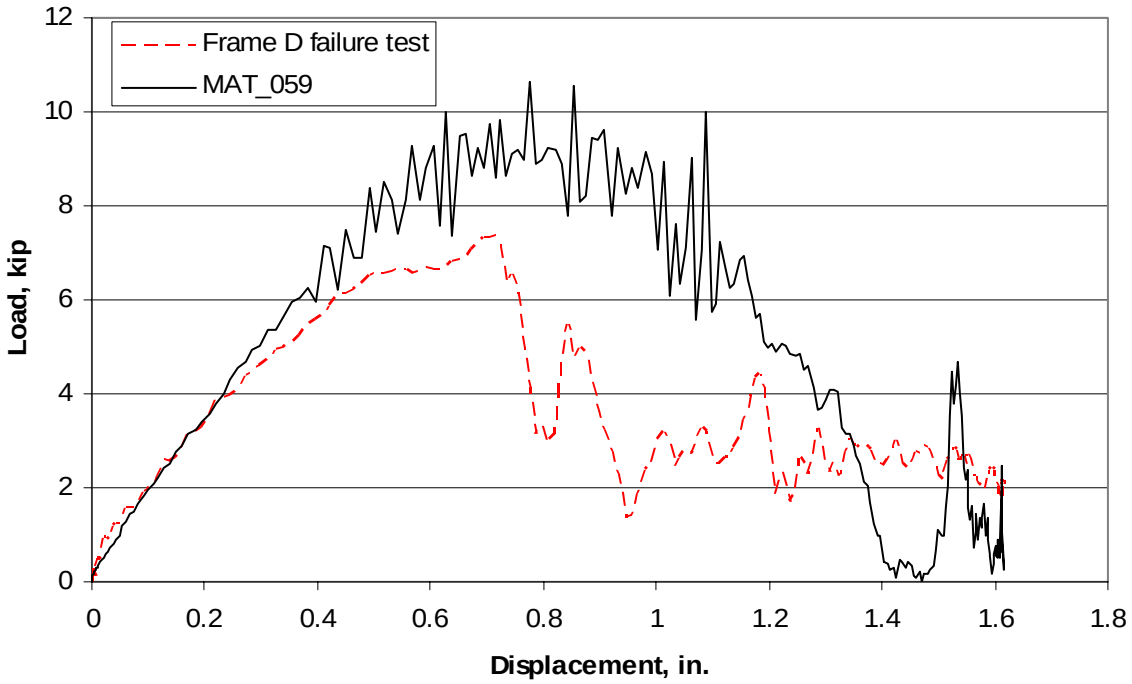

Fig. 4.11: Comparison of Load-Displacement curve of MAT_059 and experimental data.

There are other parameters that can be set in both MAT_054/055 and MAT_059 which control the softening of the fiber under tension and a reduction of fiber strength in compression after the matrix cracks.[19,20] In the interest of simplicity and direct comparison, neither of these parameters were utilized in the models discussed in this chapter.

4.2.2 Failure sequence in the FEA model

Checking the text output file that lists the elements that fail and the time of each failure, and using PostGL, an animation and visualization program that is part of LSDyna, the failure sequence of the best MAT_054 FEA model was observed. The first element to fail was on the back edge of the outer flange at -1.2˚, at 0.008566 s. This 'crack' propagated straight to the junction of the web and the flange, leaving a gap in the back side of the outer flange at -1.2˚. When the 'crack' reached the junction of the web and outer flange, it propagated along the junction from -1.2˚ to -2.2˚ and +1.6˚ (Fig. 4.12). This failure corresponded to the first load drop (see the green curve for *EFS*=1.5 in Fig. 4.10). A similar pattern was observed in the experiments, both static and

dynamic, although the cracks in the outer flange only propagated along the junction in the test of Frame C; the other three frames simply exhibited fracture of the outer flange.

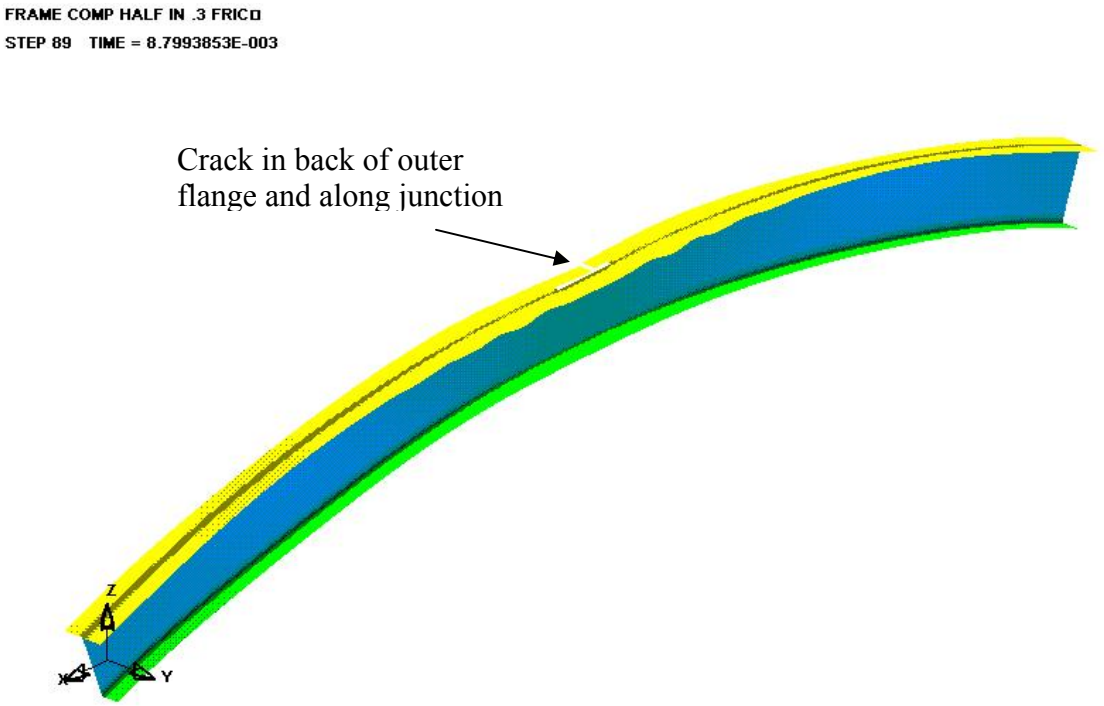

Fig. 4.12: Crack in back of outer flange and long junction of outer flange and web, corresponds to first load drop.

At 0.008943 s, the crack reached the junction of the web and the outer flange, two elements at +8˚ failed (circled in Fig. 4.13). This position corresponds to the edge of the load platen. This 'crack' did not propagate, and was not observed in the experimental tests.

At 0.008991 s, 0.000425 s after the initial 'crack' reached the junction of the outer flange and the web, the 'crack' began to propagate radially inward through the web at +1.2˚ (Fig 4.13). At the same time, the 'crack' propagated through the front of the outer flange at +1.2˚. This corresponded to the second load drop, the small peak following the initial load drop in the green curve in Fig. 4.10. When the 'crack' reached the inner flange, the frame began to reload. Again, this is similar to what was observed in the experimental tests.

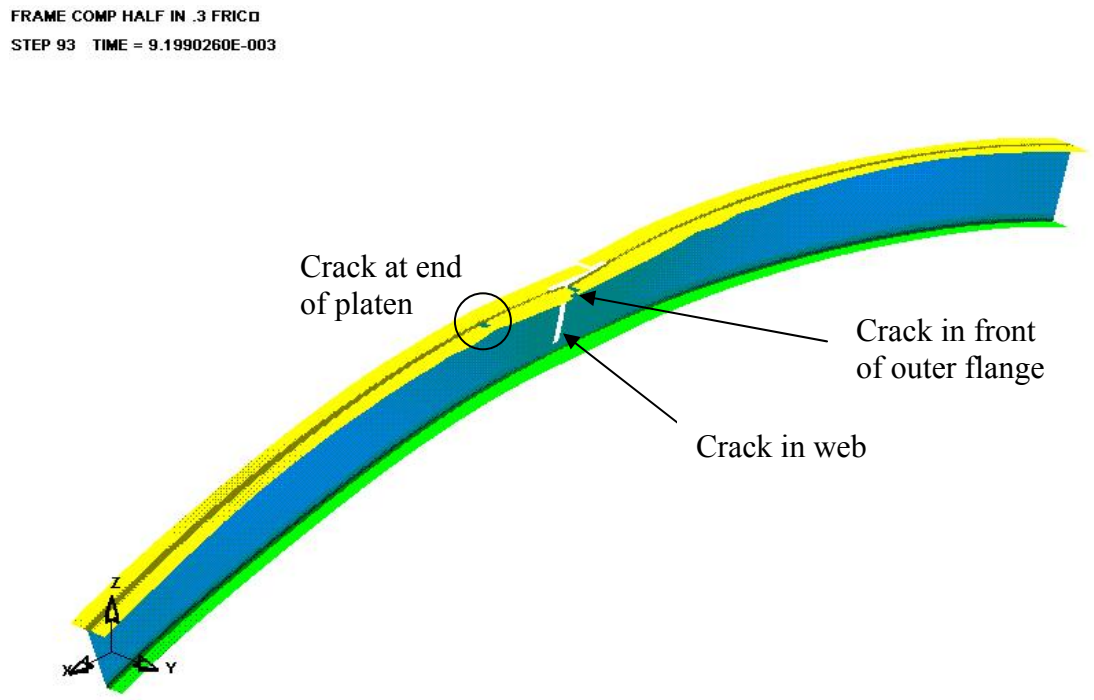

Fig. 4.13: Cracks in web, front of outer flange, and at platen end.

At 0.001028 s, 0.001 s after the 'crack' reached the inner flange, the clamped ends of the front of the outer flange failed. The second set of medium peaks in the green curve in Fig. 4.10 corresponds to this failure event. This event was not observed during the tests.

At 0.00117 s, 0.002 s after the 'crack' reached the inner flange, it propagated through the inner flange at +1.2˚, fully fracturing the frame (Fig. 4.14). This failure even corresponds to the small peak after 1.0 in. displacement in the green curve of Fig. 4.10; the large spike right at 1.0 in. is not a failure of any elements. For the rest of the FEA, half of the frame twisted and the other half just bent slightly; no more failed elements were logged in the LSDyna output.

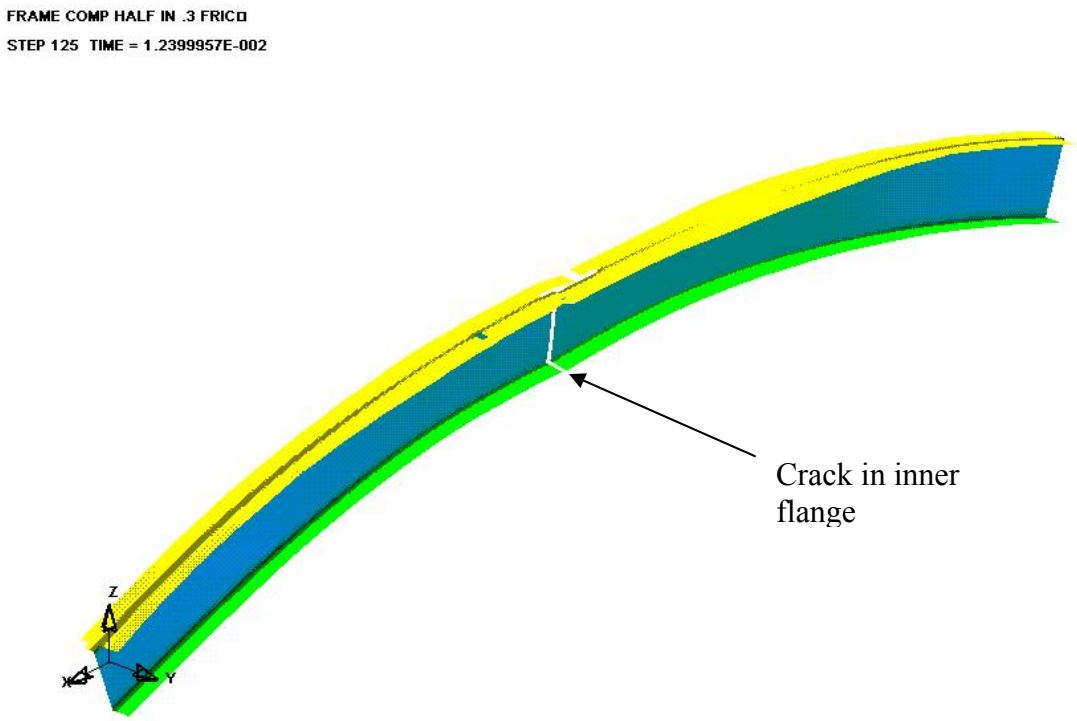

Fig. 4.14: Fully fractured frame FEA.

4.3 Strains in FEA model at failure

A strain-pattern study like the one conducted in Section 3.4 was performed with the best MAT_054 FEA data. The strains were tracked in the elements that were in positions that corresponded to the strain gage locations, and strains at various load levels were compared to the experimental data. As shown in Fig. 4.15, at a load well below failure, only 3 kips, the FEA predicted strains of similar compressive magnitude at the apex of the outer flange, but did not predict the tensile strains closer to the end blocks, beyond -10˚. At the peak load, a similar pattern was seen: the compressive strains at the apex of the outer flange were comparable to the experimental data, but the FEA predicted compressive strain all the way to the end blocks. Also of note, the FEA did not predict the lower compressive strain right at the apex of the frame at peak load.

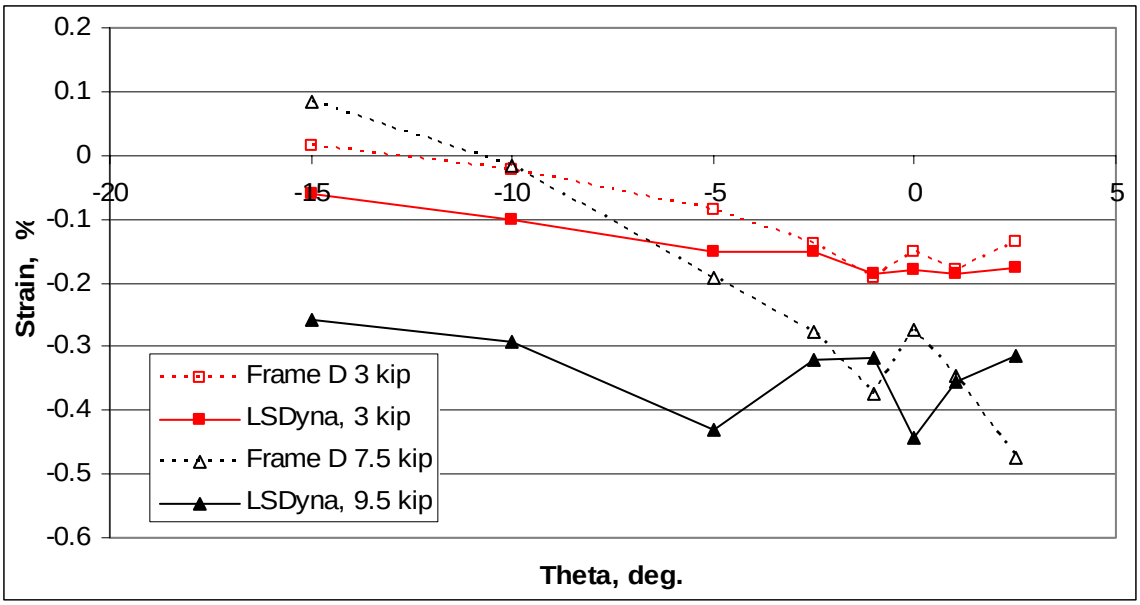

Fig. 4.15: Strain distributions in outer flange, FEA compared to Frame D failure test.

The FEA data for the inner flange at the 3 kip load level predicted a higher magnitude tensile strain at the apex, and a higher magnitude compressive strain near the end blocks, but did predict the inflection point near -6˚. At the peak load, the FEA did not predict the increase in tensile strain at the apex, or the increased compressive strain toward the end blocks (Fig. 4.16).

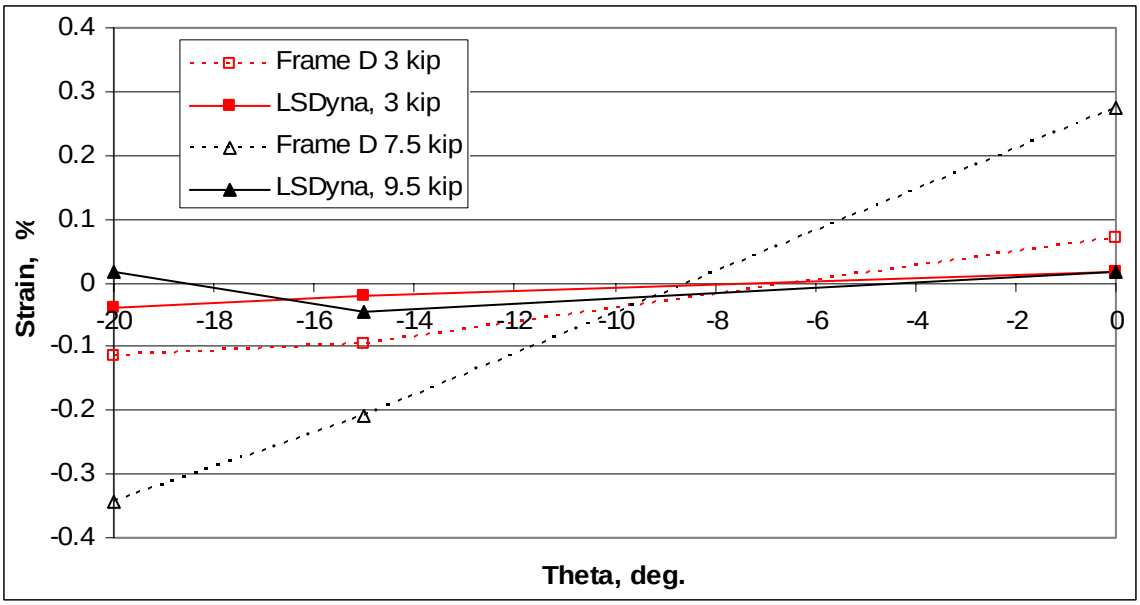

Fig. 4.16: Strain distributions in the inner flange, FEA compared to Frame D failure test.

Chapter 5 Concluding Remarks

This chapter presents a summary of the results and conclusions of the work discussed in the previous chapters. The results of dynamic failure tests of the textile composite fuselage frames are presented first, followed by a summary of the dynamic FEA conducted using LSDyna. The last section discusses recommendations for future work.

5.1 Dynamic textile composite fuselage frame tests

Dynamic tests to failure were conducted on Frames D and CF6F, and the response was compared to the quasi-static response of the Frames B and C conducted by Perez[4]. The same fixture used in the static tests was used to support the frame during the dynamic tests (Fig. 2.3). A load-introduction fixture was designed that consisted of a platen to spread the load across the apex of the frame, a trio of load cells to measure the load, and a wedge of aluminum honeycomb that tailored the load pulse to more accurately simulate a true crash-type loading (Figs. 2.3, 2.7). The frame and fixtures were placed in a small drop tower at NASA/Langley's Impact Dynamic Research Facility (Fig. 2.5). A 91.6 lb aluminum drop head was dropped from various heights which, along with various wedge sizes, imparted a potential of up to 1000, 2000, 7000, and 10,000 lbs peak loads to the frame. It was expected that the frame would fail at 6900 lbs, 115% of the static failure load.

Frame D failed at 7495 lbs and 0.7143 in. displacement, while Frame CF6F failed at 7104 lbs and 0.5651 in. This represented an average of 120% of the static failure load and 128% of the static failure displacement (Section 3.2). All frames failed by fracture near the apex of the arch. Cracks initiated in the outer flange of the frame, then propagated into the web. The crack in Frame D propagated to the inner flange, and the frame eventually fractured completely. Frame CF6F did not fracture completely, leaving

the inner flange intact. Cracks were also observed along the strand of unidirectional filler material placed at the outer junction of the web and the outer flange (Section 3.3). The energy absorbed by Frame CF6F during the failure test was 6.84 kip-in, 75.5% of the total energy absorbed during the test. Frame D absorbed 6.15 kip-in, 71% of the total energy absorbed during the test. The rest of the initial energy imparted to the system by the drop mass (9.47 kip-in) was absorbed by the honeycomb wedge or by the out-of-plane bending and twisting of the frame (Table 3.2).

Results from the lower peak load tests showed that the response of the frames to non-failure dynamic loads is very close to the static response to that same peak load (Section 3.4). The patterns of tensile and compressive strain are also similar between the two load cases, with the magnitudes of the dynamic strains generally higher for a given load than the static tests (Section 3.5).

5.2 Dynamic finite element analysis using LSDyna

A dynamic transient FEA was conducted using LSDyna, a commercially available FEA code from Livermore Software Technology Corp. Confidence in the LSDyna simulations was established by 1) comparing the response of a model using discrete-beam spring and discrete mass elements to the modal analysis of the two-spring, two-mass system discussed in Section 2.2, and 2) modeling composite coupon tests conducted by van Wamelen.[13] The response of the element-test model exactly matched the modal analysis. The material-test model matched the failure stress and strain of the off-axis coupon load test, and was -16% off the failure load of the on-axis load case.

The FEA model of the full frame was built using three material models, and the response of each was compared to the dynamic experimental data. Only the frame and lower load platen were modeled. The final FEA model of the frame was made of 3441 four node shell elements, roughly 0.5 in. on a side, with 21,548 active degrees of freedom. Clamped boundary conditions were applied to the nodes at the ends of the frame model. The platen was modeled as a rigid body with a prescribed displacement that was derived from the time history of the displacement of the platen during the experimental tests.

Several material models were used to model the textile composite material. The first model used MAT_022, a composite damage model that compared the stress of each element to the failure criteria, and set the material constants of the element to zero, effectively failing the element, if the failure criteria were met. This model only used the tensile fiber strength in the failure criteria for tensile and compressive failure in the fiber direction, and the response of the model was not very accurate, the best case being 42.5% higher in failure load, 6.7% lower in failure displacement, and 23.3% lower in energy absorbed with respect to the tests data. MAT_054/055 used similar failure criteria to MAT_022, but incorporated the compressive strength in the fiber direction, X^C, and allowed the strains of the element to control failure. The use of failure strains led to a slightly better model, 30.1% higher in failure load, 12.0% lower in failure displacement, and 8.6% lower in energy absorbed with respect to the test data. The third material model, MAT_059, was not well documented; it did not use failure strains, but did incorporate both tensile and compressive fiber direction strengths. This model's response was very similar to MAT_054/055 with the same failure load and displacement, but with more energy absorption, 43.7% high compared to the experimental data.

The failure sequence of the best MAT_054 FEA model was observed through an animation program and by checking the text output file written by LSDyna. It was found that the FEA exhibited similar failure events, starting with failure of the outer flange, then the web, and finally the inner flange. There were other failure events registered by the FEA, in particular the clamped ends of the outer flange failed, that were not observed in the experimental tests.

The strain patterns predicted by the FEA model were similar in magnitude and in direction for a load well below the peak load, but the FEA predicted that the entire outer flange was under high compressive strain and the inner flange was under little strain near failure, while the experiment showed the outer flange to transition from compression to tension near ±9˚ and the inner flange to transition from tension to compression near ±6˚.

5.3 Recommendations for future work

The data set for the experimental work is very small, only two frames in each of the static and dynamic test cases. Additional tests, possibly with frames that are not as

complex or expensive to manufacture, would strengthen the result that the dynamic response exhibits similar load and strain patterns, but with higher magnitudes.

The dynamic FEA conducted used only built-in material models in LSDyna. Additional parameters are available in these models that control 1) the softening of the fiber under tensile load, and 2) the reduction in compressive strength of the fiber after the matrix has cracked. The response of MAT_054, with the same curve up to failure, suggests that using these parameters could soften the overall stiffness of the frame, possibly leading to a reduction in the slope of the Load-Displacement curve of the FEA response. The LSDyna software cannot model delamination fractures that were observed in the post mortem examination of the failed frames. Hence, a more comprehensive failure modeling of the textile composite material in the frame is necessary to more closely capture the transient response and progressive damage in these frames.

No attempt was made to model the full test apparatus. A model that included the aluminum honeycomb wedge and drop mass, and imparted an initial velocity to the drop mass, may provide increased insight into the behavior of the frame during the test because the platen would be allowed to rotate as the response of the frame dictated.

Finally, it is possible to create a user-defined material in LSDyna. A progressive-failure cohesive zone interface element, similar to the one implemented in the quasi-static simulation in ABAQUS by Hart,[9] may be possible in LSDyna; use of such an element may increase the accuracy of the response of the model.

References

[1]Woodson, M. B., Johnson, E. R., Haftka, R. T, Hyer, M. W., Griffin, O. H, Jr., "Optimal Design of Composite Fuselage Frames for Crashworthiness," Doctor of Philosophy Dissertation in Aerospace Engineering, Virginia Tech, Blacksburg, VA 24061-0203, December 1994.

[2]Carden, H.D., Boitnott, R.L., and Fasanella, E.L., "Behavior of Composite/Metal Aircraft Structural Elements and Components Under Crash-Type Loads - What Are They Telling Us?", Proceedings of the 17th Congress of the International Council of Aeronautical Sciences Vol. 2, (Stockholm, Sweden, Sept. 9-14, 1990), American Institute of Aeronautics and Astronautics, Inc., Washington DC, 1990, p. 1195-1208.

[3]Moas, E., Boitnott, R. L., and Griffin, O. H., Jr., "An Analytical and Experimental Investigation of the Response of Curved Composite Frame/Skin Specimens," Journal of the American Helicopter Society, 1994, pp. 58-66.

[4]Perez, Jose G., "Energy Absorption and Progressive Failure Response of Composite Fuselage Frames", Master of Science Thesis in Aerospace Engineering, Virginia Tech, Blacksburg, VA 24061-0203, July 1999.

[5]Barrie, R.E., Skolnik, D.Z.,"Evaluation of Textile Composites for Fuselage Frames", Proceedings 4th NASA/DoD Advanced Composites Technology Conference, NASA CP-3299, pp. 719-735.

[6]Jackson, A. C., 1994, "Development of Textile Composite Preforms for Aircraft Primary Structures", Proceedings of the 35th AIAA/ASME/ASCE/AHS/ASC Structures, Structural Dynamics, and Materials Conference, (Hilton Head, South Carolina, April 18-20, 1994), American Institute of Aeronautics and Astronautics, Reston, Virginia, Part 2, pp. 1008-1012 (AIAA Paper No. 94-1430).

[7]Chou, T., 1992, "Microstructural Design of Fiber Composites", Cambridge University Press, Cambridge, Massachusetts.

[8]Naik, R. A., "TEXCAD - Textile Composite Analysis for Design: Version 1.0 User's Manual", NASA CR-4639, National Aeronautics and Space Administration, Hampton, Virginia.

[9]Hart, D. C., "Development of a Progressive Failure Finite Element Analysis For a Braided Composite Fuselage Frame," Master of Science Thesis in Aerospace Engineering, Virginia Tech, Blacksburg, VA 24061-0203, July 2002.

[10]Clarke, C. W., Townsend, W., Boitnott, R. L., "Crash Testing of Helicopter Airframe Fitting", Presented at the American Helicopter Society annual conference, Baltimore, MD, June 7-10, 2004.

[11]The MathWorks, "Signal Processing Toolbox," [online help manual], URL: http://www.mathworks.com/access/helpdesk/help/toolbox/signal/signal.html [cited 15 June 2004].

[12]Livermore Software Technology Corp., "LSDyna User's Guide," [online manual], pp. 1.1-1.12, URL: http://portal.ecadfem.com/fileadmin/files/lsdyna/website/pdf/pdf_lsdyna/Users_Guide.pdf?PHPSESSID=2789ac9230a8c6ad7acad2f4ac55c4b3 [cited 13 July 2004].

[13]van Wamelen, A. A., "Optimal Design and Testing of Laminated Specimens to Evaluate Competing Failure Criteria," Masters of Science Thesis in Aerospace Engineering, Virginia Tech, Blacksburg, VA 24061-0203, July 1993.

[14]Livermore Software Technology Corp., "LSDyna Theoretical Manual," [online manual], pp. 9.1-9.13, URL: http://portal.ecadfem.com/fileadmin/files/lsdyna/website/pdf/pdf_lsdyna/Theory_Manual.pdf?PHPSESSID=2789ac9230a8c6ad7acad2f4ac55c4b3 [cited 13 July 2004].

[15]Livermore Software Technology Corp., "LSDyna Keyword User's Manual," [online manual], pp. 26.20-26.28, URL: http://portal.ecadfem.com/fileadmin/files/lsdyna/website/pdf/pdf_lsdyna/Keyword_Manual_970.pdf?PHPSESSID=2789ac9230a8c6ad7acad2f4ac55c4b3 [cited 13 July 2004].

[16]Livermore Software Technology Corp., "LSDyna Theoretical Manual," [online manual], pp. 16.33-16.34, URL: http://portal.ecadfem.com/fileadmin/files/lsdyna/

website/pdf/pdf_lsdyna/Theory_Manual.pdf?PHPSESSID=2789ac9230a8c6ad7acad2f4ac55c4b3 [cited 13 July 2004].

[17]Hyer, W. M., *Stress Analysis of Fiber-Reinforced Composite Materials*, McGraw-Hill, New York, 1998, pp. 58.

[18]Livermore Software Technology Corp., "LSDyna Keyword User's Manual," [online manual], pp. 7.91-7.95, URL: http://portal.ecadfem.com/fileadmin/files/lsdyna/website/pdf/pdf_lsdyna/Keyword_Manual_970.pdf?PHPSESSID=2789ac9230a8c6ad7acad2f4ac55c4b3 [cited 13 July 2004].

[19]Livermore Software Technology Corp., "LSDyna Keyword User's Manual," [online manual], pp. 26.175-26.180, URL: http://portal.ecadfem.com/fileadmin/files/lsdyna/website/pdf/pdf_lsdyna/Keyword_Manual_970.pdf?PHPSESSID=2789ac9230a8c6ad7acad2f4ac55c4b3 [cited 13 July 2004].

[20]Livermore Software Technology Corp., "LSDyna Keyword User's Manual," [online manual], pp. 26.191-26.194, URL: http://portal.ecadfem.com/fileadmin/files/lsdyna/website/pdf/pdf_lsdyna/Keyword_Manual_970.pdf?PHPSESSID=2789ac9230a8c6ad7acad2f4ac55c4b3 [cited 13 July 2004].

Appendix A

This appendix presents the scripts that were used to perform the modal analysis of the two-spring, two-mass model of the dynamic frame test describes in Section 2.2. First is the script that sets the input variables and output, then the supporting scripts are presented.

```
%-----------------------------------------------------------------
%twostwom.m finds the time history of the loading of the arch
%when impacted by a mass, traveling at a given velocity.
clear
format short e

%units of lb-in-s

%mass matrix
Ww=2.4+46.22+42.98; %lbf, weight of drop platen + upper section + lower
section
Wf=17.8670;%lbf, load introduction fixture weight
mw=Ww./386; %lbf/g (with in/s2)
mf=Wf/386; %lbf/g (with in/s2)
%Mass matrix:
mr=[mw 0
    0 mf];

%Building aluminum honeycomb "spring":
%Aluminum honeycomb crush strength
Xc= 680;%psi from IDRF testing

%Wedge geometric parameters:
S=6; %in., base depth, parallel to arch ***VARIABLE***
b=4; %in., base width
h=3.25; %in., heigth, ***VARIABLE***
%Wedge "spring stiffness":
Kc=Xc*b*S(k)./h;

%Frame "spring stiffness":
Kf= 15000;%lbf/in

%Drop head impact velocity:
V=23;%ft/s  ***VARIABLE***
```

```
V=V.*12; %ft/s -> in/s

%Modal analysis (numeric solution to the equations of motion)
%***Must have mdofmodes.m and mdofstepresponse.m available!***
%this script may be set up for multiple wedge geometries for use in
papmetric studies.
for j=1:length(Xc)
    for i=1:length(h)
        kr= [Kc(j,i) -Kc(j,i)
            -Kc(j,i) (Kc(j,i)+Kf)];

        [omega,phi]=mdofmodes(mr,kr);

        M = transpose(phi)*mr*phi;

        w = omega;
        Nhat = 2;
        zt = [0 0];
        t = 0:.000001:.02; %s, length of test, ***VARIABLE
        u0 = transpose([0 0]);
        du0 = transpose([-V 0]);
        P = transpose(386*[-mw -mf]);

      u(:,:,i,j)=mdofstepresp(mr,w,phi,Nhat,zt,t,u0,du0,P);

        F(i,:)=u(2,:,i,j)*Kf;

        MaxForce(i)=abs(min(F(i,:)));
        u1max(i,j)=abs(min(u(1,:,i,j)));
        u2max(i,j)=abs(min(u(2,:,i,j)));
        differ(i,:)=u(1,:,i,j)-u(2,:,i,j);
        maxdiffer(i)=abs(min(differ(i,:)));

        if maxdiffer(i)>=.8*h(i)
            MaxForce(i)=NaN;
        end
    end

    MaxForce2(j,:)=MaxForce;
    maxdiffer2(j,:)=maxdiffer;

end

%Print wanted output:
MaxForce2'
maxdiffer2
u2max

%Plot time history of load platen displacement:
figure
plot(t,u(2,:,1,1)), grid on
%-----------------------------------------------------------------
```

The supporting scripts, mdofmodes.m and mdofStepResp.m, were written by Dr. William Hallauer, Department of Aerospace and Ocean Engineering Department,

Virginia Tech, for an introductory class in structural dynamics. The first script defines a Matlab function that finds the modes and associated frequencies of a lumped-mass system, and the second script takes the output of the first to find the time history of the displacements of the given system to a step input.

```
function [omega,phi]=mdofmodes(mr,kr);
%------------------------------------------------------------------
%PURPOSE:
%Given mass and stiffness matrices, calculates circular natural
%frequencies (rad/sec) and the mode shape (modal) matrix. Each
%mode shape (column of the modal matrix) is normalized so that
%the corresponding modal mass is unity.
%
%FORMAT:  [omega,phi]=mdofmodes(m,k)
%
%INPUT QUANTITIES - m, k - mass and stiffness matrices
%OUTPUT QUANTITIES - omega - natural frequencies (rad/sec)
%                    phi - modal matrix, each column a mode shape.
%------------------------------------------------------------------
[v,d]=eig(kr,mr);%Solve structural dynamics eigenvalue problem
[lambda,j]=sort(diag(d));%Sort eigenvalues and eigenvectors
v=v(:,j);%(mode shapes) in ascending order of eigenvalues
gmass=diag(v'*mr*v);%Generalized masses, eigenvector scaling
phi=v*diag(1 ./sqrt(gmass));%Eigenvectors for unit modal masses
omega=(sqrt(lambda))';% Natural frequencies (rad/sec), ascending order
%------------------------------------------------------------------------



function u=mdofstepresp(mr,w,phi,Nhat,zt,t,u0,du0,P);
%-------------------------------------------------------------
%PURPOSE:
%Calculates step response and/or initial-condition response
%of an N x N MDOF model (for which modes have already been
%calculated) using modal expansion by the mode-displacement
%method, user must specify number of modes to include
%
%FORMAT:  u=mdofstepresp(mr,w,phi,Nhat,zt,t,u0,du0,P);
%*****BE SURE TO SUPPRESS PRINTING WITH THE SEMICOLON ";"*****
%
%INPUT QUANTITIES
%mr = mass matrix of restrained structure, N x N
%w = row matrix of nat freqs (rad/sec), 1 x N, in ascending order
%phi = orthonormal modal matrix, N x N, ordered just as w
%Nhat = number of modes in modal expansion, r = 1, 2, ... , Nhat
%       where 1 .LE. Nhat .LE. N
%t = array of time instants, t = 0:delt:endt; for accuracy, delt
%       must be less than half of 2*pi/w(Nhat), where w(Nhat) is
%       the highest natural frequency in the expansion
%zt = row matrix of modal viscous damping ratios, Nhat x 1
%u0 = vector of initial displacements, N x 1
%du0 = vector of initial velocities, N x 1
%P = vector of physical step inputs, N x 1
```

```
%
%OUTPUT QUANTITY
%u = matrix of displacement response, N x length(t), not printed,
%       the user should plot the desired output time series, using,
%       for example, plot(t,u(7,:),'k',t,u(5,:),'r',t,u(3,:),'g')
%-------------------------------------------------------------
N = length(mr(:,1));%number of DOFs in the MDOF model
ntimes= length(t);%length of the time series
w((Nhat+1):N)=[];%removes unused higher elements from matrix of nat
freqs
phi(:,(Nhat+1):N)=[];%removes unused vectors from modal matrix
eta0=phi'*mr*u0;%initial values of modal coordinates, Nhat x 1
deta0=phi'*mr*du0;%initial velocities of modal coordinates, Nhat x 1
Hps=(phi'*P).*((1./w').^2);%modal step pseudo-static resp vector, Nhat
x 1
wd=w.*sqrt(1-zt.^2);%row matrix of damped nat freqs, 1 x Nhat
for r=1:Nhat
   wdt=wd(r)*t;
   eta(r,:)=Hps(r)+exp(-zt(r)*w(r)*t).*((eta0(r)-Hps(r))*cos(wdt)+...
       (deta0(r)+zt(r)*w(r)*(eta0(r)-Hps(r)))/wd(r)*sin(wdt));
end
u=phi*eta;%response matrix, N x ntimes
%-------------------------------------------------------------------------
```

Appendix B

The Matlab script presented here was used to take the raw ASCII experimental data, perform the needed analysis described in Section 3.1, and output ASCII files that were then used to create plots in Microsoft Excel.

```
%frameloadanal.m
%this script takes the assembled matix of data, splits it into usable
matrices,
%and performs the analysis that is done in Excel.

%The reason for duplicating the Excel analysis is that filtering can be
implemented
%in Matlab.
clear

load C:\LOP\Project\TestData\D3_09162003_3\ASCII_Data\D10kdata.ASC;

%these are (in order):
%1=time
%2=load cell 1 (left side) for CF6F, load cell 2 for D
%3=load cell 2 (right front) for CF6F, load cell 3 for D
%4=load cell 3 (right rear) for CF6F, load cell 4 for D (left side)
%5=accel 1 (lower front)
%6=accel 2 (lower rear)
%7=accel 3 (upper left)
%8=accel 4 (upper right)
%9-23=strain gages 1 through 15
%24=channel 31, a sine wave input

data=D10kdata; %to type less :)
time=data(:,1);
% data spread (from excel, for D10K):
% zero          FF
% 1to3900   5800t11450

sumload=data(:,2)+data(:,3)+data(:,4);
sum0=data(1,2)+data(1,3)+data(1,4);
corrload=(sumload-sum0)/.725; %.725 is the calibrated load correction
factor
```

```
aluavg0=mean(data(1:3900,7));
aruavg0=mean(data(1:3900,8));
alucorr=data(:,7)-aluavg0;
arucorr=data(:,8)-aruavg0;



m=length(corrload);
%lower platen zero is to end of free fall
aflavg0=mean(data(1:11450,5));
arlavg0=mean(data(1:11450,6));
aflcorr=data(:,5)-aflavg0;
arlcorr=data(:,6)-arlavg0;

%4-point averaging:
%loading is 9760 to 7150
ba= ones(1,4)/4;
faafl=filtfilt(ba,1,aflcorr(11460:12000));
faarl=filtfilt(ba,1,arlcorr(11460:12000));
%Butterworth, 5th-order, 60Hz cutoff, 10,000Hz sampling:
%used to smooth data before and after failure events
[bb,ab]=butter(5,60/5000);
fbafl1=filtfilt(bb,ab,aflcorr(1:11459));
fbarl1=filtfilt(bb,ab,arlcorr(1:11459));
fbafl2=filtfilt(bb,ab,aflcorr(12001:m));
fbarl2=filtfilt(bb,ab,arlcorr(12001:m));
filtafl=[fbafl1;faafl;fbafl2];
filtarl=[fbarl1;faarl;fbarl2];

filtal=(filtafl+filtarl)./2;

%intergral checks for filters:
int1=0;
int2=0;
int3=0;
for k=1:12000
    int1a=.0001/2*(aflcorr(k)+aflcorr(k+1));
    int1=int1+int1a;
    int2a=.0001/2*(arlcorr(k)+arlcorr(k+1));
    int2=int2+int2a;
    int3a=.0001/2*(filtal(k)+filtal(k+1));
    int3=int3+int3a;
end
int1
int2
int3

%finding velocity and displacement of drop head:
velalu(1)=data(1,7)*(data(2,1)-data(1,1))*32.2;
velaru(1)=data(1,8)*(data(2,1)-data(1,1))*32.2;
xalu(1)=velalu(1)*(data(2,1)-data(1,1));
xaru(1)=velaru(1)*(data(2,1)-data(1,1));

%and of load-introduction fixture:
velal(1)=filtal(1)*(data(2,1)-data(1,1))*32.2;
xal(1)=velal(1)*(data(2,1)-data(1,1));
```

```
for n=2:m
    velalu(n)=.5*(alucorr(n-1)+alucorr(n))*...
      (data(n,1)-data((n-1),1))*32.2+velalu(n-1);
    velaru(n)=.5*(arucorr(n-1)+arucorr(n))*...
      (data(n,1)-data((n-1),1))*32.2+velaru(n-1);
    xalu(n)=.5*(velalu(n-1)+vlealu(n))*...
      (data(n,1)-data((n-1),1))+xalu(n-1);
    xaru(n)=.5*(velaru(n-1)+velaru(n))*...
      (data(n,1)-data((n-1),1))+xaru(n-1);

    velal(n)=.5*(filtal(n-1)+filtal(n))*...
      (data(n,1)-data((n-1),1))*32.2+velal(n-1);
    xal(n)=.5*(velal(n-1)+velal(n))*...
      (data(n,1)-data((n-1),1))+xal(n-1);
end

%average for free fall data:
aluavgff=mean(data(5800:11450,7));
aruavgff=mean(data(5800:11450,8));

%load as seen by the drop head:
massd=91.6/1000;
loadalu=(data(:,7)-aluavgff)*massd;
loadaru=(data(:,8)-aruavgff)*massd;

%load as seen at the platen:
massp=17.867/1000;
loadinafl=data(:,5)*massp;
loadinaflcorr=aflcorr*massp;
loadinarl=data(:,6)*massp;
loadinarlcorr=arlcorr*massp;
loadinavg=(loadinafl+loadinarl)./2;
loadinavgcorr=(loadinaflcorr+loadinarlcorr)./2;
loadincorr2=corrload+loadinavg;
loadincorr3=corrload+loadinavgcorr;

%this is the final load that is imparted to the frame:
loadincorr=corrload+(filtal*massp);
infilt=loadincorr;

%plot range is about 11450to11700 for D10K for time-dependent plots.
Other plot vary

load C:\LOP\Project\TestData\FrameC1txt.ASC;
dataC=FrameC1txt;
%known columns are: 1:4=load, disp, load(press), calibrate.  The rest
are strain gages, but
%there are no files with the labels on the columns, so the data can't
be matched to a gage.

load C:\LOP\Project\TestData\FrameBcut1.ASC;
dataB=FrameBcut1;
%for Frame B data, the columns are: "LOAD, LB"  "DISP, IN"
      "LOAD(PRESS), LB" CALIBRATE
%"SG1,%"    "SG2,%"     "SG3,%"     "SG4,%"     "SG5,%"     "SG6,%"
      "SG7,%"     "SG8,%"     "SG9,%"     "SG10,%"
```

```
%"SG11,%"   "SG12,%"    "SG13,%"    "SG14,%"    "SG15,%"    "SG16,%"
      NONE  NONE  NONE
%"SG45,%"   "SG21,%"    "SG22,%"    "SG23,%"    "SG24,%"    "SG25,%"
      "SG26,%"    "SG27,%"
%"SG28,%"   "TIME, MS"
%1=load
%2=disp
%3=load(press)
%4=calibrate
%5:20=strains 1:16
%24:32=strains 45,21:28
%33=time

%plotting the dyanmic and static load-displacement curves:
figure
plot((-
12*xal(11450:11700))+0.0825,infilt(11450:11700),'k',dataB(1:1460,2),dat
aB(1:1460,3)/1000,':k',...
    dataC(1:2500,2),dataC(1:2500,3)/1000,'--k'),...
    legend('Dyn., D','Static, B','Static, C'), xlabel('displacement,
in.'), ylabel('load, klb'),...
    title('Load-Displacement curves, dynamic vs. static')
```

Appendix C

An example LSDyna input file is presented in this appendix. In this input file, a '$' at the beginning of the line means the line is a comment. A '*' in front of a word in caps at the beginning of a line defines the word as a keyword, which defines the following section of the input file. For example:

```
*PART
$HEADING
FRAMEIF
$      PID     SECID       MID     EOSID      HGID      GRAV    ADPOPT      TMID
       101       201       301         0         0         0         0         0
```

defines the part 'frameif.' The last two lines are called a 'card' and define attributes for the part. Some sections, such as the material models, have many cards. If the user is placing spaces between the variables, the spacing is very important in the LSDyna input files, as outlined in the User's Guide. The size of the font for this appendix is so that each card will fit on one line, as is required of the input file. Alternatively, the user may use a comma-delimited format. For example, the above could be written:

```
*PART
$HEADING
FRAMEIF
$      PID     SECID       MID     EOSID      HGID      GRAV    ADPOPT      TMID
101,201,301,0,0,0,0,0
```

The commented line may also be compressed or simply removed if the user so chooses. Both forms are used in this input file, specifically in the list sections of the file because these lists were generated in Microsoft Excel or Matlab as comma-delimited files, then copied into the input file. These lists are quite lengthy and have been truncated; please contact the author at lopilk@alum.mit.edu if you wish to obtain the entire file.

The following is the LSDyna input file that generates the 0.5-in. full frame model with MAT_054 as described in Section 4.2, framecomphalf.dyn:

```
$---+----1----+----2----+----3----+----4----+----5----+----6----+----7----+----8
$  LS-DYNA(970) DECK WRITTEN BY : eta/FEMB-PC version 28.0
$  ENGINEER :
$   PROJECT :
$     UNITS : M,  KG,  SEC,  N
$      TIME : 12:23:51 PM
$      DATE : Thursday, June 03, 2004
$---+----1----+----2----+----3----+----4----+----5----+----6----+----7----+----8
*KEYWORD
$---+----1----+----2----+----3----+----4----+----5----+----6----+----7----+----8
*TITLE
FRAME COMP half IN .3 fric
*CONTROL_TERMINATION
2.500E-02,0,0.000E+00,0.000E+00,0.000E+00
*CONTROL_TIMESTEP
0,0.9,0,0.000E+00,0.000E+00,0,0,0
*CONTROL_HOURGLASS
1,1.0E-03
*CONTROL_ENERGY
2,2,2,2
*CONTROL_OUTPUT
0,0,0,0,0.000E+00,0,100,5000
0
*DATABASE_BINARY_D3PLOT
1.000E-04,0
*DATABASE_BINARY_D3THDT
1.000E-04,0
*DATABASE_EXTENT_BINARY
0,0,3,1,1,1,1,1
0,0,0,0,0,0,2
1
*DATABASE_GLSTAT
1.0E-04,1
*DATABASE_RCFORCE
1.0E-04,1
$---+----1----+----2----+----3----+----4----+----5----+----6----+----7----+----8
$                                                                             $
$                                PART CARDS                                   $
$                                                                             $
$---+----1----+----2----+----3----+----4----+----5----+----6----+----7----+----8
*PART
$HEADING
FRAMEIF
$      PID     SECID       MID     EOSID      HGID      GRAV    ADPOPT      TMID
       101       201       301         0         0         0         0         0
*PART
$HEADING
FRAMEWEB
$      PID     SECID       MID     EOSID      HGID      GRAV    ADPOPT      TMID
       102       202       301         0         0         0         0         0
*PART
$HEADING
FRAMEOF
$      PID     SECID       MID     EOSID      HGID      GRAV    ADPOPT      TMID
       103       203       301         0         0         0         0         0
*PART
$HEADING
PLATEN1
$      PID     SECID       MID     EOSID      HGID      GRAV    ADPOPT      TMID
       104       204       302         0         0         0         0         0
$---+----1----+----2----+----3----+----4----+----5----+----6----+----7----+----8
$                                                                             $
$                              SECTION CARDS                                  $
$                                                                             $
$---+----1----+----2----+----3----+----4----+----5----+----6----+----7----+----8
*SECTION_SHELL
```

```
$IF
$      SECID   ELFORM  SHRF    NIP     PROPT   QR/IRID ICOMP   SETYP
201,1,.8333,2,0,0,0
$      T1      T2      T3      T4      NLOC    MAREA
5.08E-03,5.08E-03,5.08E-03,5.08E-03,0,0
*SECTION_SHELL
$WEB
$      SECID   ELFORM  SHRF    NIP     PROPT   QR/IRID ICOMP   SETYP
202,1,.8333,2,0,0,0
$      T1      T2      T3      T4      NLOC    MAREA
4.318E-03,4.318E-03,4.318E-03,4.318E-03,0,0
*SECTION_SHELL
$OF
$      SECID   ELFORM  SHRF    NIP     PROPT   QR/IRID ICOMP   SETYP
203,1,.8333,2,0,0,0
$      T1      T2      T3      T4      NLOC    MAREA
2.286E-03,2.286E-03,2.286E-03,2.286E-03,0,0
*SECTION_SOLID
$    SECID    ELFORM       AET
       204         1         0
$---+----1----+----2----+----3----+----4----+----5----+----6----+----7----+----8
$                                                                             $
$                                MATERIAL CARDS                               $
$                                                                             $
$---+----1----+----2----+----3----+----4----+----5----+----6----+----7----+----8
*MAT_ENHANCED_COMPOSITE_DAMAGE
$FRAME
$      MID        RO        EA        EB        EC      PRBA      PRCA      PRCB
       301   1691.26 4.87E+010 4.54E+010 1.05E+010    0.2156    0.0475    0.0692
$      GAB       GBC       GCA     KFAIL      AOPT
 1.32E+010 4.447E+09 4.144E+09         0         0
$       XP        YP        ZP        A1        A2        A3    MANGLE
         0         0         0         0         0         0         0
$       V1        V2        V3        D1        D2        D3    DFAILM    DFAILS
         0         0         0         0         0         0       2.5       2.5
$    TFAIL      ALPH      SOFT      FBRT     YCFAC    DFAILT    DFAILC       EPS
         0      0.25         1       1.0       1.0       1.5      -1.0      .015
$       XC        XT        YT        YC        SC      CRIT      BETA
 4.895E+08 6.300E+08 5.043E+08 3.922E+08 2.200E+08      54.0         0
*MAT_RIGID
$ALUMINUM, PLATEN 1 AND 2
$      MID        RO         E        PR         N    COUPLE         M     ALIAS
       302   2.7E+03 6.89E+010      0.33       0.0       0.0       0.0
$      CMO      CON1      CON2
       1.0         4         7
$       XP        YP        ZP        A1        A2        A3
         0         0         0         0         0         0
$---+----1----+----2----+----3----+----4----+----5----+----6----+----7----+----8
$                                                                             $
$                              LOAD CURVES                                    $
$                                                                             $
$---+----1----+----2----+----3----+----4----+----5----+----6----+----7----+----8
*DEFINE_CURVE
701,0,1,1,0,0,0
0,0
0.0001,-3.05E-06
0.0002,-3.05E-06
.
.
.
0.0249,-4.09E-02
0.025,-4.09E-02
$---+----1----+----2----+----3----+----4----+----5----+----6----+----7----+----8
$                                                                             $
$                              LOAD CARDS                                     $
$                                                                             $
$---+----1----+----2----+----3----+----4----+----5----+----6----+----7----+----8
*LOAD_BODY_Z
901,9.81
*DEFINE_CURVE
901
```

```
0,1
1,1
$---+----1----+----2----+----3----+----4----+----5----+----6----+----7----+----8
$                                                                              $
$                              NODE SET CARDS                                  $
$                                                                              $
$---+----1----+----2----+----3----+----4----+----5----+----6----+----7----+----8
*SET_NODE_LIST
$      SID       DA1       DA2       DA3       DA4
       401       0.0       0.0       0.0       0.0
$     NID1      NID2      NID3      NID4      NID5      NID6      NID7      NID8
1,174,347,520,693,866,1039,1212
1385,1558,1731,1904,2077,2250,2423,2596
2769,2942,3115,3288,3461,173,346
519,692,865,1038,1211,1384,1557,1730
1903,2076,2249,2422,2595,2768,2941,3114
3287,3460,3633
*SET_NODE_LIST
$      SID       DA1       DA2       DA3       DA4
       402       0.0       0.0       0.0       0.0
$     NID1      NID2      NID3      NID4...
10001,10002,10003,10004,10005,10006,10007,10008
*SET_PART_LIST
403,0,0,0,0
101,102,103
$---+----1----+----2----+----3----+----4----+----5----+----6----+----7----+----8
$                                                                              $
$                           BOUNDARY SPC CARDS                                 $
$                                                                              $
$---+----1----+----2----+----3----+----4----+----5----+----6----+----7----+----8
*BOUNDARY_SPC_SET_ID
$       ID
       501
$     NSID       CID      DOFX      DOFY      DOFZ     DOFRX     DOFRY     DOFRZ
       401         0         1         1         1         1         1         1
*BOUNDARY_SPC_SET_ID
$       ID
       502
$     NSID       CID      DOFX      DOFY      DOFZ     DOFRX     DOFRY     DOFRZ
       402         0         1         1         0         1         1         1
*BOUNDARY_PRESCRIBED_MOTION_RIGID
104,3,2,701,1.0,0,1.0E+28,0.0
$---+----1----+----2----+----3----+----4----+----5----+----6----+----7----+----8
$                                                                              $
$                              CONTACT CARDS                                   $
$                                                                              $
$---+----1----+----2----+----3----+----4----+----5----+----6----+----7----+----8
*CONTACT_AUTOMATIC_NODES_TO_SURFACE_ID
$      CID
       601
$     SSID      MSID     SSTYP     MSTYP    SBOXID    MBOXID       SPR       MPR
       403       104         2         3                            0         0
$       FS        FD        DC        VC       VDC    PENCHK        BT        DT
       0.3       0.3       0.0  1.21E+08       0.0         0       0.01.0000E+20
$      SFS       SFM       SST       MST      SFST      SFMT       FSF       VSF
       1.0       1.0       0.0       0.0       1.0       1.0       1.0       1.0
$     SOFT    SOFSCL    LCIDAB    MAXPAR     SBOPT     DEPTH     BSORT    FRCFRQ
          0      0.10                1.025       0.0       2.0         0         1
$   PENMAX    THKOPT    SHLTHK     SNLOG      ISYM     I2D3D    SLDTHK    SLDSTF
       0.0         0         0         0         0         0       0.0       0.0
$     IGAP    IGNORE
          2         0
$---+----1----+----2----+----3----+----4----+----5----+----6----+----7----+----8
$                                                                              $
$                           NODE INFORMATION                                   $
$                                                                              $
$---+----1----+----2----+----3----+----4----+----5----+----6----+----7----+----8
*NODE
$FRAME
1,-1.0741E+00,0.0000E+00,-1.9907E-01
2,-1.0622E+00,0.0000E+00,-1.9452E-01
```

```
3,-1.0502E+00,0.0000E+00,-1.9002E-01
.
.
.
3631,1.0929E+00,3.5560E-02,-7.5829E-02
3632,1.1054E+00,3.5560E-02,-8.0513E-02
3633,1.1178E+00,3.5560E-02,-8.5251E-02
$PLATEN1
10001,-0.3048,-0.0508,0.124059
10002,0.3048,-0.0508,0.124059
10003,0.3048,0.0508,0.124059
10004,-0.3048,0.0508,0.124059
10005,-0.3048,-0.0508,0.162159
10006,0.3048,-0.0508,0.162159
10007,0.3048,0.0508,0.162159
10008,-0.3048,0.0508,0.162159
$---+----1----+----2----+----3----+----4----+----5----+----6----+----7----+----8
$                                                                              $
$                            ELEMENTS INFORMATION                              $
$                                                                              $
$---+----1----+----2----+----3----+----4----+----5----+----6----+----7----+----8
*ELEMENT_SHELL
$    EID     PID    NID1...
$FRAMEIF
1,101,1,2,175,174
2,101,2,3,176,175
3,101,3,4,177,176
.
.
.
687,101,690,691,864,863
688,101,691,692,865,864
$FRAMEWEB
689,102,1,2,867,866
690,102,2,3,868,867
.
.
.
2063,102,2074,2075,2940,2939
2064,102,2075,2076,2941,2940
$FRAMEOF
2065,103,2077,2078,2251,2250
2066,103,2078,2079,2252,2251
.
.
.
3439,103,3458,3459,3632,3631
3440,103,3459,3460,3633,3632
*ELEMENT_SOLID
$PLATEN1
10001,104,10001,10002,10003,10004,10005,10006,10007,10008
$---+----1----+----2----+----3----+----4----+----5----+----6----+----7----+----8
*END
```

Appendix D

The Matlab script that was written to generate the node and element lists for the LSDyna input file is presented in this appendix. Lists were save as ASCII text files, then opened in Microsoft Excel and resaved as comma-delimited files. These files were then opened in a text editor and copied into the LSDyna input file.

```
%framenodes.m creates the nodes for the beam based on element size.

clear

%frame dimensions
theta=42; %total arc of frame
theta=theta/2; %coordinates go +/- about center of arc
yif=1.25; %in., inner flange y-dimension
yof=2.8; %in., outer flange y-dim total
yof=yof/2; %coordinates go +/- about web
zof=4.8; %in., outer flange z-dim
ri=118; %radius on inner flange

%element size ***VARIABLE!
eifn=8; %# of elements across inner flange (y-dir), even or odd
ewn=16; %# of ele up web (z-dir), even or odd
eofn=16; %# of ele across outer flange (y-dir), even ONLY!!!
earcn=344; %# of ele along arc (x-z plane, s-dir), even ONLY!!!
    %inner arc is about 86 in., so earc=86 is about 1 in. ele

%splitting the sections into stations for the nodes:
eif=0:yif/eifn:yif; %inner flange, y-dir
ew=0:zof/ewn:zof; %web, z-dir
eof=-yof:2*yof/eofn:yof; %outer flange, y-dir
earc=-theta:2*theta/earcn:theta; %inner arc, theta

%node coordinates:
%inner flange:
for j=1:length(eif)
    for k=1:length(earc)
        nodeif(k+(j-1)*length(earc),2) = ri * sin(earc(k)*pi/180);
        nodeif(k+(j-1)*length(earc),4) = ...
            -(ri * (1-cos(earc(k)*pi/180)));
```

```
        nodeif(k+(j-1)*length(earc),3) = eif(j);
    end
end

%web:
%this list starts at the second row and stops one row short of the
%top so that the node number list is consistent in the flanges.
%this affects how the element list is built for the web.
for m=2:length(ew)-1
    for n=1:length(earc)
        nodew(n+(m-2)*length(earc),2) = ...
            (ri + ew(m)) * sin(earc(n)*pi/180);
        nodew(n+(m-2)*length(earc),4) = ...
            -(ri * (1-cos(earc(n)*pi/180))) + ...
            cos(earc(n)*pi/180)*ew(m);
        nodew(n+(m-2)*length(earc),3) = 0;
    end
end

%outer flange
for p=1:length(eof)
    for q=1:length(earc)
        nodeof(q+(p-1)*length(earc),2) = ...
            (ri+zof) * sin(earc(q)*pi/180);
        nodeof(q+(p-1)*length(earc),4) =  ...
            -(ri * (1-cos(earc(q)*pi/180))) + cos(earc(q)*pi/180)*zof;
        nodeof(q+(p-1)*length(earc),3) = eof(p);
    end
end

%node list assembly:
node=[nodeif
    nodew
    nodeof];
node=node.*0.0254; %in to m

%adding the node numbers to the first column:
for f=1:length(node)
    node(f,1)=f;
end



%elements list:

%inner flange
for a=1:length(eif)-1
    for b=1:length(earc)-1
        eleif(b+(a-1)*(length(earc)-1),3) = ...
            b + (a-1)*length(earc);
        eleif(b+(a-1)*(length(earc)-1),4) = ...
            eleif(b+(a-1)*(length(earc)-1),3) + 1;

        eleif(b+(a-1)*(length(earc)-1),5) = ...
            b + (a)*length(earc) +1 ;
        eleif(b+(a-1)*(length(earc)-1),6) = ...
            eleif(b+(a-1)*(length(earc)-1),5) - 1;
```

```
    end
end
%part number, second column:
eleif(:,2)=101;

%web
%for first row (because node numbers are not consistent in web):
for c=1
    for d=1:length(earc)-1
        elew(d,3) = d;
        elew(d,4) = elew(d,3) + 1;

        elew(d,5) = d + length(nodeif) +1;
        elew(d,6) = elew(d,5) - 1;
    end
end

%for inner section:
for c=2:length(ew)-2
    for d=1:length(earc)-1
        elew(d+(c-1)*(length(earc)-1),3) = ...
            d + length(nodeif) + (c-2)*length(earc);
        elew(d+(c-1)*(length(earc)-1),4) = ...
            elew(d+(c-1)*(length(earc)-1),3) + 1;

        elew(d+(c-1)*(length(earc)-1),5) = ...
            d + length(nodeif) + (c-1)*length(earc) +1;
        elew(d+(c-1)*(length(earc)-1),6) = ...
            elew(d+(c-1)*(length(earc)-1),5) - 1;
    end
end

%for top row:
for c=length(ew)-1
    for d=1:length(earc)-1
        elew(d+(c-1)*(length(earc)-1),3) = ...
            d + length(nodeif) + (c-2)*length(earc);
        elew(d+(c-1)*(length(earc)-1),4) = ...
            elew(d+(c-1)*(length(earc)-1),3) + 1;

        elew(d+(c-1)*(length(earc)-1),5) = ...
            d + length(nodeif) + length(nodew) + ...
            (length(eof)-1)/2*length(earc) + 1;
        elew(d+(c-1)*(length(earc)-1),6) = ...
            elew(d+(c-1)*(length(earc)-1),5) - 1;
    end
end
%part number, second column:
elew(:,2)=102;

%outer flange
for e=1:length(eof)-1
    for f=1:length(earc)-1
        eleof(f+(e-1)*(length(earc)-1),3) = ...
            f + length(nodeif) + length(nodew) + (e-1)*length(earc);
        eleof(f+(e-1)*(length(earc)-1),4) = ...
            eleof(f+(e-1)*(length(earc)-1),3) + 1;
```

```
        eleof(f+(e-1)*(length(earc)-1),5) = ...
            f + length(nodeif) + length(nodew) + e*length(earc) + 1;
        eleof(f+(e-1)*(length(earc)-1),6) = ...
            eleof(f+(e-1)*(length(earc)-1),5) - 1;
    end
end
%part number, second column:
eleof(:,2)=103;

%element assembly:
ele=[eleif
    elew
    eleof];
%adding element number to the first column:
for h=1:length(ele)
    ele(h,1)=h;
end

%saving the ascii files; convert to .csv in Excel:
save ele.asc ele -ascii
save node.asc node -ascii

%all output is supressed, so this tells you when you're done:
disp('done')
```

Vita

Larry Pilkington was born 2 December 1978 to Jim Pilkington and Susan Kelton in Ouray, CO. He graduated valedictorian from Hyannis High School in Hyannis, NE, in 1997. While in high school he earned his private pilot's certificate, leading to an interest in the design and manufacturing of small aircraft. In 2001, he earned a B.S. in Aero/Astro Engineering from the Massachusetts Institute of Technology in Cambridge, MA, and capped his education with a M.S. in Aerospace Engineering from Virginia Polytechnic Institute and State University in Blacksburg, VA.